INVESTIGATING THE INTERACTIONS OF POLY(A)-CORALYNE IN CROWDED ENVIRONMENTS AND THE EFFECT OF DNA METHYLATION ON DDD-LYSINE AND DDD-ARGININE INTERACTIONS

A THESIS SUBMITTED TO
THE GRADUATE SCHOOL OF NATURAL AND APPLIED SCIENCES
OF
MIDDLE EAST TECHNICAL UNIVERSITY

BY

ZEYNEP SUVACI

IN PARTIAL FULFILLMENT OF THE REQUIREMENTS
FOR
THE DEGREE OF MASTER OF SCIENCE
IN
CHEMISTRY

JANUARY 2022

Approval of the thesis:

INVESTIGATING THE INTERACTIONS OF POLY(A)-CORALYNE IN CROWDED ENVIRONMENTS AND THE EFFECT OF DNA METHYLATION ON DDD-LYSINE AND DDD-ARGININE INTERACTIONS

submitted by **ZEYNEP SUVACI** in partial fulfillment of the requirements for the degree of **Master of Science** i**n Chemistry, Middle East Technical University** by,

Prof. Dr. Halil Kalıpçılar
Dean, Graduate School of **Natural and Applied Sciences** _____

Prof. Dr. Özdemir Doğan
Head of the Department, **Chemistry** _____

Assoc. Prof. Dr. Özgül Persil Çetinkol
Supervisor, **Chemistry, METU** _____

Examining Committee Members:

Prof. Dr. Levent Toppare
Chemistry, METU _____

Assoc. Prof. Dr. Özgül Persil Çetinkol
Chemistry, METU _____

Assist. Prof. Dr. Şebnem Eşsiz
Molecular Biology and Genetics, Kadir Has University _____

Assist. Prof. Dr. Çağatay Dengiz
Chemistry, METU _____

Assist. Prof. Dr. Süreyya Özcan Kabasakal
Chemistry, METU _____

Date: 24.01.2022

I hereby declare that all information in this document has been obtained and presented in accordance with academic rules and ethical conduct. I also declare that, as required by these rules and conduct, I have fully cited and referenced all material and results that are not original to this work.

Name Last name: Zeynep Suvacı

Signature:

ABSTRACT

INVESTIGATING THE INTERACTIONS OF POLY(A)-CORALYNE IN CROWDED ENVIRONMENTS AND THE EFFECT OF DNA METHYLATION ON DDD-LYSINE AND DDD-ARGININE INTERACTIONS

Suvacı, Zeynep
Master of Science, Chemistry
Supervisor: Assoc. Prof. Dr. Özgül Persil Çetinkol

January 2022, 98 pages

Poly(A) tail is an essential determinant of mRNA stability and maturation and is required for translation initiation. Small molecules recognizing poly(A) tails might interfere with mRNA processing. Hence, they have the potential to act as therapeutic agents. Coralyne (COR), a strong poly(A) binder, is shown to induce the formation of a stable, double-stranded poly(A) self-structure under dilute solution conditions. Although studies in dilute solutions are very informative, they do not necessarily reflect DNA structure and stability in vivo. Within the first part of this thesis, poly(A)-COR interactions under molecular crowding conditions were investigated to shed light on the behavior of poly(A)-COR in intracellular environments. PEG200, sucrose, and glycerol were used to mimic the cellular environment. Results of thermal denaturation experiments revealed a decrease in poly(A)-COR stability, especially with increasing PEG concentration. CD spectroscopy results confirmed that while the characteristic spectrum of poly(A)-COR was conserved, it was altered slightly in the presence of crowding agents, especially PEG. In the second part of this thesis, the effect of DNA methylation on the interactions of Dickerson

Dodecamer (DDD) with lysine (Lys) and arginine (Arg) amino acids, which are profoundly found in histones, was investigated. The methylation of cytosines at the 5th position (d5mC) is one of the most common epigenetic modifications and is believed to alter gene expression. CD spectroscopy results revealed the conservation of B-form structure upon DNA methylation. Increasing the amino acid concentrations is found to alter the B-DNA structure, where the effect was noteworthy in the unmethylated DDD compared to DDD8, which has 8 methylated cytosines. In addition, the effect of Arg on DNA stability was found to be more substantial compared to Lys via UV-Vis thermal denaturation experiments.

Keywords: Poly(A), Coralyne, Molecular Crowding, DNA Methylation, Dickerson Dodecamer

ÖZ

KALABALIK ORTAMDA POLY(A)-CORALYNE ETKİLEŞİMLERİNİN VE DNA METİLASYONUNUN DDD-LİZİN VE DDD-ARGİNİN ETKİLEŞİMLERİNE ETKİSİNİN İNCELENMESİ

Suvacı, Zeynep
Yüksek Lisans, Kimya
Tez Yöneticisi: Doç. Dr. Özgül Persil Çetinkol

Ocak 2022, 98 sayfa

Poly(A) kuyruğu, mRNA stabilitesi ve olgunlaşmasının temel bir belirleyicisidir ve translasyonun başlatılması için gereklidir. Poly(A) kuyruklarını tanıyan küçük moleküller mRNA içeren süreçlere müdahil olabilirler ve bu nedenle terapötik ajan olarak kullanılma potansiyeline sahiptirler. Poly(A)'ya güçlü bir şekilde bağlanan Coralyne'in seyreltik çözelti koşulları altında kararlı, çift sarmallı bir poly(A) öz yapısının oluşumunu indüklediği gösterilmiştir. Seyreltik çözeltilerdeki çalışmalar oldukça bilgilendirici olsa da in vivo DNA yapısını ve kararlılığını tam olarak açıklayamamaktadır. Bu tezin ilk bölümünde, poly(A)-COR'un hücre içi ortamlardaki davranışına ışık tutmak için moleküler kalabalık koşulları altında poly(A)-COR etkileşimleri araştırılmıştır. Hücresel ortamı taklit etmek için PEG200, sükroz ve gliserol kullanılmıştır. Termal denatürasyon deneylerinin sonuçları özellikle artan PEG derişimi ile poly(A)-COR kararlılığında bir düşüş olduğunu ortaya çıkarmıştır. CD spektroskopi sonuçları poly(A)-COR'un karakteristik spektrumunu korurken, kalabalıklaştırıcı ajanların, özellikle PEG'in varlığında poly(A)-COR yapısının hafif değiştiğini doğrulamıştır. Bu tezin ikinci bölümünde,

DNA metilasyonunun Dickerson Dodecamer (DDD) ile histonlarda fazlaca bulunan lizin (Lys) ve arginin (Arg) amino asitlerinin etkileşimleri üzerindeki etkisi araştırılmıştır. Sitozinlerin 5. pozisyonda metilasyonu (d5mC) en yaygın epigenetik modifikasyonlardan biridir ve gen ekspresyonunu değiştirdiğine inanılmaktadır. CD spektroskopi sonuçları, DNA metilasyonunun, DNA'nın B-form yapısını değiştirmediğini ortaya çıkartmıştır. Amino asit derişimlerinin arttırılmasının ise B-DNA yapısında değişikliklere sebep olduğu ve bu etkinin metillenmemiş DDD'de, 8 adet metillenmiş sitozin bulunduran DDD8'e kıyasla daha belirgin olduğu tespit edilmiştir. Ayrıca, UV-Vis termal denatürasyon deneyleri ile Arg'nin DNA kararlılığı üzerindeki etkisinin, Lys'ye kıyasla daha fazla olduğu tespit edilmiştir.

Anahtar Kelimeler: Poly(A), Coralyne, Moleküler Kalabalıklaşma, DNA Metilasyonu, Dickerson Dodecamer

To my parents who made everything possible for me…

ACKNOWLEDGMENTS

I would like to thank Assoc. Prof. Dr. Özgül Persil Çetinkol for her guidance, patience, and support. Joining her research group and working with her was the best decision I have ever made in my life.

I gratefully appreciate Scientific and Technological Research Council of Turkey (TÜBİTAK) for the financial support to the second part of this thesis via project number 118Z339.

I would like to thank to my committee members, Prof. Levent Toppare, Assist. Prof. Şebnem Eşsiz, Assist. Prof. Çağatay Dengiz and Assist. Prof. Süreyya Özcan Kabasakal for their valuable presence at my thesis defense.

I would like to thank my lab mates, OPC Lab, for creating the greatest environment that a person can work at and with.

I would like to express my special thanks to Kübra Doğan. Without her company, this thesis would probably be incomplete, and my morning coffee would probably be tasteless.

I would express my sincere gratitude to Dr. Mehrdad Forough for his continuous support, his precious advices, and being the big brother I never had.

I also would like to thank to my parents for always being there for me; to Deroji for make me laugh whenever I felt down; to İrem, for being a one-woman-band to me; and to my grandmother Nurten, for her incredible supports; and to my dearest friends, Pelin, Semin, Ecenaz and Müge, for their valuable company and friendship.

I would like to express my gratitude for the Nanografi family, especially Dr. Ahmet Çağlar Özketen, Ayşenur, Gizem and Evren for their irreplaceable supports.

Last but not least, I would like to thank to my best friend, Tuna Yıldız for his love, encourage and persistence. Without him, nothing would be the same.

TABLE OF CONTENTS

LIST OF TABLES

TABLES

LIST OF FIGURES

FIGURES

LIST OF ABBREVIATIONS

Arg	Arginine
BPE	Buffered Phosphate EDTA
CD	Circular Dichroism
COR	Coralyne
DDD	Dickerson Dodecamer
DNA	Deoxyribonucleic Acid
EG	Ethylene Glycol
ncRNA	Non-Coding RNA
Lys	Lysine
PEG	Polyethylene Glycol
RNA	Ribonucleic Acid
Tf	Final Temperature
Ti	Initial Temperature
Tm	Melting Temperature
UV-Vis	Ultraviolet-Visible

CHAPTER 1

INTRODUCTION

1.1 Nucleic Acids

Nucleic acids are the class of macromolecules that carry genetic code in all living organisms. They are long chainlike molecules composed of nucleotides as building blocks. A nucleotide has three components: a nitrogenous base, a phosphate group, and a pentose (five-carbon) sugar. Phosphodiester bonds link together nucleotides to form nucleic acids. A nucleoside is formed by a base linked to a sugar molecule through a glycosidic bond. The nitrogenous bases for coding the genetic information in deoxyribonucleic acid (DNA) are purines, adenine (A), and guanine (G); and pyrimidines, cytosine (C), and thymine (T), whereas in ribonucleic acid (RNA) A, G, C and uracil (U) in place of T [1].

1.2 Structure of DNA and RNA

The structure of genomic DNA was firstly revealed by Watson and Crick in 1953 [2]. According to their report, DNA has a helical structure composed of two antiparallel strands with H-bonded bases in the core and phosphate groups located outside of the helix. Forces that give stability to this so-called B-form DNA helical structure are base stacking (hydrophobic forces), H-bonding between bases, and ionic interactions. Watson-Crick base pairs were defined in this report for the first time as A base pairs with T and G base pairs with C. Base pairing is given in Figure 1.

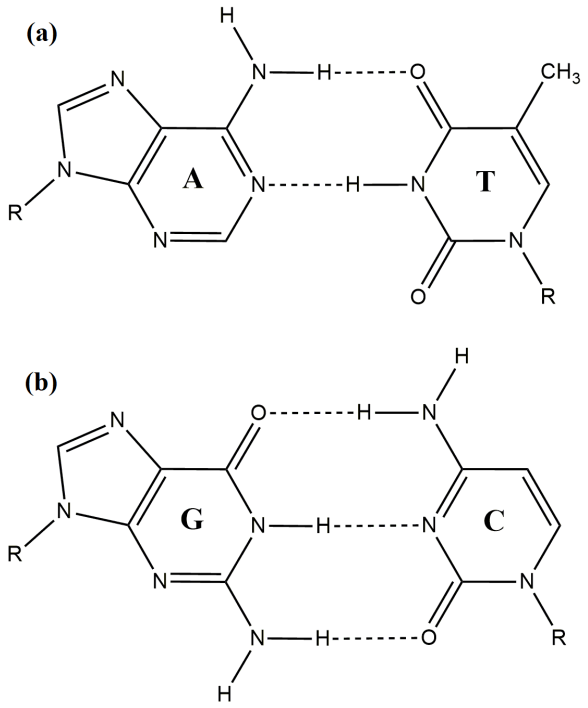

Figure 1. Watson-Crick base pairing. (a) A base pairs with T, (b) G base pairs with C. Dotted lines represent the H-bonding.

1.3 The Central Dogma

The Central Dogma, first stated by Francis Crick in 1958 [3], is an explanation of flow of information within the living organisms. Crick originally hypothesized that in all living cells, including human cells, the flow of information is from DNA to RNA to proteins. Even though, it was revised in 1970's by Crick, the Central Dogma of molecular biology is still valid today guiding many scientists [4].

Figure 2. The Central Dogma of Molecular Biology

The first process in the Central Dogma is the DNA replication. DNA replication is the process in which two identical DNA strands are produced in a semi-conservative way [5]. DNA is made up of two strands that are in opposite directions. These strands are separated during the replication process, and new daughter DNA strands are synthesized from the parent DNA molecule. DNA replication occurs in all living organisms and is the most critical element of biological inheritance. This process is also essential for cell division during damaged tissues' growth and repair mechanisms [2,6,7].

The transcription is the process of copying a region of DNA into an RNA molecule. The segments copied into messenger RNA (mRNA) are later utilized mostly to synthesize proteins. Other regions copied into RNA are called non-coding RNAs (ncRNAs). The transcription process has three stages; initiation, elongation, and termination [8].

The translation process is the event of decoding the genetic information found within the mRNA molecule to generate a specific sequence of amino acids in a polypeptide chain. Translational machinery reads the ribonucleotides in a series of nucleotide triplets (codons). One triplet encodes one specific amino acid. It occurs in the cytoplasm of the cell. Similar to the transcription process, translation has initiation, elongation, and termination steps [9–11].

1.3.1 Post-Transcriptional Modifications

At the end of the transcription process, immature mRNA (precursor mRNA, pre-mRNA) is produced. Post-transcriptional modifications are essential for the pre-mRNA's maturation, stability, and degradation. These modifications can be divided into three parts; splicing, 5'-capping, and polyadenylation [12,13].

1.3.1.1 Splicing

The process of removal of introns (non-coding sequences) and ligation of exons (coding sequences) in order is called constitutive splicing. Alternative splicing is the process that includes skipping specific exons and producing various forms of mature mRNA. This concept was first proposed in 1978 by Gilbert [14]. The mechanism explains the difference between the number of generated proteins and the number of protein-coding genes in humans [15].

The essential and fundamental role of alternative splicing in biological systems has been reported in the literature [16]. Higher eukaryote species have been shown to have a higher fraction of alternatively spliced genes, implying that the mechanism has played a significant role in evolution. Alternative splicing is involved in various biological events throughout an organism's existence [17]. Conserved and species-specific splicing is very critical in differentiation of species and genome evolution [18].

1.3.1.2 5'-Capping

After initiation of the transcription process, a 5' cap (also called RNA m^7G cap, RNA cap, or RNA 7-methylguanosine cap) is added to the first transcribed nucleotide, forming a 5'-5'-triphosphate bond. This cap contains a 7-methylguanosine (methylated guanosine at 7^{th} position) residue at the terminal position. 5'-capping is essential for the protection of mRNA from phosphatases and other nucleases at the terminal position. The process also acts as a promoter for initiating the translation event [19].

1.3.1.3 Polyadenylation

All eukaryotic and prokaryotic mRNAs have a long adenosine chain at their 3'- end that is synthesized by poly(A) polymerase (PAP) at the end of the transcription

process. This sequence contains about 200-250 repeats of adenosines and is called the poly(A) tail. The poly(A) tail is essential for nuclear transportation, mRNA stability, and translation process initiation [20,21]. Prokaryotic poly(A) tails are usually shorter than that of eukaryote's [22].

1.3.2 Targeting Poly(A) with Small Molecules

It has been reported that the poly(A) tails of mRNA may represent a tumor-specific target since the discovery of the overexpression of Neo-PAP, a human PAP, in human cancer cells, compared to normal cells [23–25]. Several molecules have been found to bind poly(A) with high affinity and selectivity (Figure 3) [25–28]. These molecules mostly have four fused six-membered rings and crescent shapes. For instance, coralyne (COR) and palmatine have dimethoxy groups, and berberine and sanguinarine have methylenedioxy groups. Stable self-structure formation is induced by coralyne and sanguinarine upon their binding to poly(A) [25,27].

The binding of coralyne and sanguinarine and self-structure formation of poly(A) is similar to that of poly(dA) upon binding of COR. The self-structure of poly(dA) formed in the presence of COR is an antiparallel duplex that is most stable under neutral pH conditions [29]. On the other hand, the parallel duplex structure of poly(A) is hemi-protonated and stable only under slightly acidic conditions [25].

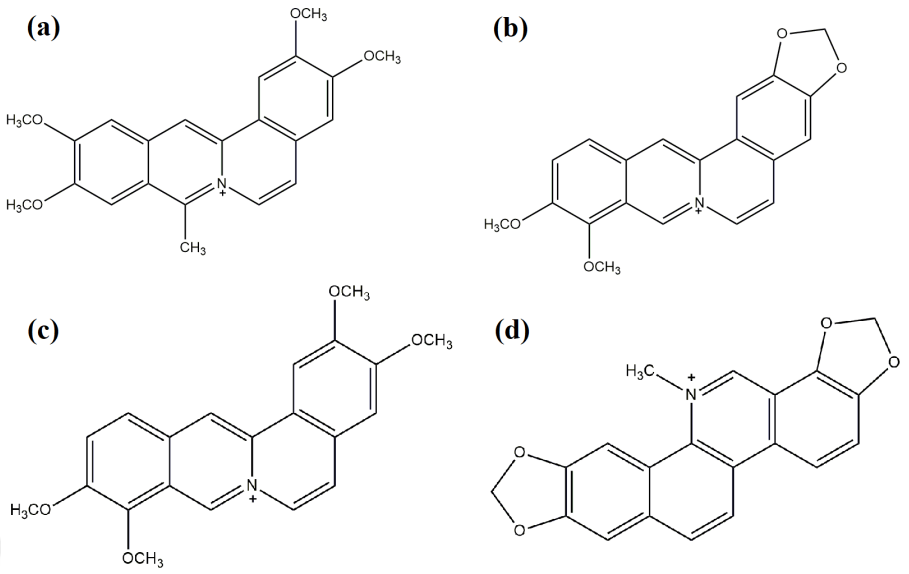

Figure 3. Chemical structures of (a) coralyne, (b) berberine, (c) palmatine, (d) sanguinarine.

1.3.2.1 Coralyne and Its Binding to Poly(A)

Coralyne (2,3,10,11-tetramethoxy-8-methylisoquinolino[2,1-b]isoquinolin-7-ium) is a proto-berbinium alkaloid, a class of isoquinoline alkaloid family related to the benzo[c]phenanthridines. A unique structural feature is present in this alkaloid which is a quaternized nitrogen atom at a bridgehead position in the tetracyclic fused ring system. COR has been reported to show significant antitumor activity against both P388 and L1210 leukemias in mice [30]. The activity together with relatively low toxicity has emerged an interest in this compound. The binding of COR to many nucleic acid structures was reported previously [31–34]. COR binds to triplexes more favorably than duplexes. The reason is that the shape of Pu-Py-Pu base triplets matches the shape of COR more closely than that of Watson-Crick base pairs. Also, COR binds preferentially to poly(dA) than Watson-Crick DNA [31]. The binding of COR to DNA triplexes occurs through intercalation [33,35]. Intercalators bind to nucleic acids by obeying the nearest neighbor exclusion principle. The binding of an intercalator between base pairs prohibits the binding of another intercalator between the next base pair, or neighboring binding site, according to this principle. The

reasons of an intercalating molecule to be unable to bind to a binding site that is already occupied by an intercalator are not known; it could be steric factors, changes in DNA structure caused by the first molecule's binding, electrostatic changes in DNA structure, or repulsion between two closely-placed intercalators. For the first time in 2005, Xing et al. reported that the COR binds preferentially and strongly to poly(A) and induces the formation of a duplex structure. Also, they determine the binding constant of COR to poly(A) at pH 7.0 as 1.8 x 10^{-6} M^{-1} [25]. After that, in 2009, Persil Çetinkol determined -by using a different method- that COR binds with the highest affinity to poly(A) among other poly(A) binding small molecules which were acquired [36]. According to their results, the binding affinity of COR to poly(A) was even higher. Then, several studies were conducted especially in sensor area by taking advantage of poly(A)-COR interactions [37–40]. All these works conducted under dilute aqueous conditions. Even though they are informative in thermodynamic and kinetic findings, they do not reflect the in vivo conditions in a complete and absolute manner.

1.4 Molecular Crowding

Various oligonucleotide technologies benefit significantly from quantitative data of nucleic acid interactions. The efficiency and stability of nucleic acid structures are determined by the strength of interbase H-bonding and base stacking. Hydration is also an important determinant of nucleic acid stability because water and cations are associated with polar purine and pyrimidine bases and the negatively charged phosphate backbone. The composition of the solution in which the nucleic acid is present significantly affects the dissociation or association of water molecules and ions, consequently, the base-pairing formation [41–44]. Watson-Crick base pairing stability has been studied extensively in dilute aqueous solutions containing salts [45–48]. According to the thermodynamic data obtained, accurate predictions could be made about the secondary structures of sequences [49–51]. The energy characteristics of oligonucleotide sequence design are crucial. In addition,

incorporating the chemical modification data helped improve the predictions for large RNA sequences. The prediction parameters found for RNA•DNA hybrid duplexes [46,52,53] can be utilized as a guideline for developing antisense DNA sequences as an example of mRNA targeting treatments employing antisense oligonucleotides.

Living cells are composed of several organelles, biomolecules, soluble and insoluble components [54–59]. Biomolecules occupy up to 40% of the cellular volume [60]. Cations are also present in cells, and they play important roles in regulating the biological functions of nucleic acids [43,61,62]. Crowded conditions of the cell significantly affect the activity coefficients and the chemical potentials of biomolecules due to the excluded volume effect. The physical properties such as viscosity, osmotic pressure, and dielectric constant differ for crowded and dilute solutions [59]. Hence, the stability and structure of biomolecules are different according to the changes in the physical properties of the environment.

1.5 Chromatin Structure

DNA is a heteropolymer that is both lengthy and strongly charged. It has one elementary negative charge per 0.17 nm of the double helix on average. The diameter of DNA is roughly 2 nm, yet the length of a stretched single molecule, depending on the organism, might be several dozens of centimeters [63]. The size of the DNA molecule in eukaryotes is substantially larger than the size of the DNA in viruses and bacteria [64].

DNA is organized in nucleoprotein particles called nucleosomes, which are only the first level of DNA packing. A nucleosome is a structure that has 147 base pairs wrapped around an octamer of histone proteins containing two copies of H2A, H2B, H3, and H4. These polynucleosomal arrays are seen as “beads on a string” with electron microscopy in which the string is the DNA, and the beads are nucleosomes [65]. Individual nucleosomes are distinguished by many characteristic properties.

For instance, the position of a nucleosome concerning the underlying genomic sequence impacts the accessibility of regulatory regions. Hence nucleosome's translational position can have a significant regulatory impact [63]. A chromatin is the structure whose repeating unit is nucleosome. The nucleosomal structure of chromatin is an effective packing strategy that allows chromosomal DNA to be densely packed and tightly condensed to the lowest level while maintaining full access to its specific regions for highly regulated expression [66].

Additionally, histones come in several isoforms that combine to generate a variety of octamers. They can also undergo multiple covalent modifications. Since the discovery of the nucleosome's fundamental structure in 1974, the importance of chromatin structure has been understood in many different functions, including recombination, transcription, cell cycle control, and cancer. Furthermore, although it is widely assumed that at least some parts of chromatin architecture are epigenetically inherited, this is not as well established as many believe [67].

1.6 Epigenetics

Epigenetics is a relatively recent field that refers to the regulation of gene expression without changes in the DNA sequence and with a heritable pattern during cell division. Progresses in this field were mainly made by using the data of normal and diseased tissues [68,69]. In fact, these modifications are reversible and play an essential role in the evolution of numerous disorders including neurodevelopmental disorders (multiple sclerosis, epilepsy, Parkinson's, Alzheimer's, and Huntington's diseases) [69,70], and autoimmune disorders (type 1 diabetes, lupus erythematosus, and rheumatoid arthritis) [71–73]. The main types of epigenetic modifications are DNA methylation, non-coding RNAs, and histone modifications.

1.6.1 DNA Methylation

DNA methylation involves the covalent attachment of a methyl group to the 5th carbon of cytosine (d5mC) via the catalysis of DNA methyltransferases (DNMTs) [74]. d5mC makes up 1% of the human genome's nucleic acids with the fact that the brain has some of the greatest levels of DNA methylation of any tissue in the body, [75]. A partial widening in the major groove and a partial narrowing in the minor grove provided by methyl groups are observed as a result of the methylation of cytosine residues. The sterically hindered methyl groups were positioned close to the phosphate backbone in the major groove. This situation is thought to limit the weak interactions of DNA with histone proteins. As interactions decrease, unpacking of the nucleosome becomes more manageable, and DNA becomes more accessible [76,77]. Moreover, due to the hydration of cytosines, the 3D structure of DNA recognition regions may be changed. With this chance, recognition of cytosines by polar groups in DNA-binding proteins might be highly affected [77,78]. DNA methylation predominantly occurs in CpG islands, which are cytosines preceding a guanine nucleotide. CpG islands are about 1000 bp long sections of DNA with a higher CpG density than the rest of the genome yet are frequently unmethylated [79]. Most of the CpG islands are initiation sites starts [80]. CpG islands appear to be conserved sequences to promote gene expression by regulating the structure of chromatins and binding of transcription factors. Nucleosomes are tiny, packed pieces of DNA that are wrapped around histone proteins on a regular basis. DNA becomes less permissive for gene expression as it becomes more closely bound with histone proteins. CpG islands have fewer nucleosomes than other DNA regions, which is one of its most distinguishing characteristics [81–83]. Very few of the CpG islands are methylated throughout embryonic development, resulting in transcriptional silencing of the associated genes. Methylation of CpGs is thought to have an essential role in regulating tissue-specific gene expression [84–88], X chromosome inactivation [89], silencing retroviral elements [90], and genomic imprinting [91–93].

1.6.2 Non-Coding RNAs

Non-coding transcribed regions, or non-coding RNAs, have been implicated as crucial participants in a variety of gene regulation mechanisms [94,95]. It was recently discovered that eukaryotic genomes transcribe up to 90% of genomic DNA, including a large number of RNAs with no coding ability, using second-generation sequencing methods such as RNA-Seq [96], tiling arrays [97,98] and whole transcriptome analyses [99]. Furthermore, these new technologies revealed that eukaryotic genomes are highly dynamic, with numerous structural changes emerging in normal cells, such as large deletions and insertions [100]. Until recently, it was considered that eukaryotic genomes contained just a small number of protein-coding genes (2-3%) and a few non-coding RNAs (ncRNAs) that functions in protein translation, such as ribosomal RNAs and transfer RNAs. Yet, many long ncRNAs related to chromatin modifications [101,102], small RNAs transcribed from promoter regions [103], and bidirectional promoters generating ncRNAs of various sizes [104,105] have recently been discovered. There has also been evidence of widespread transcription of repetitive sequences [106,107] and noncoding RNAs produced by mitochondrial DNA [108]. MicroRNAs (miRNAs), Piwi-interacting RNAs (piRNAs), small RNAs, and long or large RNAs (lncRNAs) are the types of ncRNAs with different functions [109].

1.6.3 Histone Modifications

Histone proteins, together with DNA, form the nucleosomes, the basic building blocks of chromatin. As the essential subunits of chromatin, nucleosomes, include octamers of histones H2A, H2B, H3, and H4, as described in section 1.5. And these proteins are among the most evolutionarily preserved proteins known [110,111]. In eukaryotic cells, this preservation reflects the invariant way that DNA is wrapped around the histone proteins [112]. Besides histone proteins, histone tails are hypothesized to interact with DNA and neighboring nucleosomes in a secondary and

more flexible manner, allowing for dynamic changes in the accessibility of the underlying genome [113]. Histones proteins are highly basic and abundant in lysine and arginine residues [114,115]. Post-transcriptional modifications (PTMs) of histones (methylation, acetylation, phosphorylation, and ubiquitylation) construct an epigenetic layer with DNA methylation [116–118], affecting gene transcription. Acetylation of histones at lysine residues is often linked with transcriptionally active genes, while lysine methylation, depending on the specific site and degree of methylation, causes gene activation or repression [116,117,119]. Changes in histone PTMs and their interactions with other nuclear proteins on gene promoter regions may result in very stable epigenetic modifications that affect chromatin structure. As a result, long-term gene expression dysregulation and disease progression may occur [120].

1.7 DNA-Protein Interactions

Protein recognition of DNA and particular interactions of these proteins with the nucleic acid bases of DNA are required for the basic functions of living cells such as growth, differentiation, maturation, and so on. The complicated interplay of non-covalent contacts is at the heart of biomolecular recognition. These include canonical hydrogen bonds, electrostatic and van der Waals interactions, as well as non-canonical interactions such as cation–π interactions, CH–π interactions, and π–π stacking. Many of these non-covalent interactions guide the recognition principles of protein–protein and protein–DNA interfaces. The cation–π interactions are found to be operational between a side chain carrying a positive charge, such as arginine (Arg), lysine (Lys), or a side chain carrying a partial charge, such as asparagine (Asn) or glutamine (Gln), and a π system, among the non-canonical interactions. The π system might be a nucleic acid base or an aromatic ring of phenylalanine (Phe), tyrosine (Tyr), tryptophan (Trp), or histidine (His) [121]. Many ligand–receptor interactions in proteins are recognized by cation – π interactions [122]. Cation – π interactions, π – π stacking, and hydrogen bonds were discovered as molecular

determinants of ATP binding in proteins [123]. The presence of the cation – π interaction between a divalent cation like Mg^{2+} and DNA bases has previously been demonstrated [124]. The cation – π interaction has been identified as having a role in the specificity and stability of the protein – DNA interface [125,126]. H2A, H2B, H3 and H4 are small, positively charged proteins. Because the phosphate groups in DNA's sugar-phosphate backbone are negatively charged, histone proteins bind to DNA very tightly [111].

1.8 Purpose of the Study

The first part of this thesis focuses on revealing the effects of molecular crowding on poly(A) double helical structures in the presence of COR.

It is known that both DNA and RNA can transform into unusual nucleic acid structures that can act as switches that respond to parameters such as temperature, pH, ions, and small molecules [127–132]. RNA is similarly known to form more diverse, higher-order structures, including the homopolymer duplex formed by poly(rA), first described by Rich, Davies, Crick, and Watson [133]. The long poly(A) tail is an important determinant of mRNA stability and maturation and is required for translation initiation [20,21]. Poly(A) polymerase (PAP) catalyzes the synthesis of poly(A) participates in an endonucleolytic cleavage step and is a key factor in the polyadenylation of the 3'-end of mRNA. Neo-PAP, a human PAP, is significantly overexpressed in human cancer cells compared to its expression in normal or virally transformed cells [23] and may represent a tumor-specific target. Drugs that can recognize and bind to single-stranded A-rich regions of mRNA may interfere with the full processing of mRNA by PAP and represent a new type of potential therapeutic agent.

Despite many studies examining the interactions of small molecules with nucleic acids, little is known about the recognition of single-stranded, A-rich RNAs by small molecules. Depending on solution conditions such as pH, salt, and temperature,

poly(A) can adopt a parallel double-stranded conformation created by the involvement of adenine bases at the N1 position [133–136]. The formation of such structures has strengthened the hypothesis of the existence of double-stranded poly(A) in eukaryotic cells. The termination of the polyadenylation process is thought to occur with the formation of the double-stranded poly(A) structure [137]. Therefore, the transition of poly(A) from a single-stranded to a double-stranded structure is of great importance for nucleic acids in terms of the structure-function relationship. Small molecules that can bind strongly to double-stranded poly(A) may be an opportunity to modulate double-stranded poly(A) and nucleic acid structure-function relationships of single-stranded poly(A). It was reported in the studies of Giri and Kumar in 2008 [138] as well as Xing et al. in 2005 [139] that COR binds to poly(A) and stabilizes the resulting double helix structure. In these studies, the stoichiometry of the binding was determined as four nucleotides per one coralyne molecule. Moreover, thermodynamic parameters showed that the binding is exothermic and both enthalpy and entropy driven, typically intercalative binding. The ability of this alkaloid to interpolate and stabilize the double helical structure of poly(A) has made it clear that this alkaloid will be an important agent for its therapeutic potential. Coralyne's therapeutic potential is also enhanced by its binding to other nucleic acids. It has been proven by studies that Coralyne binds T*A•T triple helices, transforms duplex poly(dT)•poly(dA) into triplex poly(dT)*poly(dA)•poly(dT) and stabilizes triplex structures [33,140–142]. However, all these studies were carried out using very dilute solutions prepared in vitro. The existence of these structures and how their formation mechanisms will respond in case of molecular crowding, similar to intracellular conditions, have not been studied before and are not available in the literature. It has a great importance to examine the double helix structure formed by poly(A), which acts as a key factor in gene expression, in the presence of molecular crowding, apart from in dilute aqueous vitro studies. Consequently, we aimed to design crowded environments for the formation of self-structure of poly(A) in the presence of COR by using

polyethylene glycol (PEG, MW 200), sucrose and glycerol (Figure 4) as crowding agents.

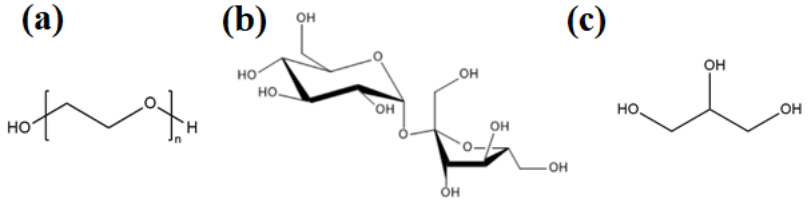

Figure 4. Chemical structures of (a) PEG, (b) sucrose and (c) glycerol.

The second part of this thesis focuses on the effects of DNA methylation on DNA-amino acid interactions.

In eukaryotic cells, DNA is packaged into a structure called a nucleosome. This structure acts as a barrier that prevents or enables replication, transcription, and repair. For DNA in the nucleosome to become available, nucleosome stability must be reduced. Studies have shown that the more flexible nature of DNA, the stronger the attachment of histone proteins to the structure formed [74]. The formation of 5-methylcytosine can prevent alterations in the 3D structure. The methyl group gets close to the phosphodiester bonds and prevent structural changes [77], reduce DNA flexibility and nucleosome stability, prevent transcription activators from binding to promoters and ensure gene regulation by binding their repressors, and as a result, it can cause gene silencing [76].

It is known that DNA-protein interactions depend on the degree of methylation of DNA, but the mechanisms by which proteins recognize and bind to DNA are not yet fully understood. The first observed results of the studies are the effects of cytosine modifications on the geometry, dynamics and thermal stability of the DNA helix. It was understood by observing the increase in melting temperatures of long DNA helix structures that cytosine modifications stabilize the DNA helix. However, in shorter

DNA helix structures, smaller changes were observed as the result of modifications. In the thermal denaturation temperatures of these double helical structures, only a few degrees of temperature increase was observed as a result of methylation, depending on the sequence [143]. It is thought that possible causes of thermal stability resulting from modifications may be due to changes in enthalpy, entropy or Gibbs free energy [144]. The smallest change in Gibbs free energy (hence the DNA melting temperature) may be the result of large changes in enthalpy and entropy. For this reason, observing the change in the thermodynamic properties of DNA by methylation will give better results than observing the change in thermal stability alone [143]. With this thesis, we created a model system in order to follow the effects of DNA methylation on interactions of Dickerson Dodecamer with positively charged amino acids, Lys and Arg (Figure 4). We aimed to observe the alterations in the thermal stability of DDD and methylated DDD (DDD8) upon their interactions with Lys and Arg.

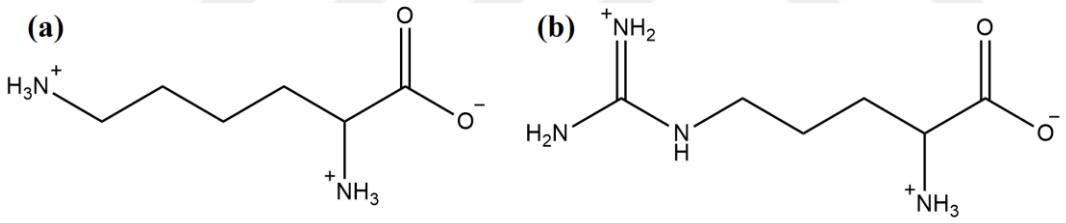

Figure 5. Chemical structures of (a) lysine and (b) arginine.

CHAPTER 2

MATERIALS AND METHODS

2.1 Investigating the Interactions of Poly(A)-COR in Crowded Environments

2.1.1 Sample Preparation

The poly(A) sequence used in the experiments was purchased from Boehringer Mannheim (West Germany) and Coralyne Chloride ($C_{22}H_{22}ClNO_4$, COR) was purchased from Sigma Aldrich (USA). The concentration of the stock solution of poly(A) was calculated by UV-vis absorption spectroscopy using the molar extinction coefficient poly(A); ε_{258} = 9800 M^{-1} cm^{-1} $nucleotide^{-1}$ [25]. COR stock solution was prepared in Millipore water, and its concentration was determined by UV-vis spectroscopy using the molar extinction coefficient value of ε_{420} = 14500 M^{-1} cm^{-1}. All of the samples contained 1X BPE buffer with 20 mM NaCl salt at pH 7.0 [36]. The buffer and salt solutions preparations were described in Appendix A. Concentration of poly(A) was 30.0 μM in all samples. For the samples containing COR, poly(A):COR ratio of 4:1 (nucleotide:molecule) was used, hence the concentration of COR in these samples was 7.5 μM. PEG200, sucrose, and glycerol were purchased from Sigma Aldrich (St. Louis, MO, USA). 60 % (w/v) stock solutions of PEG200, sucrose, and glycerol were prepared, and required amounts were added to samples to reach the desired concentrations of crowding agents.

2.1.2 UV-Vis and CD Absorption Experiments

UV-Vis and CD absorption experiments were performed via UV-vis absorption spectroscopy (Agilent Technologies Cary 8454) and CD spectroscopy (JASCO J-1500 spectropolarimeter) with CTU-100 Circulating Thermostat Unit. UV-Vis absorption spectra of the samples were collected between 190 nm and 800 nm. CD spectra of the samples were collected between 200 nm and 400 nm at 5°C and 15°C.

2.1.3 UV-Vis Thermal Denaturation Experiments

Thermal denaturation experiments were performed via UV-vis absorption spectroscopy (Agilent Technologies Cary 8454) with Peltier Temperature Control Unit. The UV-Vis thermal denaturation experiments were carried out by changing the temperature between 15°C and 95°C with 2°C/min increments. Thermal denaturation experiments were performed for all of the samples whose descriptions were given in section 2.1.1. Igor Pro software was used for the data analysis.

2.1.4 Fluorescence Experiments

COR itself is a fluorescent molecule, and fluorescence experiments were performed with the samples containing COR. The parameters for the fluorescence measurements were: Emission spectra were collected from 425 to 650 nm, the excitation wavelength was 420 nm, excitation and emission slits: 5.0 nm and 5.0 nm, operation 600 V, scan rate 600 nm/min.

2.2 Investigating the Effects of DNA Methylation on DDD-Lysine and DDD-Arginine Interactions

2.2.1 Sample Preparation

The Dickerson Dodecamer (DDD) and the methylated Dickerson Dodecamer (DDD8) sequences used in these experiments were purchased from Integrated DNA Technologies (IDT, Leuven, Belgium). DDD and DDD8 sequences are given in Appendix C. The concentrations of stock solutions of DDD and DDD8 were calculated with UV-Vis absorption spectroscopy by using the molar extinction coefficients DDD; ε_{260}=110700 M^{-1} cm^{-1} and DDD8; ε_{260}=103900 M^{-1} cm^{-1}. In order to ensure that the secondary structures of DDD and DDD8 were correct, each oligonucleotide was heated at 95°C for 3 minutes and allowed to cool to room temperature overnight. L-Arginine monohydrochloride ($C_6H_{14}N_4O_2$.HCl) and L-Lysine monohydrochloride ($C_6H_{14}N_2O_2$.HCl) were purchased from Alfa Aesar, ThermoFisher (Kandel, Germany). All of the samples were prepared in 1X BPE buffer with 185 mM NaCl salt at pH 7.0. The preparations of the buffer, salt, and amino acid stock solutions were described in Appendix A. Concentrations of DDD and DDD8 were 30.0 μM (base pair) in all samples. Concentrations of amino acids in samples were given in figure legends.

2.2.2 UV-Vis and CD Absorption and Thermal Denaturation Experiments

Absorption experiments were performed via UV-Vis absorption spectroscopy (JASCO V-730 spectrophotometer) and CD spectroscopy (JASCO J-815 spectropolarimeter). The UV-Vis thermal denaturation experiments were carried out by varying the temperature between 15°C and 85°C with 1°C/min increments. Thermal denaturation experiments were performed for all of the samples described

in section 2.2.1. Data obtained during thermal denaturation experiments were analyzed by using Igor Pro software.

CHAPTER 3

RESULTS AND DISCUSSION

3.1 Investigating the Interactions of Poly(A)-COR in Crowded Environments

3.1.1 UV-Vis Absorption and Circular Dichroism Measurements

UV-Vis absorption spectra are usually used for demonstrating the binding of ligands to nucleic acids. As COR binds to poly(A), a redshift is observed in the UV-Vis absorption peaks of the COR due to the π-π stacking of the COR with the adenine bases [25,145–148]. Figure 6 shows the UV-Vis absorption spectra of poly(A) in the absence and presence of COR. In Figure 6, the green line represents COR, and the red line represents poly(A). The addition of COR to the poly(A) sample is represented with the blue line. As can be followed with the red line, poly(A) exhibits absorption maxima at 260 nm. COR has several peaks in the UV-Vis range. Yet, its peaks between 400 and 450 nm becomes more distinct upon addition of COR to poly(A).

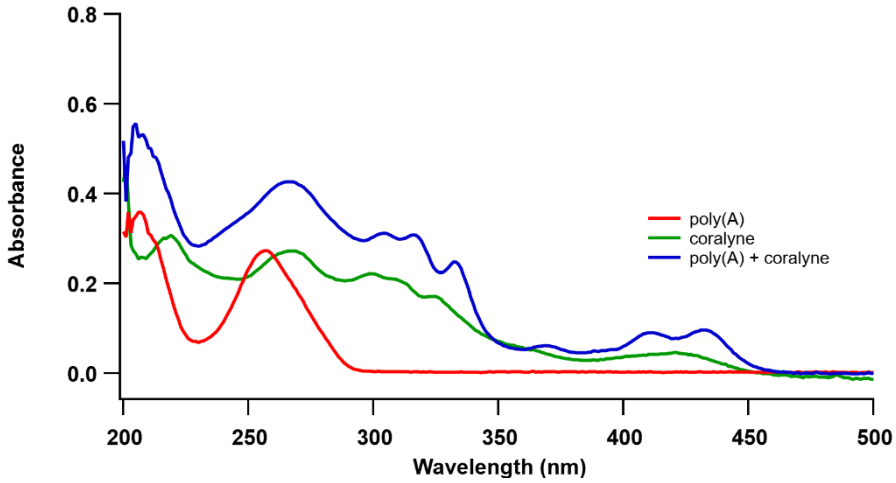

Figure 6. UV-Vis absorption spectra of poly(A), COR and poly(A) + COR samples.

Similarly, Circular Dichroism Spectroscopy is widely used in investigating small molecule-nucleic acid interactions [149,150]. Its working principle is based on the differential absorption of left and right circularly polarized light. Optically active chiral molecules such as nucleic acids will preferentially absorb one direction of the circularly polarized light. Then, the difference between the absorption of the left and right polarized light is measured. CD is generally measured in ellipticity (θ), with units of millidegrees (mdeg). Since COR is an achiral molecule, it does not give rise to a particular CD signal. However, the presence of interactions between an achiral molecule and nucleic acids can induce chirality in the small molecule's structure, resulting in the formation of a new CD band. Induced CD bands, between 290 and 350 nm, can be seen only upon binding of COR to poly(A) [25,36]. Therefore, these bands can be followed in assessing poly(A)-COR interactions. In figure 7, the green line represents the COR, and the red line represents poly(A). The addition of COR to poly(A) demonstrated by the blue line results in the appearance of induced CD bands between 290 nm and 350 nm. With the appearance of these induced CD bands, it is confirmed that COR binds to the chiral environment of poly(A). Also, the characteristic CD spectrum of poly(A) did not change upon addition of COR [36,139]. CD bands belonging to poly(A) are observed at 264 nm, 248 nm, 220 nm, and 205 nm. Intensities of the two maxima at 264 nm and 220 nm were determined as 17.8 mdeg and 7.25 mdeg, respectively. With the addition of COR to poly(A), intensities of these maximum points decreased to 10.25 mdeg and

3.32 mdeg, respectively. Also, ellipticity value on the minimum point at 248 nm was -12.63 mdeg. Adding COR to the poly(A) was resulted in a decrease in the ellipticity to -7.17 mdeg. Reports in the literature indicates similar changes in CD spectra with the addition of COR to poly(A) [25,36].

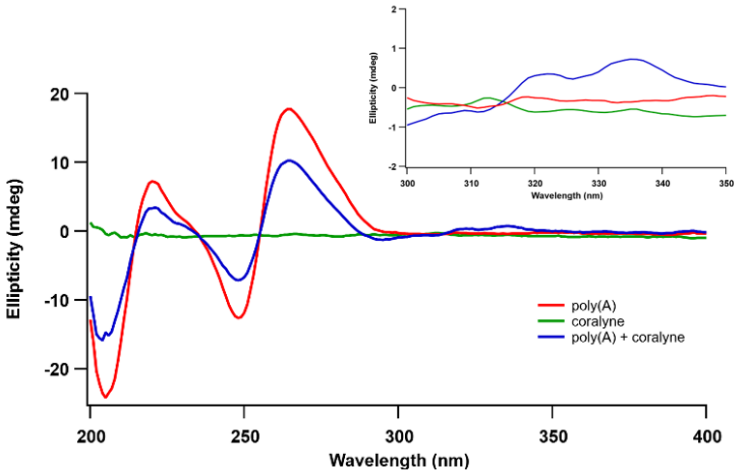

Figure 7. CD Spectra of poly(A) and COR samples. The inside spectra were obtained by expanding the wavelength range from 300 nm to 350 nm.

In order to understand the effect of molecular crowding, poly(A) + COR samples with varying concentrations of PEG were prepared. The change in UV-Vis absorption spectra upon addition of different concentrations of PEG onto poly(A) + COR can be observed in Figure 8. With the addition of increasing concentrations of PEG, a gradual increase in the absorbance of poly(A) at 260 nm was observed mainly due to absorbance of PEG [151]. No other significant change was observed in the UV-Vis spectrum of poly(A) + COR upon addition of PEG. CD spectra of the same samples are given in Figure 9. As the concentration of PEG is increased, a gradual increase in the CD spectra of the samples at around 340 nm is observed. Poly(A) maintained its characteristic spectrum in the presence of both COR and PEG. The maximum point at 220 nm which belongs to poly(A) + COR sample (the red line) has the ellipticity value of 3.45 mdeg. With the addition of 5% PEG to this sample (the yellow line), ellipticity decreased to 2.28 mdeg. On the other hand, addition of

10% (the green line) and 20% (the blue line) PEG to poly(A) + COR sample resulted in increases in the ellipticity values to 5.53 mdeg and 13.71 mdeg, respectively. In addition, 2 nm shift in the wavelength of maximum absorbance to 218 nm was observed in the spectra of both poly(A) + COR + 5% PEG and 10% PEG. The greatest change in the ellipticity upon addition of PEG was seen at this wavelength. Moreover, the minima at 248 nm of poly(A) + COR sample has the ellipticity value of -7.17 mdeg. With the addition of 5%, 10% and 20% PEG, the ellipticity was lowered to -3.81 mdeg, -3.38 mdeg and -6.39 mdeg, respectively. Addition of PEG was resulted in the 1 nm wavelength shift to 249 nm for all three samples. Furthermore, the poly(A) + COR sample has another maximum point at 264 nm with ellipticity of 10.26 mdeg. 5% and 10% PEG containing samples have decreased ellipticities of 4.61 mdeg without a shift in that wavelength. Addition of 20% PEG shifted the wavelength of the maxima to 265 nm and resulted in the ellipticity value of 6.32 mdeg. Induced CD peaks of poly(A) + COR sample were increased with the addition of increasing concentrations of PEG. Between 260 nm and 360 nm, induced CD bands were observed due to the binding of COR to the chiral environment of poly(A). At 322 nm, ellipticity of poly(A) + COR sample was determined as 0.37 mdeg and at 335 nm, it was 0.73 mdeg. Addition of increasing concentrations of PEG gradually raised the ellipticity values at both wavelengths. Ellipticity values were increased to 1.10 mdeg and 1.51 mdeg with the addition of 5% PEG, to 1.42 mdeg and 2.10 mdeg with the addition of 10% PEG and to 3.06 and 4.51 mdeg with the addition of 20% PEG, at 322 nm and 335 nm, respectively for all of the samples. The intensity in the CD spectrum increased the most with the addition of 20% PEG at around 325 nm.

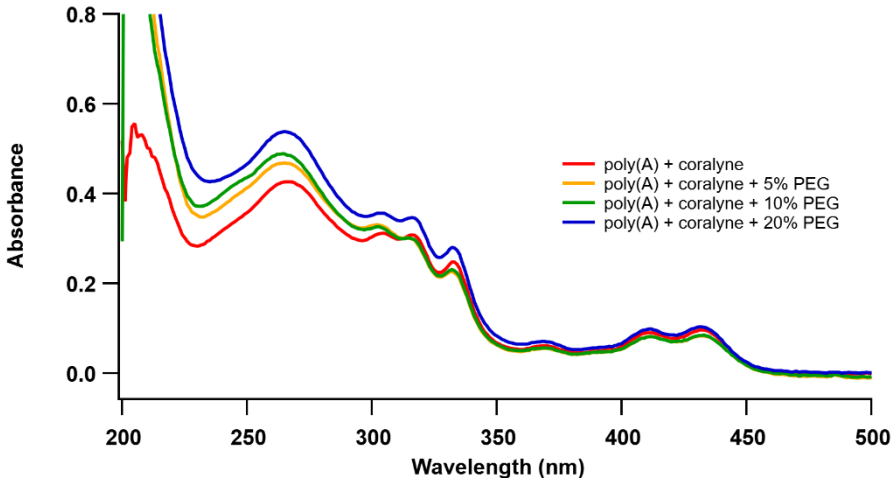

Figure 8. Change in UV-Vis absorption spectra of poly(A) + COR sample upon addition of different concentrations of PEG.

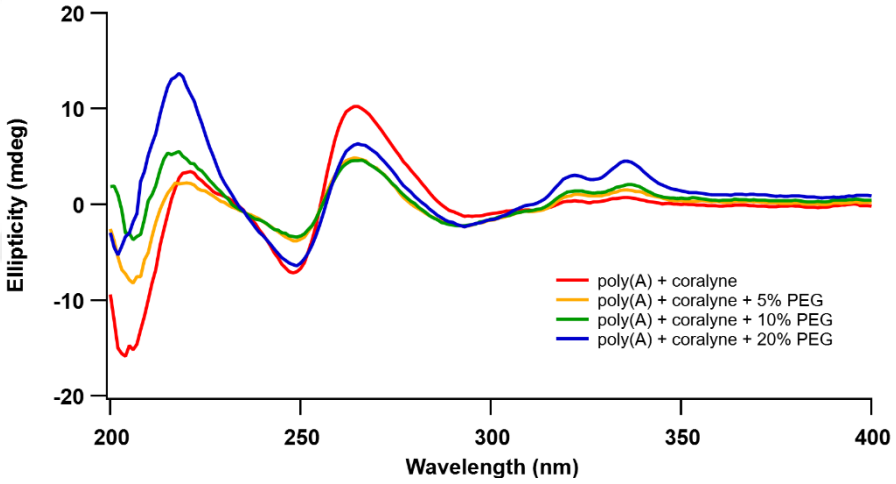

Figure 9. Change in CD spectra of poly(A) + COR sample upon addition of different concentrations of PEG.

In Figure 10, a change in UV-Vis absorption spectra upon addition of different crowding agents to poly(A) + COR is shown. Poly(A) sample containing COR was represented with the red line. Green, yellow and blue lines represent the addition of 20% PEG, sucrose, and glycerol, respectively. The addition of crowding agents increases the absorption of poly(A) at 260 nm. The most significant increase was observed with the addition of 20% sucrose to the poly(A) + COR sample. Figure 11

shows the change in CD spectra upon addition of different crowding agents to the poly(A) + COR sample. Again, the poly(A) sample containing COR represented by the red line. As seen in the spectra, poly(A) kept its characteristic spectrum due to the addition of crowding agents. At 200 nm, the maximum point of poly(A) + COR sample has an ellipticity value of 3.64 mdeg. Addition of sucrose (the yellow line) and glycerol (the blue line) decreased the intensity of the CD peaks to 2.33 mdeg and 1.21 mdeg, respectively with 2 nm shift in the wavelength to 222 nm. On the other hand, the addition of PEG (the green line) significantly increased the ellipticity to 13.88 mdeg. The ellipticity minima at 248 nm of the poly(A) + COR is -7.59 mdeg. With the addition of 20% PEG and glycerol to this sample, intensity decreased to -6.72 mdeg and -7.03 mdeg while addition of sucrose raised it to -8.72 mdeg without a shift in the wavelength. Another maxima, at 264 nm, was observed in the spectrum of the poly(A) + COR sample with an ellipticity of 11.19 mdeg. Addition of crowding agents was resulted in the following decreased ellipticity values; 7.04 mdeg with PEG, 10.84 mdeg with sucrose, and 7.57 mdeg with glycerol. The greatest decrease was observed with the addition of PEG where sucrose had the lowest effect on the intensity. Induced CD peaks of poly(A) + COR sample at 322 nm and 336 nm have the ellipticities of 0.55 mdeg and 0.62 mdeg, respectively. Ellipticity values were raised to 3.00 mdeg and 4.43 mdeg with the addition of PEG, to 1.12 mdeg and 2.02 mdeg with sucrose and to 2.27 and 3.57 mdeg with glycerol, at 322 nm and 336 nm, respectively for all of the samples. It can be seen in the spectra that the lowest effect was obtained with the addition of 20% sucrose. The CD profile of the sample containing sucrose is very similar to that of poly(A) + COR. In fact, even the induced peaks are very weak. Furthermore, the peak associated with the binding of COR to poly(A) at around 325 nm was observed in each spectrum. With the addition of 20% PEG to poly(A) + COR sample, the intensity was increased the most among the addition of crowding agents. These results indicate that the addition of PEG alters the nucleic acid structure and affects interactions of poly(A) with COR more than sucrose and glycerol.

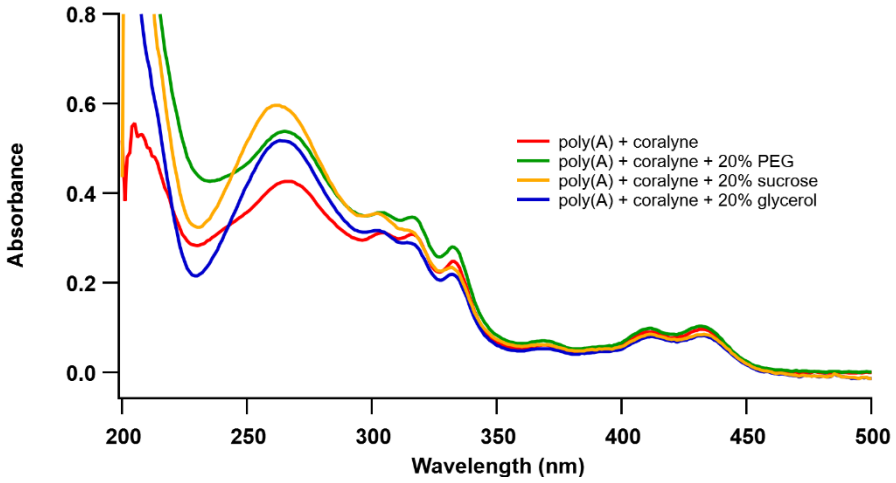

Figure 10. Change in UV-Vis absorption spectra of poly(A) + COR sample upon addition of crowding agents.

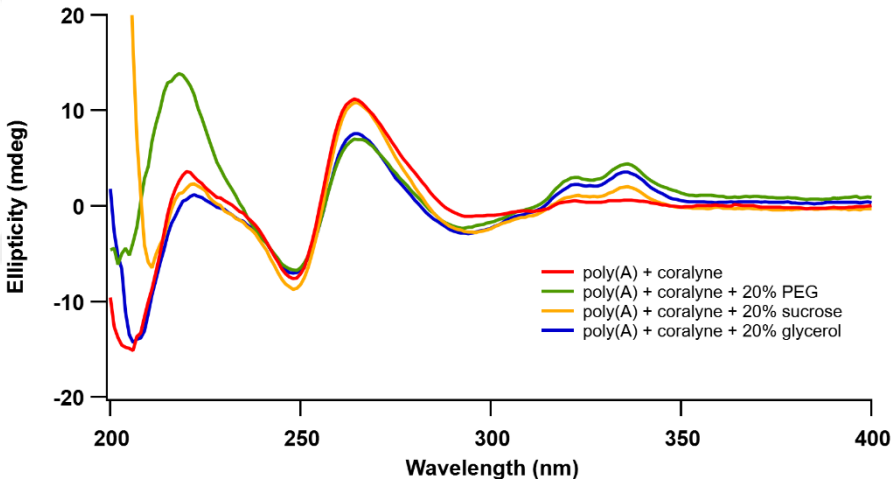

Figure 11. Change in CD spectra of poly(A) + COR sample upon addition of different crowding agents.

3.1.2 UV-Vis Thermal Denaturation Experiments

Thermal denaturation (melting) is a commonly used method performed by breaking the base stacking interactions and hydrogen bonds via heating to observe and determine the nucleic acid's stability via melting temperature (T_m) determination. An increase in the T_m indicates the increase in the thermal stability of the nucleic acid structure. In this part of the study, we aimed to demonstrate the effects of crowding

agents on the thermal stability of poly(A) double-helical structure, which is formed in the presence of COR.

In practice, poly(A) does not have a thermal denaturation profile since its structure is a random coil. However, with the intercalation of the COR, it forms a double-stranded helical structure [36,139]. Figure 12 demonstrates the thermal denaturation of poly(A) in the absence of COR. Red and blue lines represent the heating and cooling curves, respectively. As expected, the profile, due to the unstacking of the random coil poly(A) structure, was not suitable to determine a melting temperature for this sample. On the other hand, in Figures 13 and 14, a broad melting profile was observed with the addition of COR to poly(A). The red and blue lines represent the heating and cooling curves in both figures, respectively. Thermal profiles were also performed at 420 nm, where the absorption of COR occurs. From Figure 13, T_m was determined as 81°C (melt at 260 nm). From Figure 14, it was determined as 85°C (melt at 420 nm) using the normalized absorbance values.

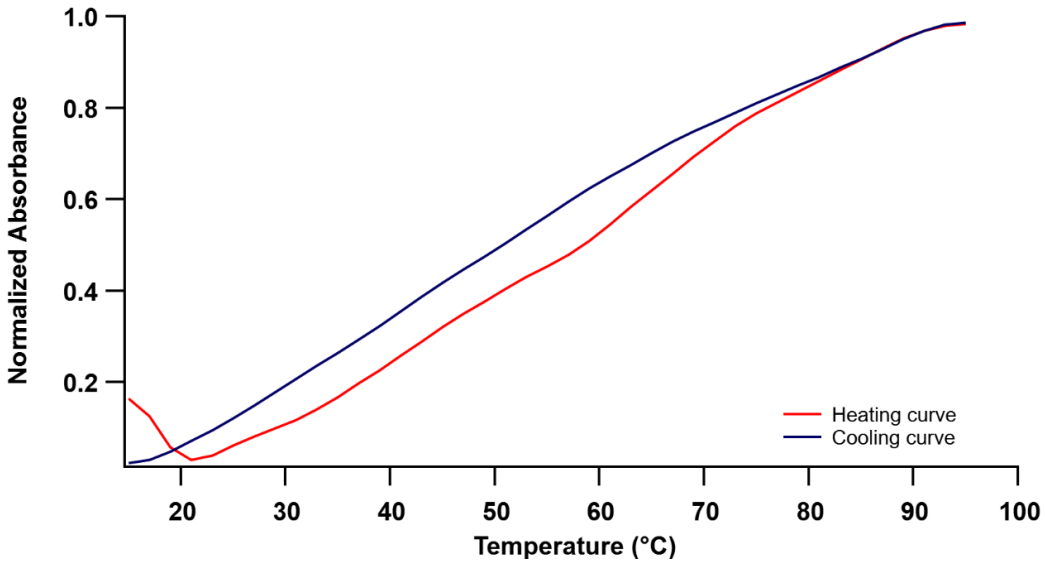

Figure 12. UV-Vis thermal denaturation profiles of 30.0 μM poly(A) at 260 nm.

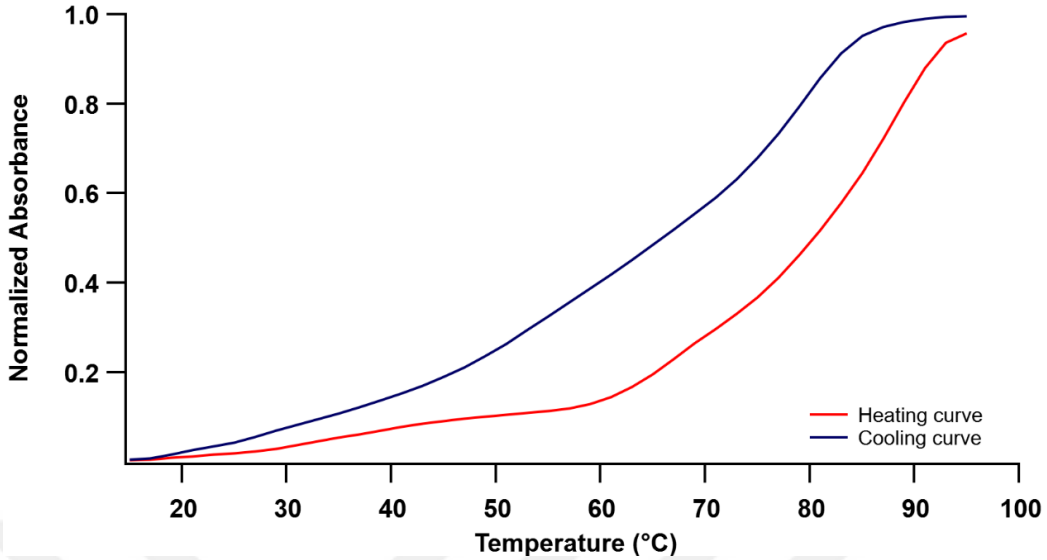

Figure 13. UV-Vis thermal denaturation profiles of 30.0 μM poly(A) in the presence of 7.5 μM COR at 260 nm.

The comparison of the melting curves of poly(A) in the absence and presence of COR can be seen in Figure 15. The green line represents poly(A) in the absence of COR, and the blue line represents poly(A) in the presence of COR. Change in the thermal denaturation profile of the poly(A) indicates the intercalation of COR to the poly(A) followed by the formation of the double-helical structure [36,139].

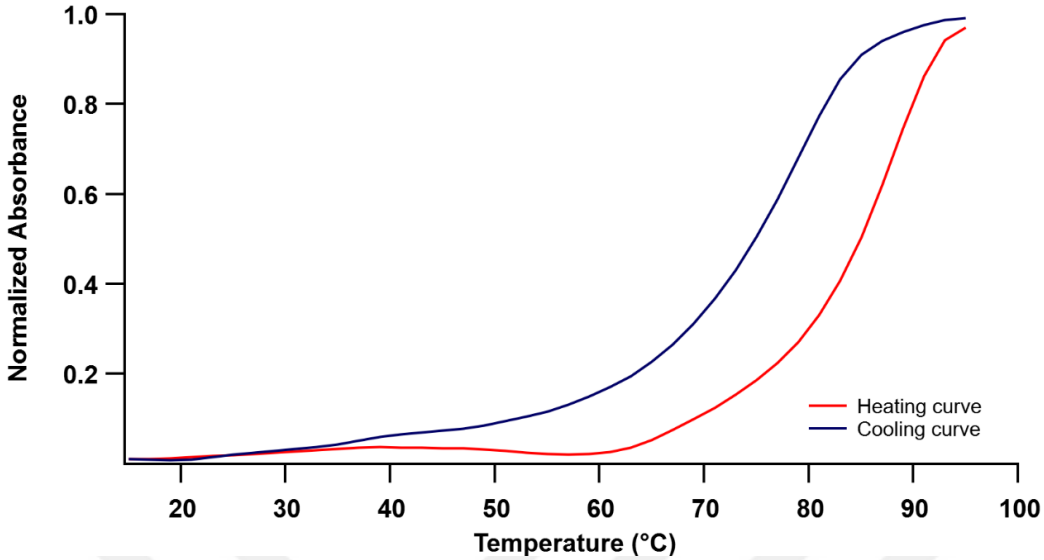

Figure 14. UV-Vis thermal denaturation profiles of 30.0 µM poly(A) in the presence of 7.5 µM COR at 420 nm.

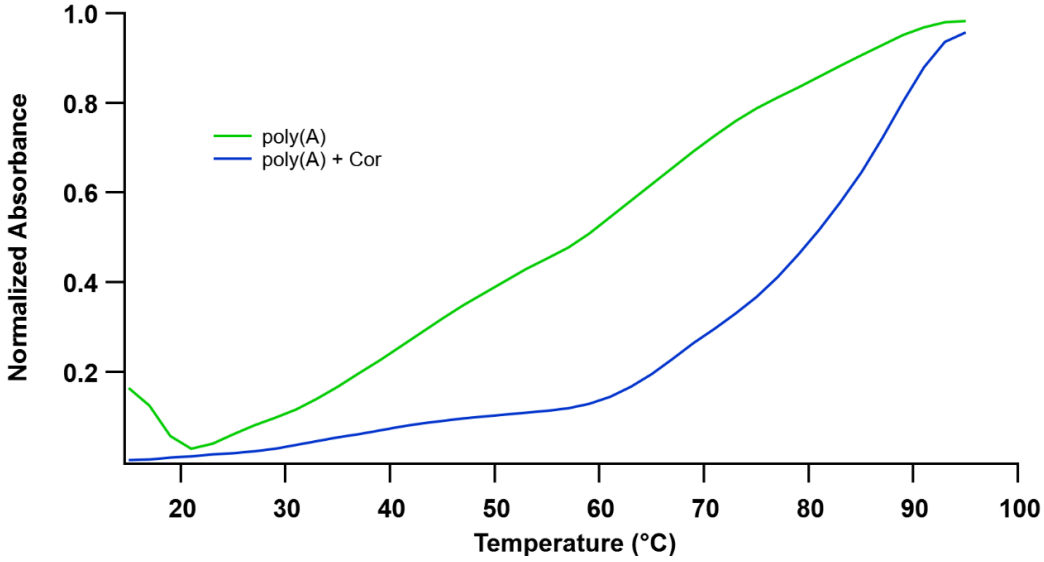

Figure 15. Change in thermal denaturation profile of poly(A) upon addition of COR at 260 nm.

Figures 16 and 17 display the thermal denaturation profiles of poly(A) + COR after the addition of 5% PEG to poly(A) at 260 nm and 420 nm, respectively. As can be seen, samples maintain to have a thermal denaturation profile. Melting temperatures

determined for these samples were 72°C and 75°C using the absorbance change at 260 nm and 420 nm, respectively. The change in the T_m represents the change in the stability of poly(A) self-structure. The decrease in the stability is due to the more crowded medium, 5% PEG. The presence of the PEG reduces the water activity and decreases the melting temperature and, consequently, stability [152,153]. It is noted that the self-structure still occurs in the presence of 5% PEG since the melting profile was obtained during thermal denaturation.

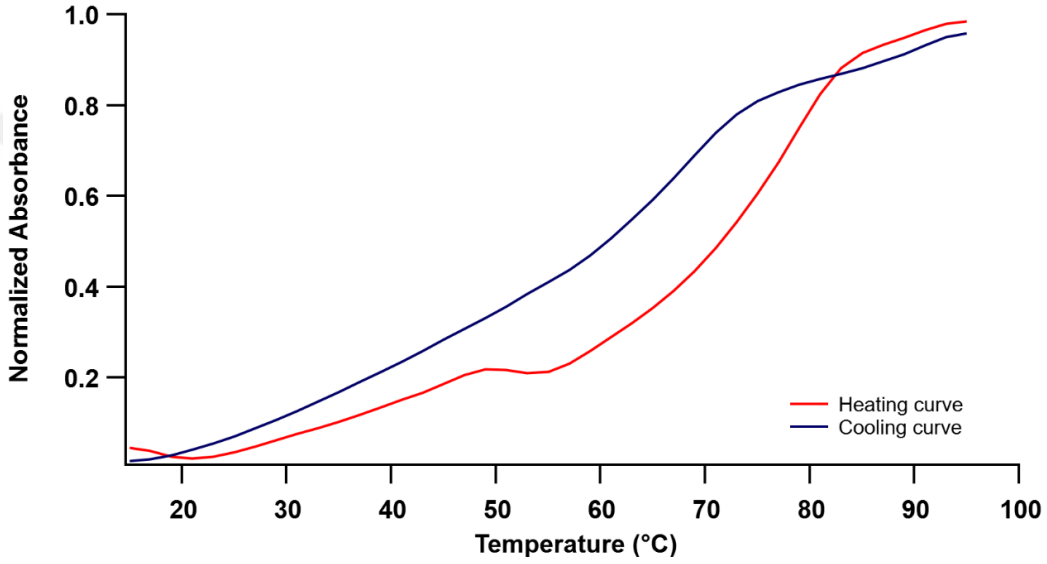

Figure 16. UV-Vis thermal denaturation profiles of 30.0 µM poly(A) in the presence of 7.5 µM COR and 5% PEG at 260 nm.

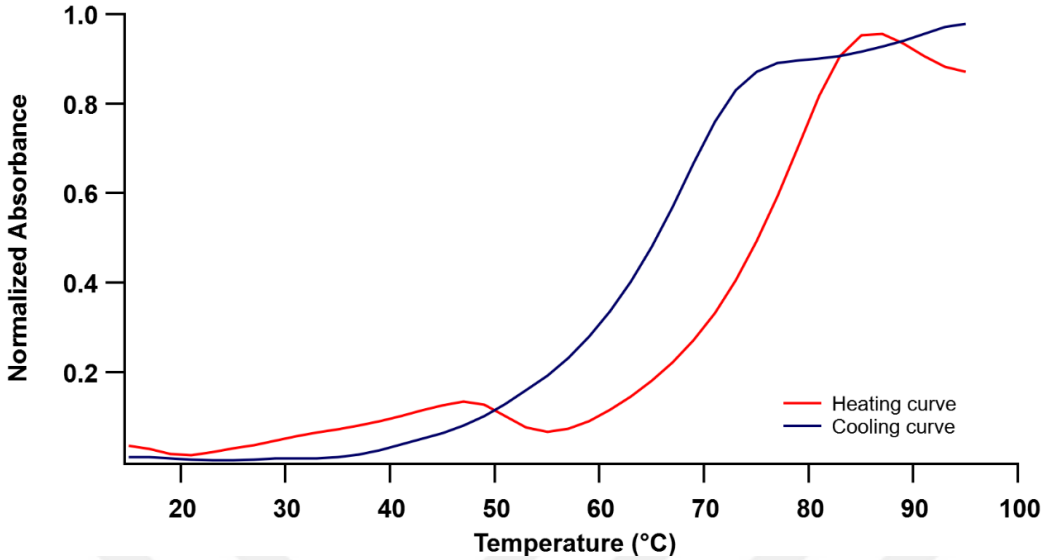

Figure 17. UV-Vis thermal denaturation profiles of 30.0 µM poly(A) in the presence of 7.5 µM COR and 5% PEG at 420 nm.

T_m of the sample poly(A) + COR is further decreased in the presence of 10% PEG and reached to 65°C at 260 nm. The addition of PEG has resulted in a decrease in the thermal stability of the self-structure of poly(A). Figures 18 and 19 represent the thermal denaturation profiles of poly(A) + COR + 10% PEG sample at 260 nm and 420 nm, respectively. As observed, increasing the crowding agent concentration clearly resulted in a decrease in the T_m and stability.

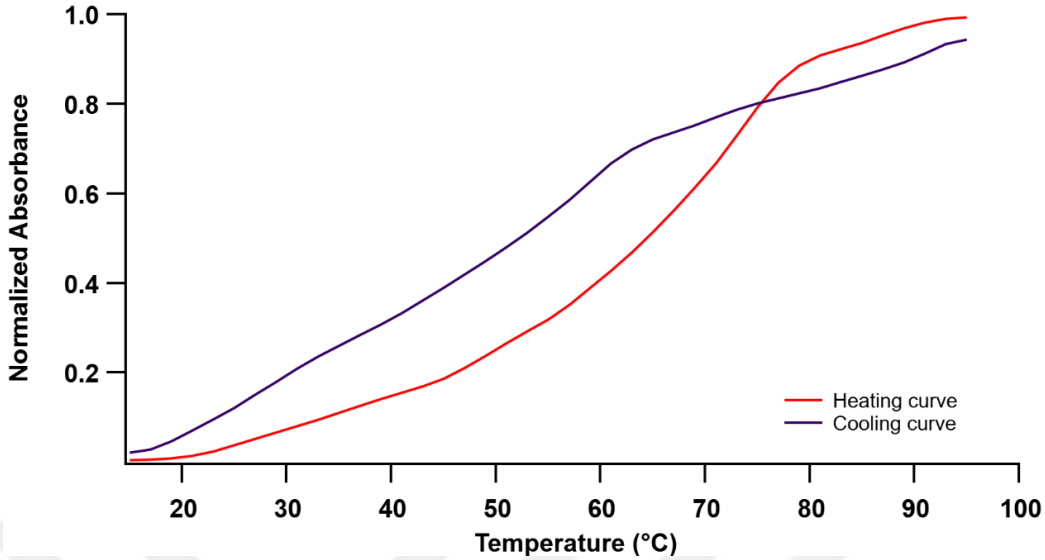

Figure 18. UV-Vis thermal denaturation profiles of 30.0 µM poly(A) in the presence of 7.5 µM COR and 10% PEG at 260 nm.

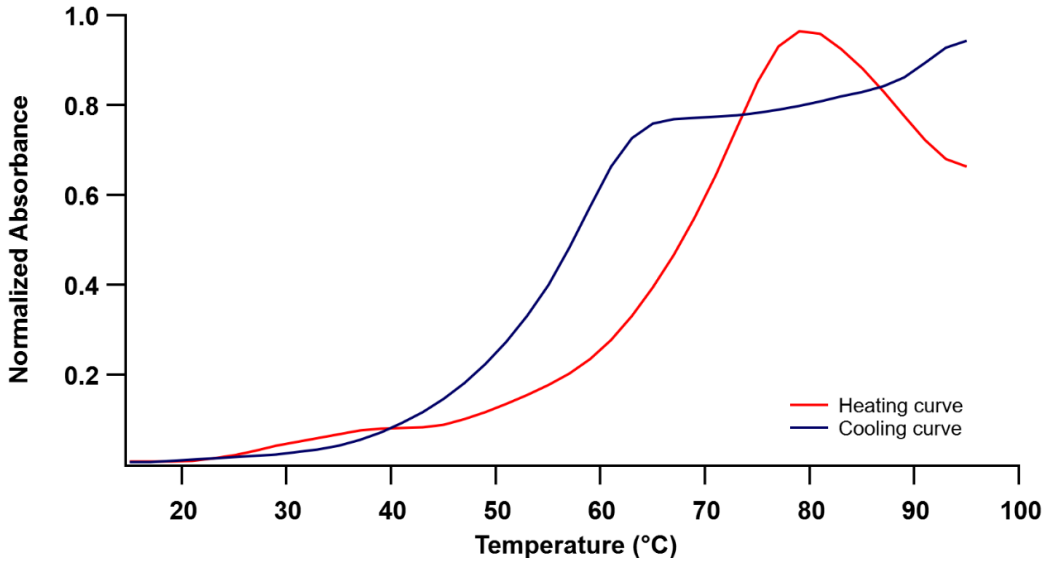

Figure 19. UV-Vis thermal denaturation profiles of 30.0 µM poly(A) in the presence of 7.5 µM COR and 10% PEG at 420 nm.

Melting curves of poly(A) + COR sample obtained at 260 nm and 420 nm in the presence of 20% PEG are shown in Figures 20 and 21, respectively. The addition of 20% PEG to poly(A) + COR sample lowered the stability resulting in melting temperatures of 61°C at 260 nm and 53°C at 420 nm.

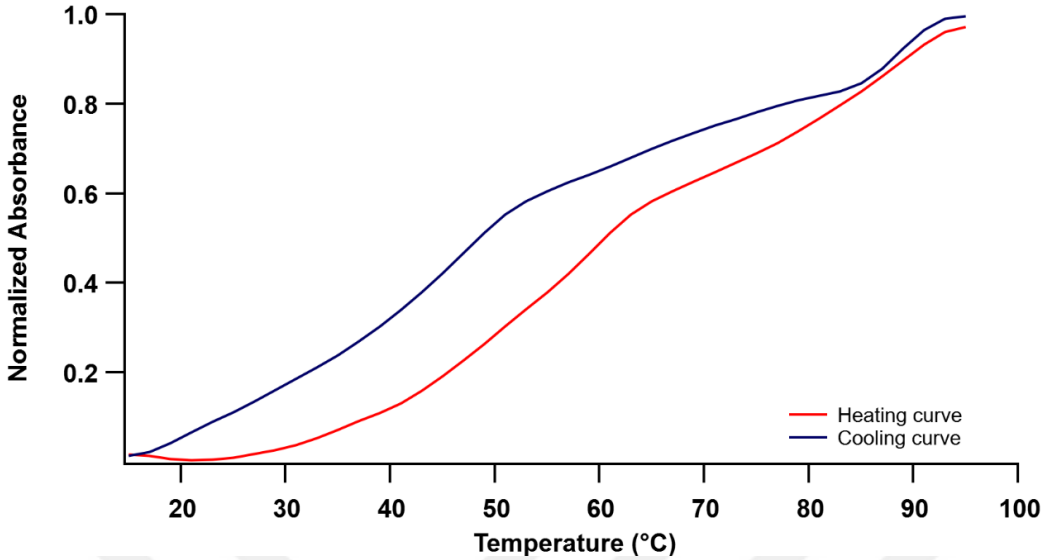

Figure 20. UV-Vis thermal denaturation profiles of 30.0 µM poly(A) in the presence of 7.5 µM COR and 20% PEG at 260 nm.

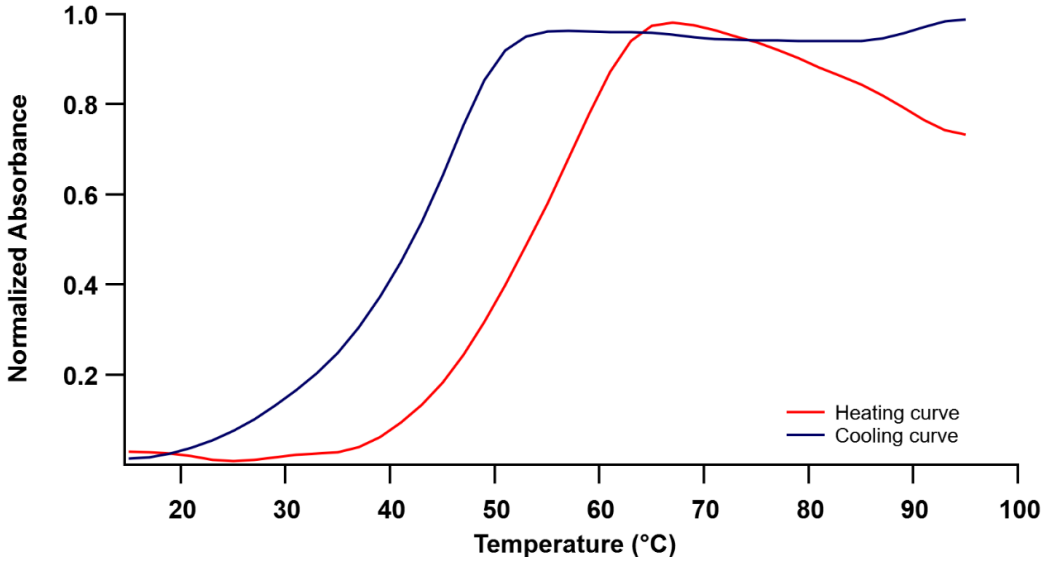

Figure 21. UV-Vis thermal denaturation profiles of 30.0 µM poly(A) in the presence of 7.5 µM COR and 20% PEG at 420 nm.

In order to compare the melting temperatures of poly(A) self-structure in the presence of 0%, 5%, 10%, and 20% PEG, figures 22 and 23 were created. Trends in the thermal stability of self-structure can be seen clearly in figures. An increase in

the final concentration of PEG in the sample has resulted in a decrease in the stability of poly(A) double-helical structure. As the sample becomes more crowded, self-structure is destabilized. In other words, the formation of the self-structure of poly(A) was prevented with increasing concentrations of PEG.

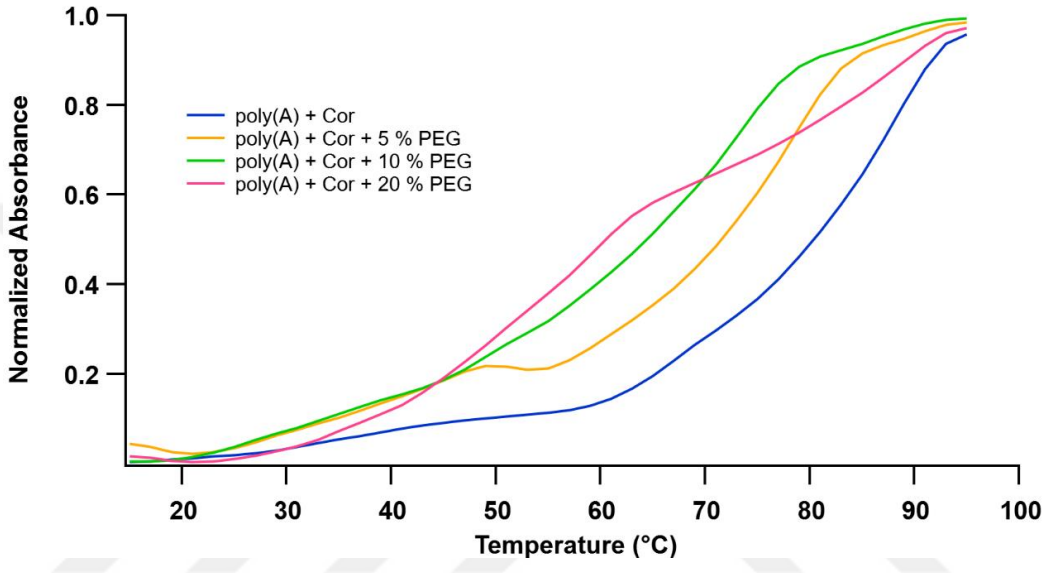

Figure 22. Change in UV-Vis thermal denaturation profiles upon addition of different concentrations of PEG to poly(A) + COR sample at 260 nm.

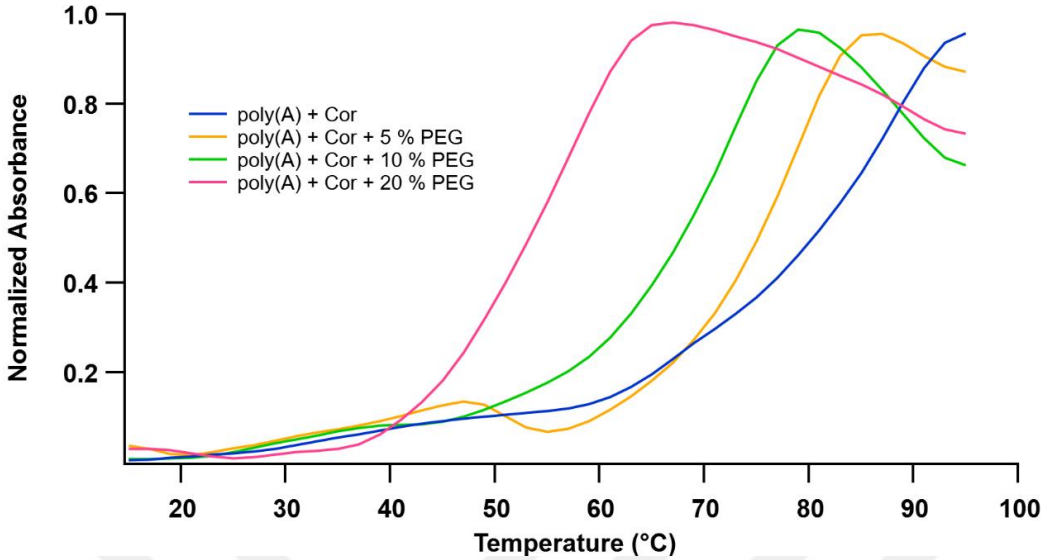

Figure 23. Change in UV-Vis thermal denaturation profiles upon addition of different concentrations of PEG to poly(A) + COR sample at 420 nm.

In view of the fact that the 20% PEG was destabilizing the self-structure of poly(A) the most, the effect of other crowding agents was examined at this concentration. In Figures 24 and 25, thermal denaturation profiles obtained at 260 nm and 420 nm, respectively for poly(A) + COR sample in the presence of 20% glycerol are given. With the addition of glycerol, T_m of poly(A) self-structure decreased to 79°C at 260 nm. T_m obtained by monitoring the absorbance change at 420 nm was 73°C.

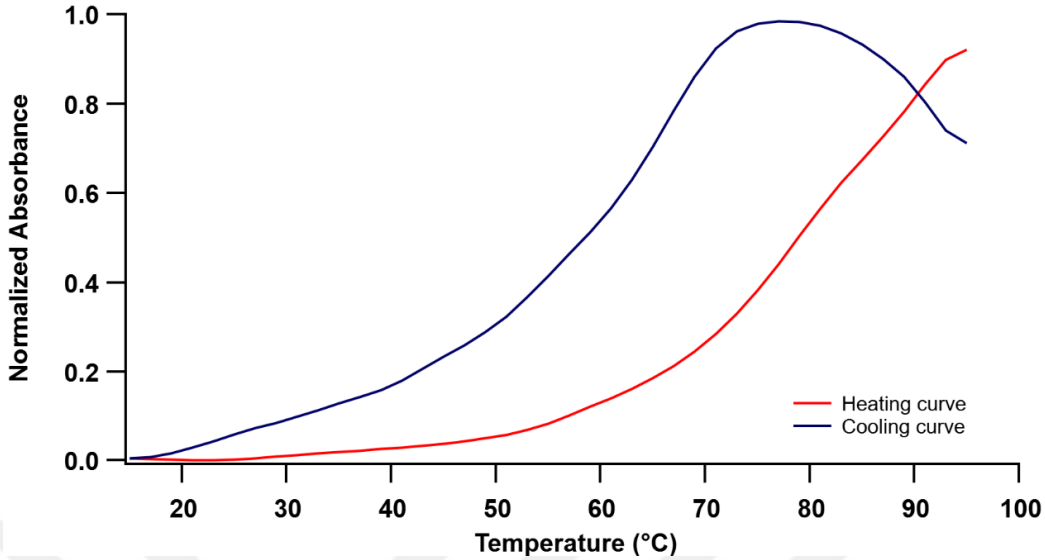

Figure 24. UV-Vis thermal denaturation profiles of 30.0 μM poly(A) in the presence of 7.5 μM COR and 20% glycerol at 260 nm.

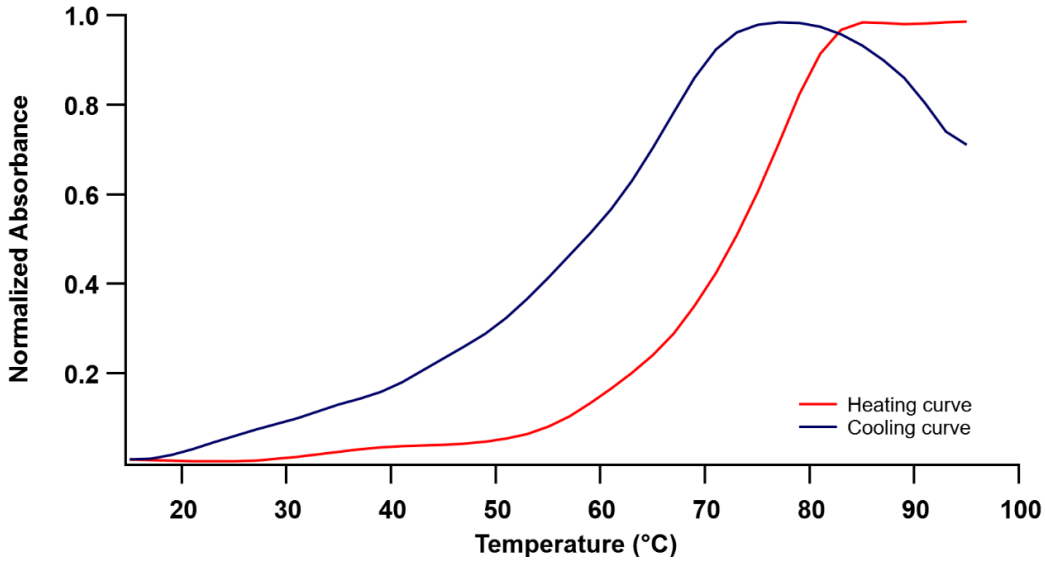

Figure 25. UV-Vis thermal denaturation profiles of 30.0 μM poly(A) in the presence of 7.5 μM COR and 20% glycerol at 420 nm.

Similarly, thermal denaturation experiments were performed for poly(A) + COR sample in the presence of 20% sucrose. Sucrose was used as a small cosolute in this

study. The melting profile of the sample remained relatively the same with the addition of sucrose. The melting temperature and, consequently, the stability of poly(A) + COR decreased less in the presence of sucrose compared to the presence of other crowding agents, in an agreement with our CD results. T_m was determined as 73°C at 260 nm and 77°C at 420 nm. Figure 26 and 27 shows the melting profiles of poly(A) + COR in the presence of sucrose.

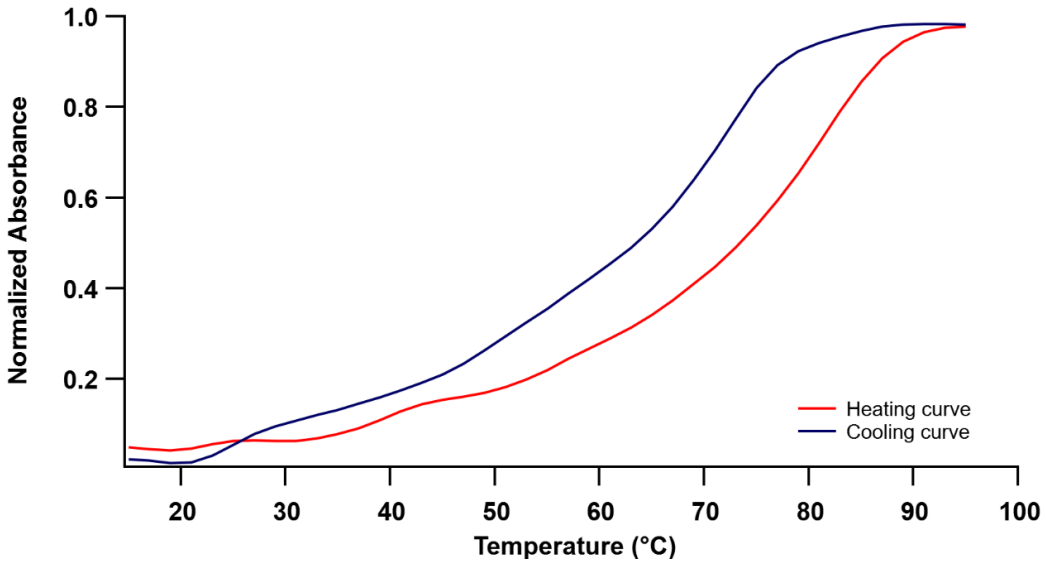

Figure 26. UV-Vis thermal denaturation profiles of 30.0 μM poly(A) in the presence of 7.5 μM COR and 20% sucrose at 260 nm.

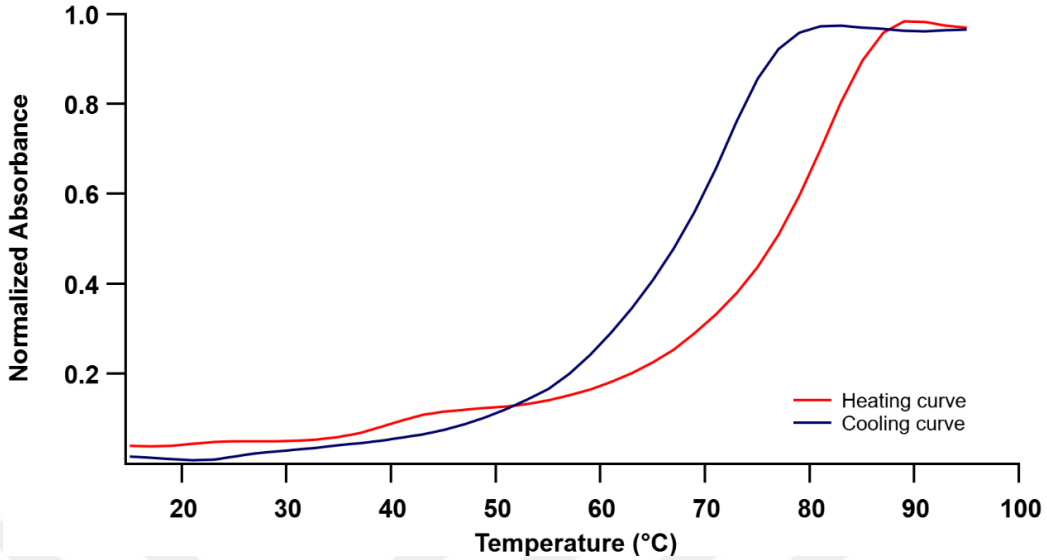

Figure 27. UV-Vis thermal denaturation profiles of 30.0 μM poly(A) in the presence of 7.5 μM COR and 20% sucrose at 420 nm.

Melting temperatures of samples determined from differential absorbance values are shown in Table 1. According to determined T_m values from normalized absorbance values, 20% sucrose decreased the T_m of poly(A) self-structure by about 8°C. With the addition of 20% glycerol, the decrease in the T_m was determined as about 2°C. In the presence of 20% PEG, the T_m decrease was about 20°C. Figures 28 and 29 show the changes in the melting temperature with different crowding agents at 20% concentration in the poly(A) + COR sample at 260 nm and 420 nm, respectively. This significant change in the T_m and hence the stability has resulted from the presence of the small cosolute. Large and small cosolute effects on nucleic acid duplexes were well studied in the literature [152–155]. Polysaccharides and PEG are highly soluble in water and have relatively low vapor pressure values. These physical properties are important to perform experiments to determine the stability change of the nucleic acid structure in the presence of a crowded environment. Studies employing high molecular weight cosolutes revealed that the stability of the duplex structure of both DNA and RNA have increased. For example, poly(I)•poly(C) RNA

duplex's stability was increased with PEGs (MW = 4000 and 20000) and dextrans (MW = 10000 and 70000) at 10% (w/v) [154]. Moreover, the Tm of poly(dA)•poly(dT) DNA duplex was also raised with increasing amount of PEG (MW = 8000) [153]. In contrast, studies conducted by using low molecular weight cosolutes (small cosolutes) such as EG, sucrose and glycerol show that the stability was decreased due to less steric hindrance of these agents and reduced water activity [152,153]. Also, in a study of calf thymus DNA in the presence of polyols, a decrease in the stability was observed due to the increased electrostatic repulsion between the DNA phosphates and the electrostatic interaction modification with counter ions [156].

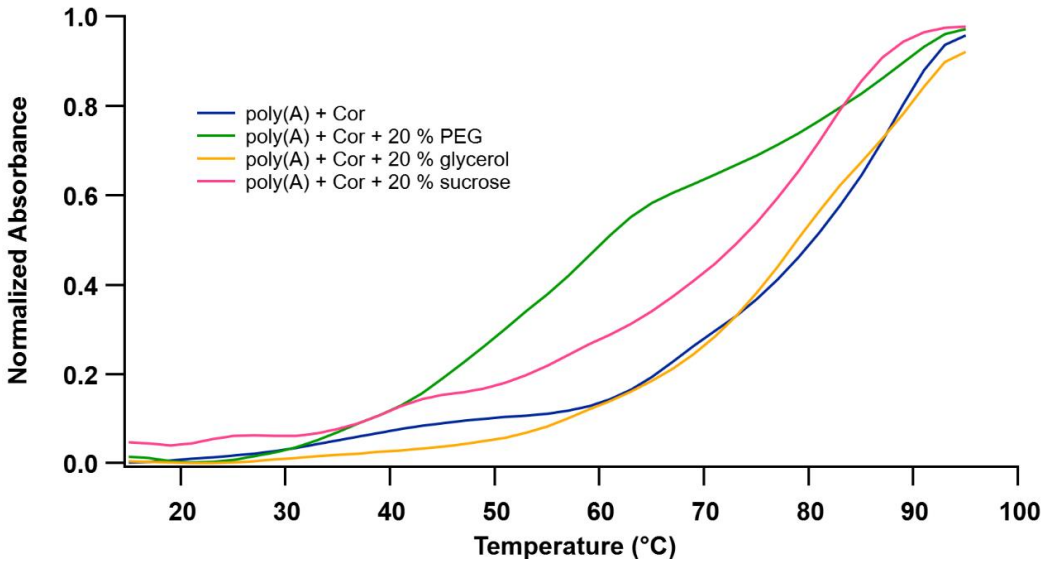

Figure 28. Change in UV-Vis thermal denaturation profiles upon addition of different crowding agents to poly(A) + COR sample at 260 nm.

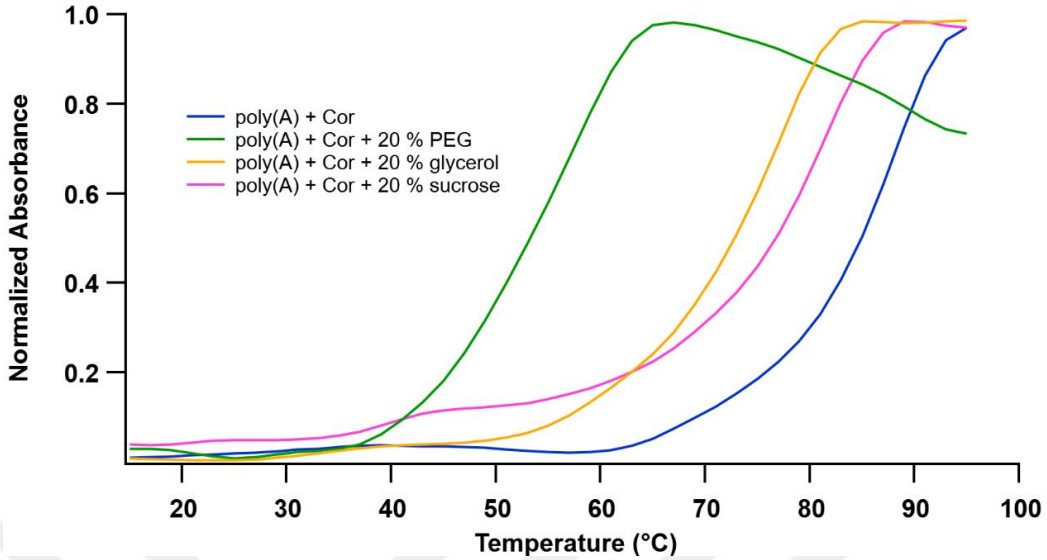

Figure 29. Change in UV-Vis thermal denaturation profiles upon addition of different crowding agents to poly(A) + COR sample at 420 nm.

In order to understand whether poly(A) samples that do not contain COR form double-helical structures with a certain T_m or not in the presence of crowding agents, thermal denaturation experiments were performed for these samples. Firstly, 20% PEG was added to the 30.0 μM poly(A) sample in the absence of COR. Figure 30 shows the results of this experiment at 260 nm. Thermal denaturation curves were not created for 420 nm since these samples do not contain COR. As expected, a melting profile was not observed, and a melting temperature was not determined for the sample that does not contain COR since the formation of self-structure of poly(A) did not occur.

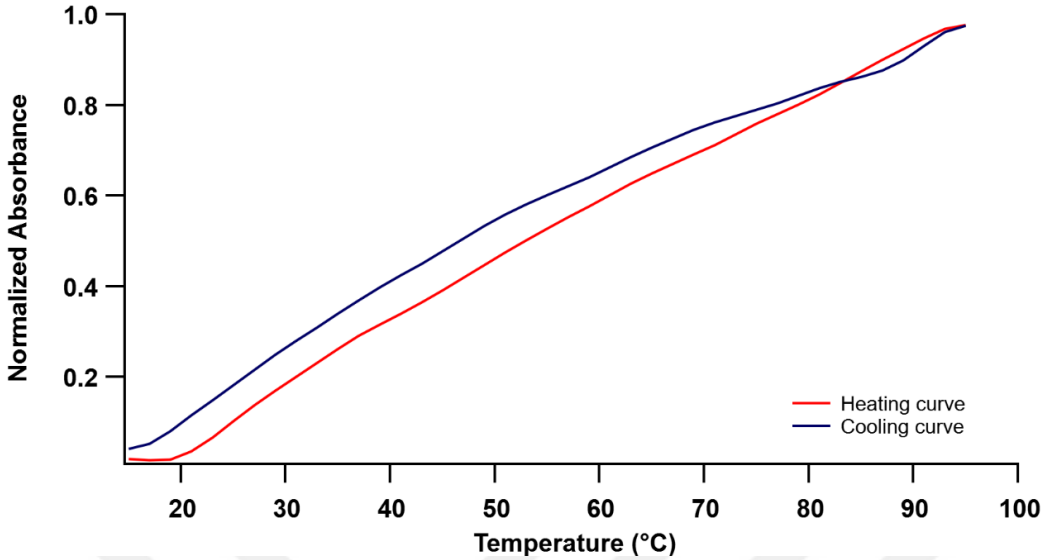

Figure 30. UV-Vis thermal denaturation profiles of 30.0 μM poly(A) in the presence of 20% PEG at 260 nm.

Figure 31 shows the thermal denaturation profiles for the 30 μM poly(A) + 20% glycerol sample. To our surprise, the heating curve obtained was resembling to the melting curve of a duplex structure. Since there was no COR in this sample, it was surprising to have such a melting profile. Therefore, as a control, a thermal denaturation experiment was performed for the sample containing only 20% glycerol. Figure 32 shows the absorption spectra of 20% glycerol obtained during the thermal denaturation experiment. As absorbance at 292 nm increases upon heating, the melt graph was constructed for this sample and given in Figure 33. As shown in Figure 33, an increase in the absorbance of 20% glycerol was reflected as a melting curve in the thermal denaturation experiment.

Thermal denaturation profiles of poly(A) in the presence of 20% glycerol at 260 nm are given in Figure 34. The heating curve of glycerol was very similar to that of poly(A) + 20% glycerol sample. In order to make a comparison between the melting curves of 20% glycerol and poly(A) + 20% glycerol samples, the graph in Figure 35 was created. In the figure, the green line represents poly(A). The yellow line represents poly(A) in the presence of 20% glycerol, and the blue line represents glycerol only. As observed, the melt curve obtained for the poly(A) + 20% glycerol

sample was not resulted from the self-structure of poly(A) but from the increase in the absorption of glycerol itself.

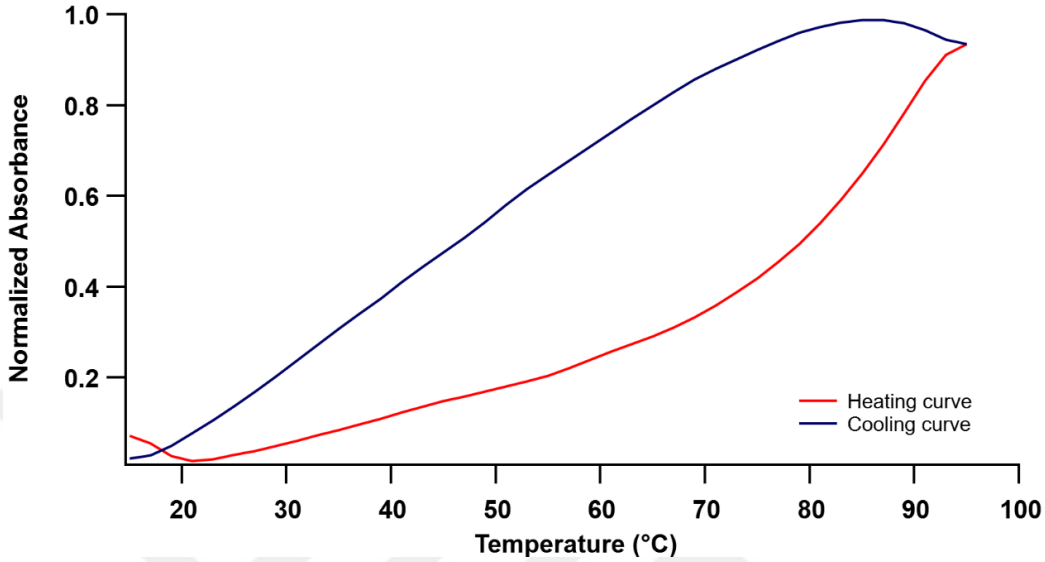

Figure 31. UV-Vis thermal denaturation profiles of 30.0 μM poly(A) in the presence of 20% glycerol at 260 nm.

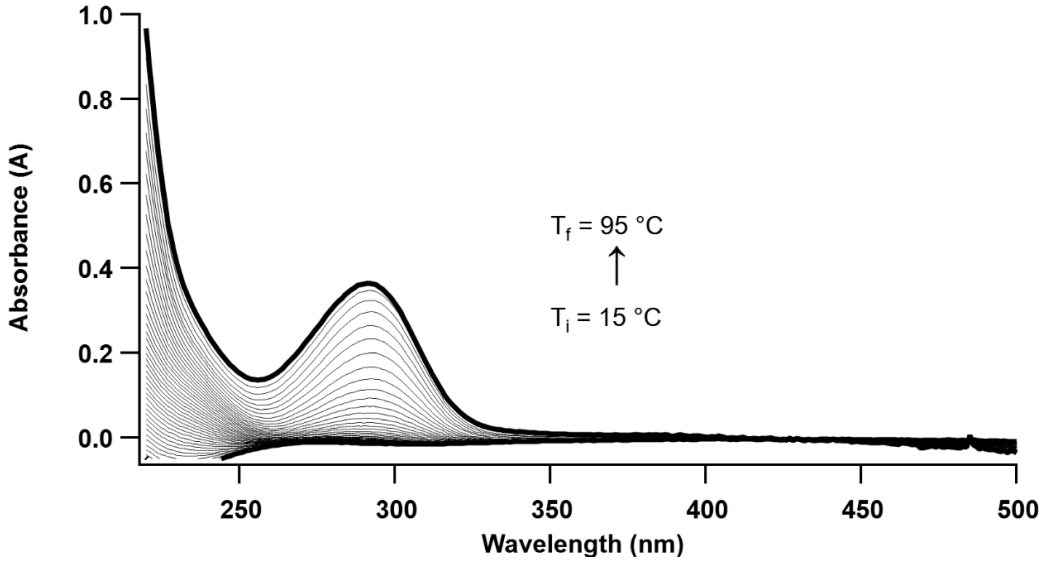

Figure 32. UV-Vis absorption spectra of 20% glycerol sample obtained during thermal denaturation.

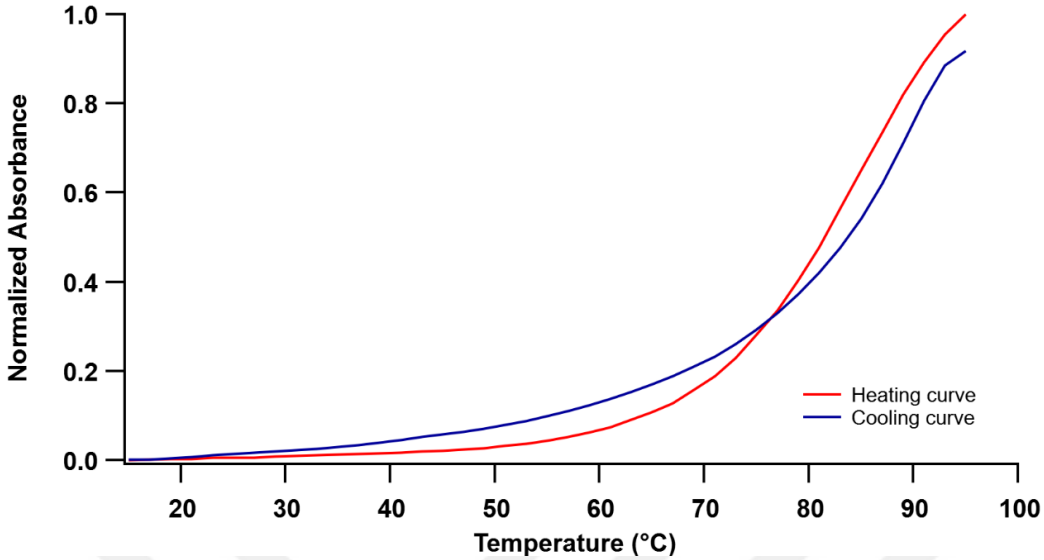

Figure 33. UV-Vis thermal denaturation profiles of 20% glycerol at 292 nm.

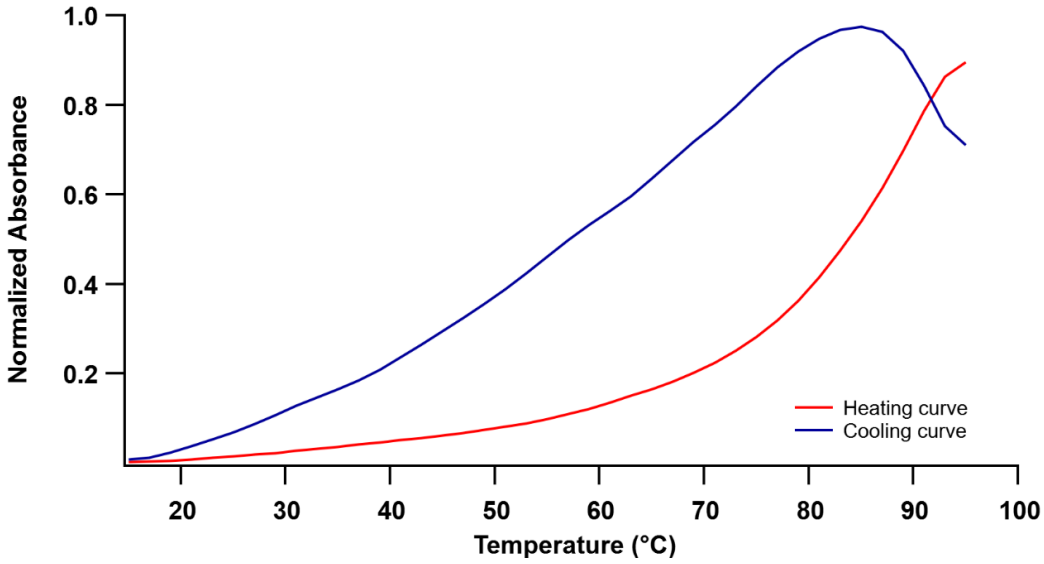

Figure 34. UV-Vis thermal denaturation profiles of 20% glycerol at 260 nm.

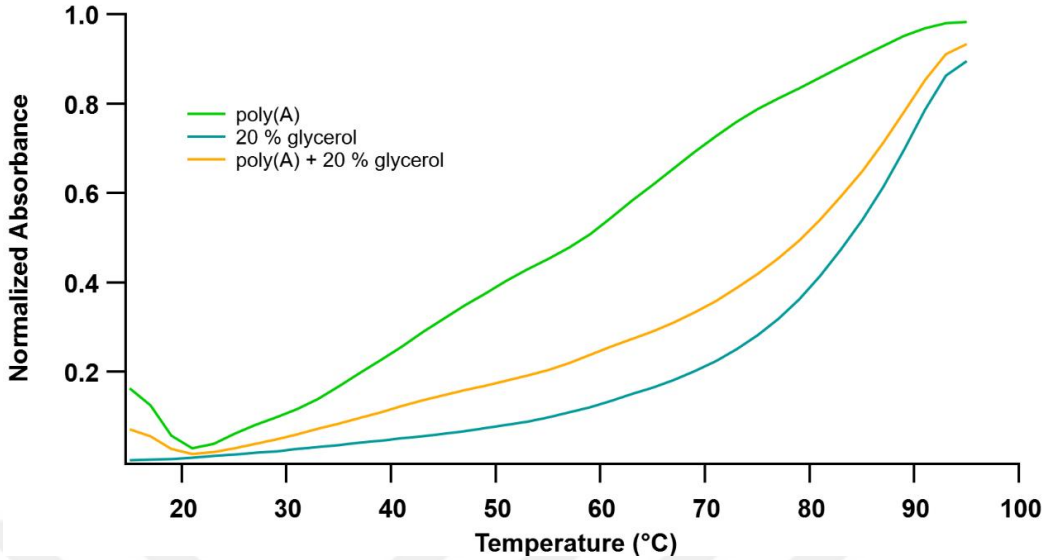

Figure 35. Change in UV-Vis thermal denaturation profile of poly(A) upon addition of 20% glycerol.

Thermal denaturation of poly(A) + 20% sucrose sample was also performed, and results of the experiment are given in Figure 36. As expected, a melting temperature cannot be determined since there was no poly(A) self-structure formation due to the absence of COR.

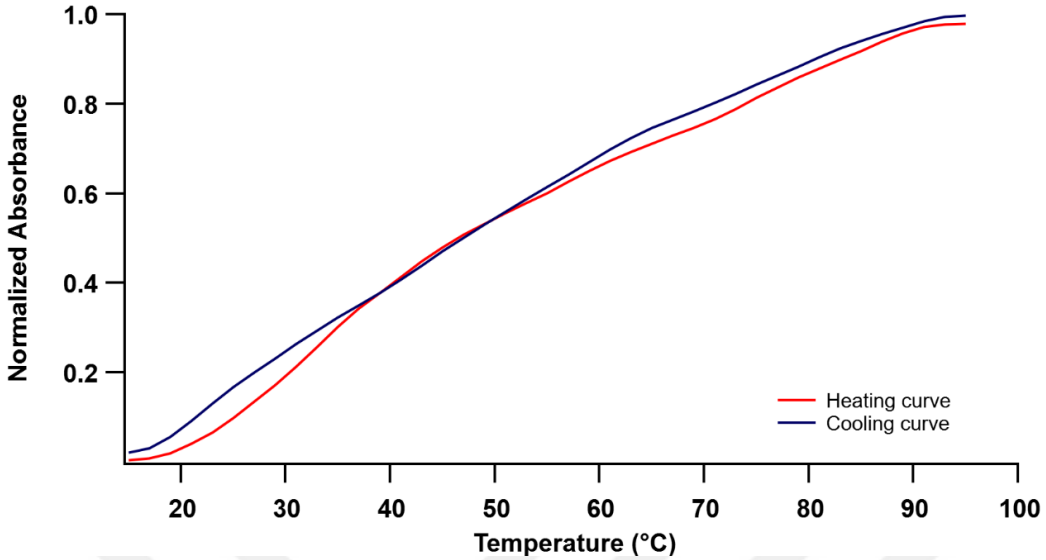

Figure 36. UV-Vis thermal denaturation profiles of 30.0 μM poly(A) in the presence of 20% sucrose at 260 nm.

Table 1. Melting temperatures of samples obtained from normalized absorbance values.

Sample	**T_m (°C) at 260 nm**	**T_m (°C) at 420 nm**
poly(A)	-	-
poly(A) + COR	81	85
poly(A) + COR + 5% PEG	72	75
poly(A) + COR + 10% PEG	65	67
poly(A) + COR + 20% PEG	61	53
poly(A) + COR + 20% sucrose	73	77
poly(A) + COR + 20% glycerol	79	73
poly(A) + 20% PEG	-	-
poly(A) + 20% sucrose	-	-
Poly(A) + 20% glycerol	-	-

3.1.3 Fluorescence Spectroscopy Experiments

Further studies were performed with fluorescence spectroscopy in order to investigate poly(A) – COR interactions. Here, changes in the fluorescence intensity of COR upon the addition of poly(A) and cosolute molecules were monitored. As shown in Figure 37, poly(A) does not show any fluorescence peak upon excitation at 420 nm since it is not fluorescent. On the other hand, the sample that contains 7.5 μM COR has a fluorescence peak with a maximum intensity at 481 nm (Figure 37, red line). The sample that contains poly(A) and COR (final concentration of poly(A):COR 30.0:7.5 μM) has a lower intensity than 7.5 μM COR itself revealing the interaction of COR with poly(A). With the intercalation of COR in poly(A) strands and the formation of self-structure, the free COR amount in the sample is thought to be decreased, resulting in a decrease in intensity. The decrease in the intensity is shown with the blue line in Figure 37. Moreover, the fluorescence intensity of 7.5 μM COR in the presence of poly(A) and 20% PEG is represented with the green line in Figure 37. The most significant change in the thermal stability was observed with the addition of 20% PEG to poly(A) + COR sample in Section 3.2. Therefore, this sample was selected for the fluorescence experiments. The fluorescence intensity of this sample (the green line) was observed as greater than the sample in the absence of PEG (the blue line). The addition of PEG to poly(A) + COR sample prevents the maximum interaction of COR and poly(A) and thought to increase the free COR amount, thus the intensity. It does not reach the intensity of COR only (the red line), which means some of the COR still interacts with the poly(A).

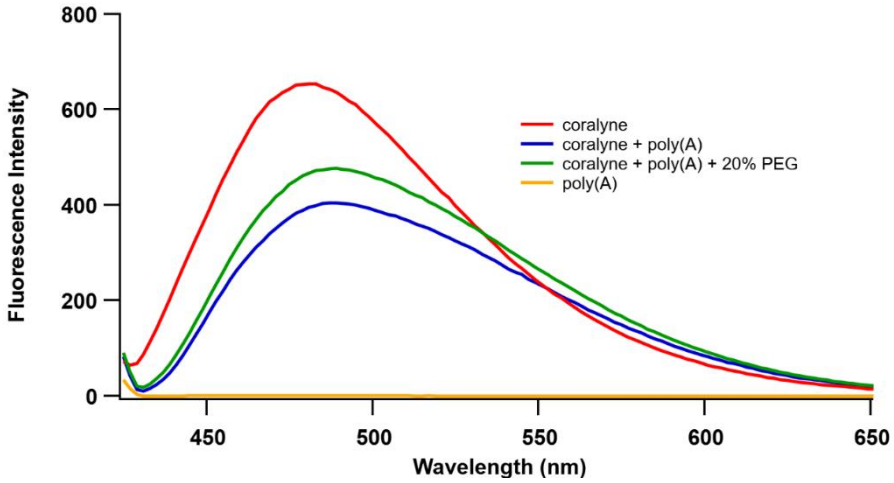

Figure 37. Change in the fluorescence intensity upon addition of 30.0 µM poly(A) and 20% PEG to 7.5 µM COR.

Figure 38 represents the changes in the fluorescence intensity of COR upon addition of different crowding agents. Intensity of COR (the red line) significantly increased and even over ranged with the addition of all of the three cosolutes. The greatest increase was observed with the addition of 20% PEG to 7.5 µM COR. On the other hand, when poly(A) was added to these samples (Figure 39), fluorescence intensities were lowered. The addition of poly(A) to COR samples that contain 20% sucrose and glycerol have lower intensities than poly(A) + COR sample. Yet, the intensity obtained by adding poly(A) to COR + 20% PEG sample, is higher than the intensity of poly(A) + COR sample.

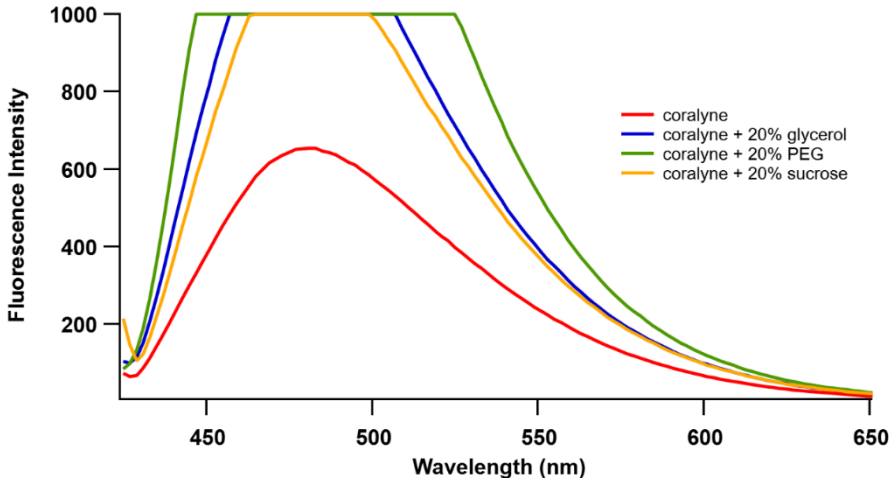

Figure 38. Change in the fluorescence intensity upon addition of 20% crowding agents to 7.5 μM COR.

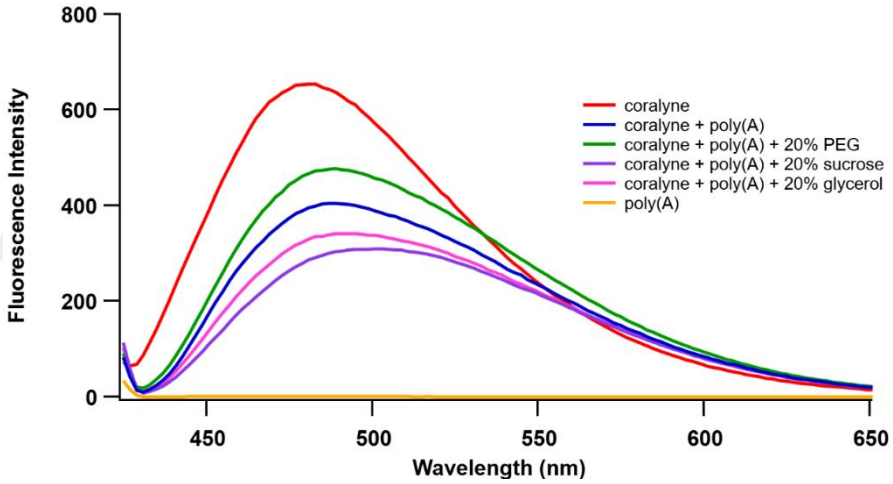

Figure 39. Change in the fluorescence intensity upon addition of 30.0 μM poly(A) and 20% PEG, sucrose, and glycerol to 7.5 μM COR.

3.2 Investigating the Effect of DNA Methylation on DDD-Lysine and DDD-Arginine Interactions

3.2.1 UV-Vis Absorption Spectroscopy

Within the scope of the study, firstly, the effect of amino acid (Lys or Arg) concentration on the thermal denaturation temperature of DDD was studied to determine the amino acid concentration that affects the structure and thermal denaturation temperature of DDD. In this context, experiments were conducted with only DDD and with different Lys concentrations. DDD + Lys samples of 50 mM, 250 mM, 500 mM and 1000 mM were prepared. Afterwards, they were carried out with Arg (250 mM, 500 mM and 1000 mM). The change in DNA stability was observed in samples containing 500 mM and 1000 mM amino acids. Therefore, DDD8-amino acid samples were also prepared at these concentrations. The UV-Vis absorption spectra of DDD and DDD8 in the absence and presence of different concentrations of amino acids at 15°C are given in Figure 40 – Figure 43. Intensity of the absorbance value of DDD and DDD8 were increased with the addition of increasing amino acid concentrations due to absorbance of the amino acids [157].

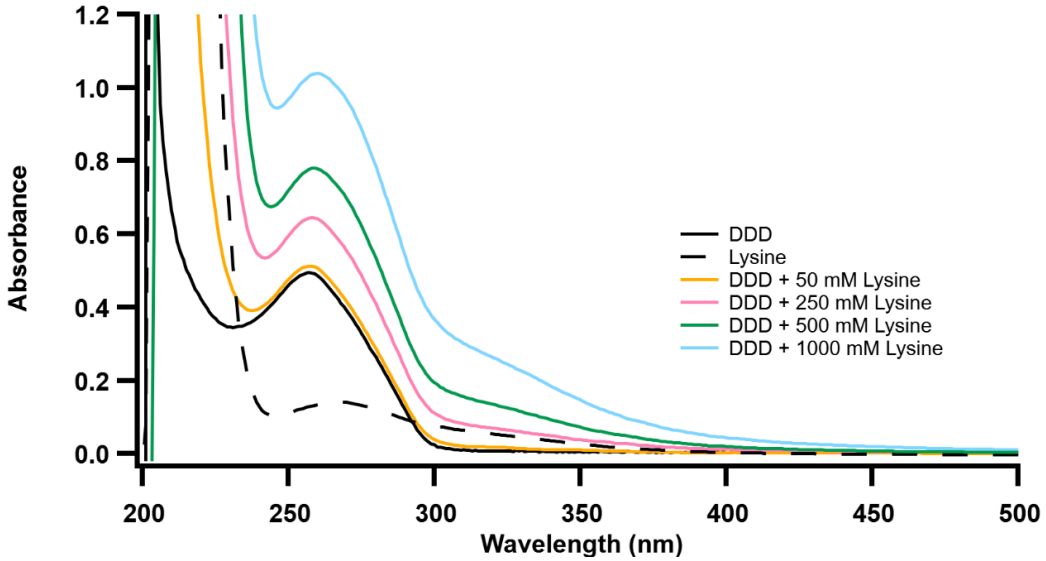

Figure 40. UV-Vis absorption spectra of DDD, Lys and DDD + Lys samples at 15°C.

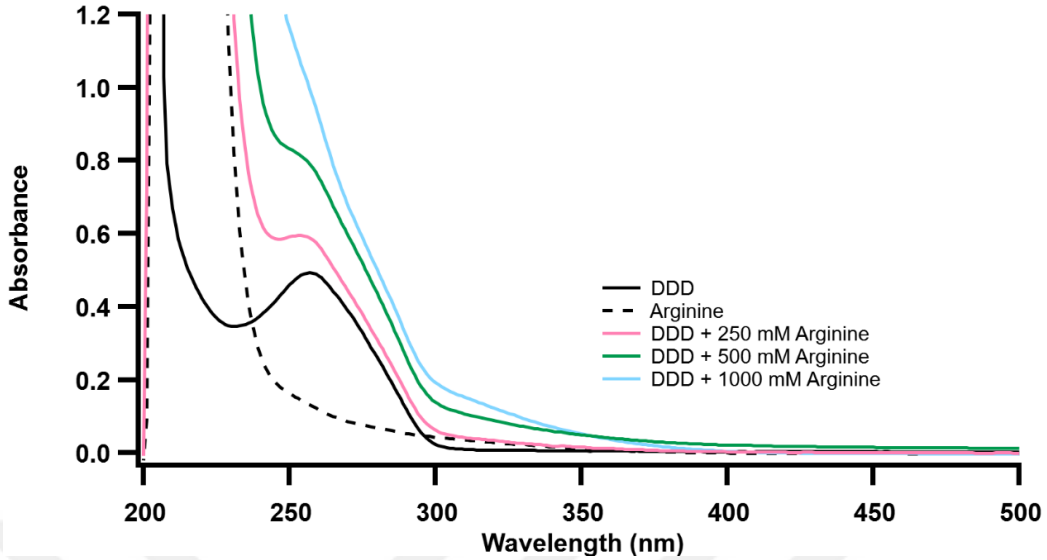

Figure 41. UV-Vis absorption spectra of DDD, Arg and DDD + Arg samples at 15°C.

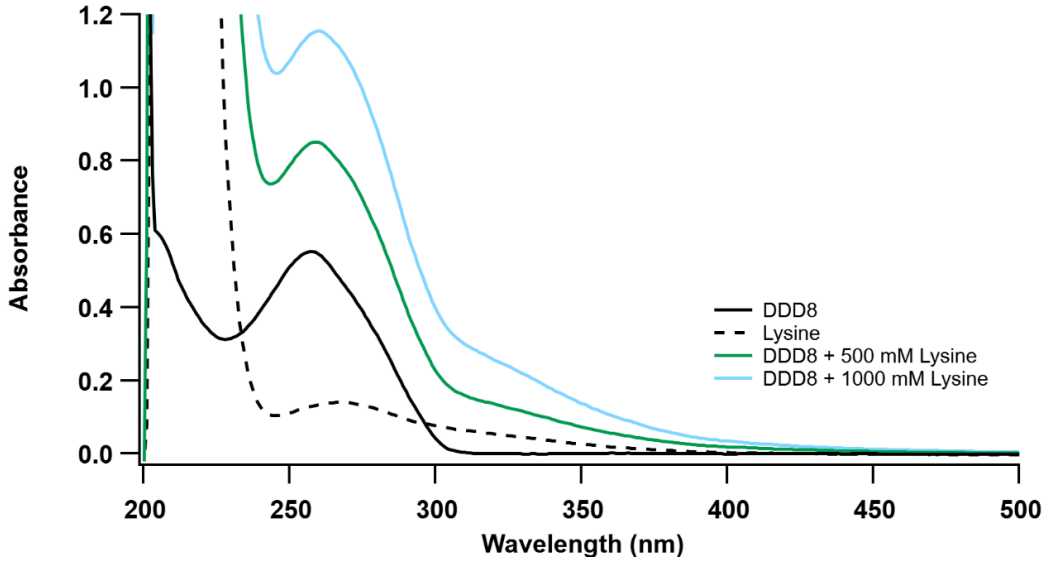

Figure 42. UV-Vis absorption spectra of DDD8, Lys and DDD8 + Lys samples at 15°C.

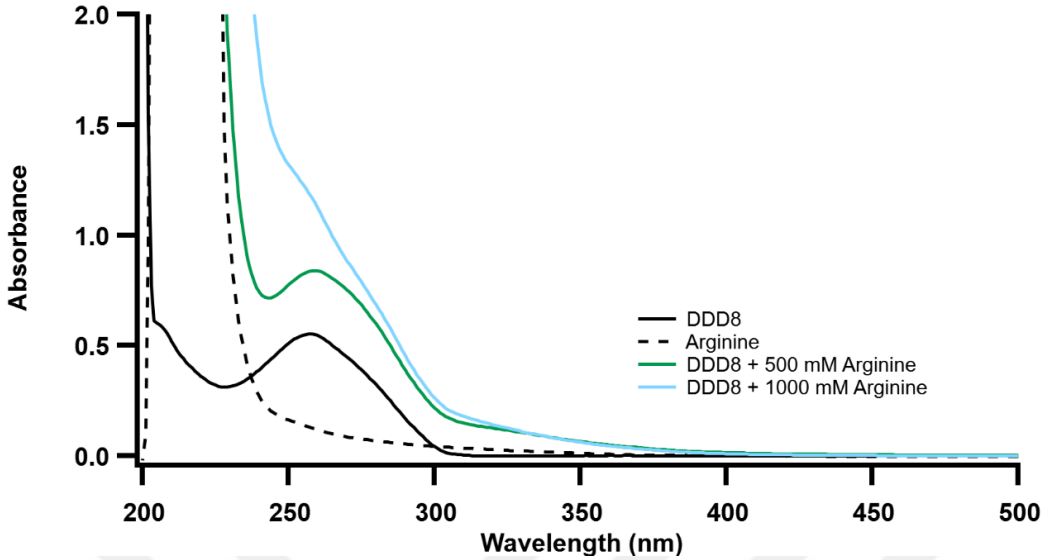

Figure 43. UV-Vis absorption spectra of DDD8, Arg and DDD8 + Arg samples at 15°C.

3.2.2 UV-Vis Thermal Denaturation Experiments

In order to determine the effects of Lys and Arg on the stability of DNA, UV-Vis thermal denaturation experiments were carried out.

Thermal denaturation (or melting) experiments are employed to enlighten the changes in the stability of DNA. Upon heating, the absorbance of oligonucleotides or polynucleotides increases at 260 nm due to base unstacking and strand separation. In the case of single strands, a gentle rise is usually observed in the absorbance due to unstacking of the bases. On the other hand, upon heating a double-stranded oligonucleotide, usually an S-shaped increase is obtained with the separation of the double-strand. Since double strand – single strand equilibrium is a phase change, the increase in the absorption is mostly very abrupt. The temperature where half of the double-strand is turned into single strands is the melting temperature and denoted as T_m. Higher T_m indicates higher stability [158].

Thermal denaturation experiments were performed in order to determine the changes in the thermal stabilities of DDD and DDD8. The thermal denaturation profiles

obtained from the temperature-dependent change of absorbance at 260 nm are shown in Figures 44 – 49. The thermal denaturation temperatures obtained using these profiles are shown in Table 2.

Figure 44 represents the change in the melting temperature of DDD upon addition of different concentrations of Lys. With the addition of 50 mM and 250 mM Lys, an insignificant change was observed. With the addition of 500 mM and 1000 mM Lys, the melting temperature of the DDD was increased by about 2°C, from 61°C to 63°C.

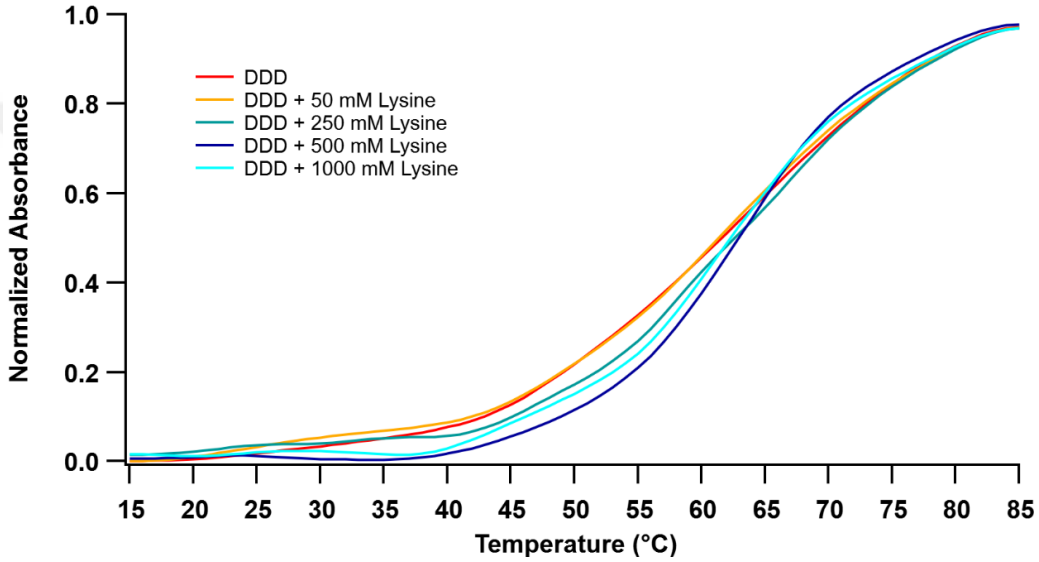

Figure 44. Thermal denaturation profiles of DDD in the absence and presence of Lys.

The thermal denaturation profiles of DDD in the absence and presence of Arg are given in Figure 45. The addition of Arg decreased the T_m of DDD. The red line represents the sample containing only DDD and has a melting temperature of 61°C. The addition of 250 mM Arg to DDD lowered the T_m to 60°C. The addition of 500 mM and 1000 mM Arg to DDD decreased the T_m to 58.5°C and 56°C, respectively. Even though the 1°C change in melting temperature does not represent a critical consequence of interactions and might possibly be in our experimental error range, the trend is noticeable among the samples.

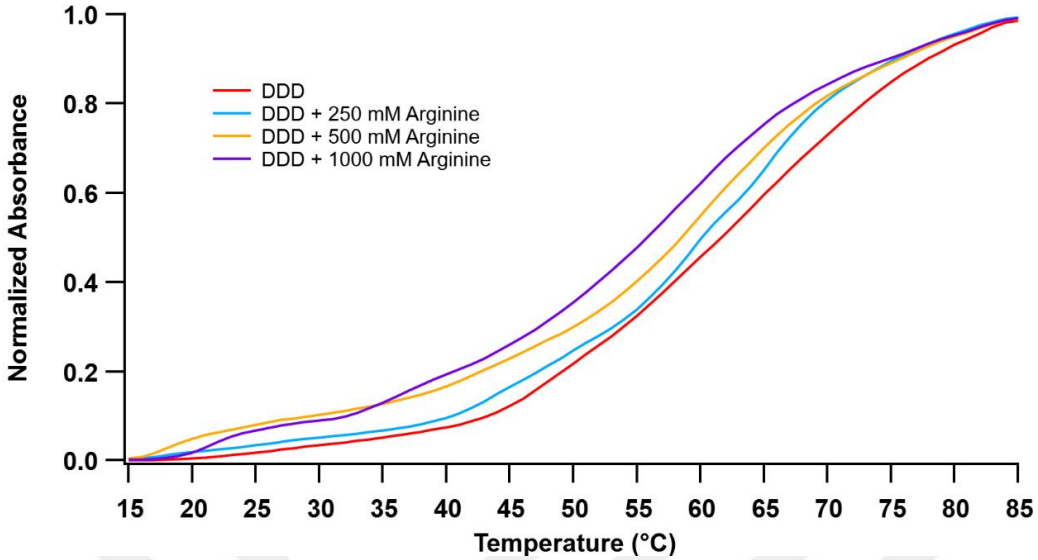

Figure 45. Thermal denaturation profiles of DDD in the absence and presence of Arg.

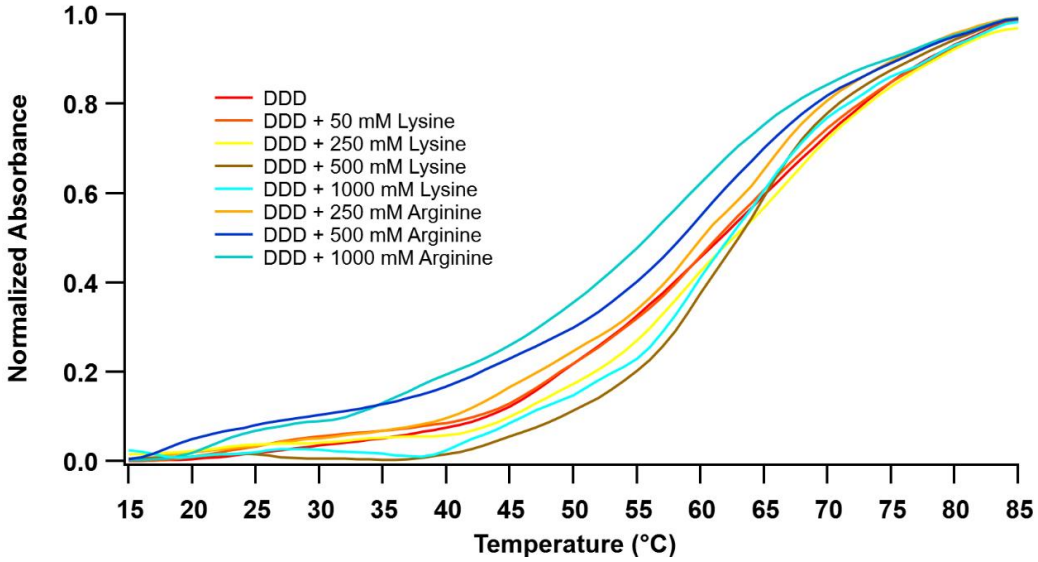

Figure 46. Thermal denaturation profiles of DDD upon addition of different concentrations of Lys or Arg.

As shown in Figure 46, 50 mM Lys addition did not change the T_m of DDD. However, addition of 250 mM and 500 mM Lys to DDD increased the T_m of DDD slightly. The stability of DDD was decreased upon increasing the Lys concentration to 1000 mM, plausibly due to higher charge neutralization. T_m of 62.5°C was

obtained in the presence of 1000 mM Lys. In fact, this T_m value is still higher than that of DDD only. On the other hand, the addition of increasing Arg concentrations to DDD has resulted in a decrease in the stability and T_m of DDD. Within the scope of these results, it is possible that the positively charged amino acids interacted with the negatively charged phosphate groups of DDD and reduced the repulsion between the phosphate groups. Usually, presence of salt in the medium increases the stability of nucleic acids up to high concentrations since helix structure is stabilized by ions. At high concentrations, helix becomes saturated due to strong interaction between cations of the salt and the negatively charged phosphate backbone and the further enhancement of the stability is small [159]. There are several studies displaying the fact that the DNA stability is reduced in the presence of salts at above a specific salt concentration [160,161].

Figures 47 and 48 display the addition of 500 mM and 1000 mM Lys and Arg to DDD8, respectively. The addition of Lys did not have a considerable effect on T_m of DDD8, which is 63.5°C. Only a slight increase was observed. The effect of Arg on DDD8 was more profound, but perplexing. The addition of 500 mM Arg raised the T_m of DDD8 to 65°C. However, further increase in Arg concentration to 1000 mM decreased the T_m of the DDD8 to 60°C.

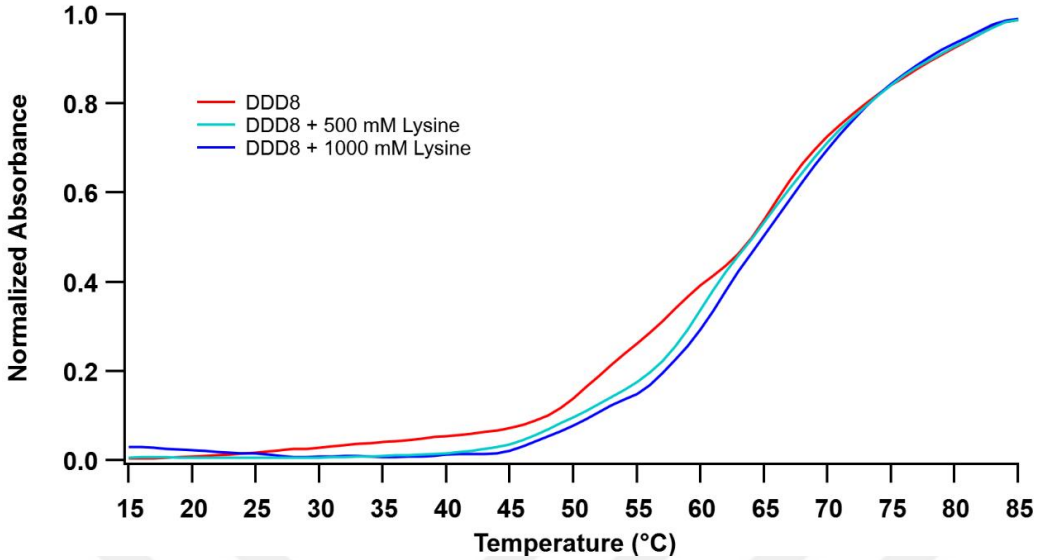

Figure 47. Thermal denaturation profiles of DDD8 in the absence and presence of Lys.

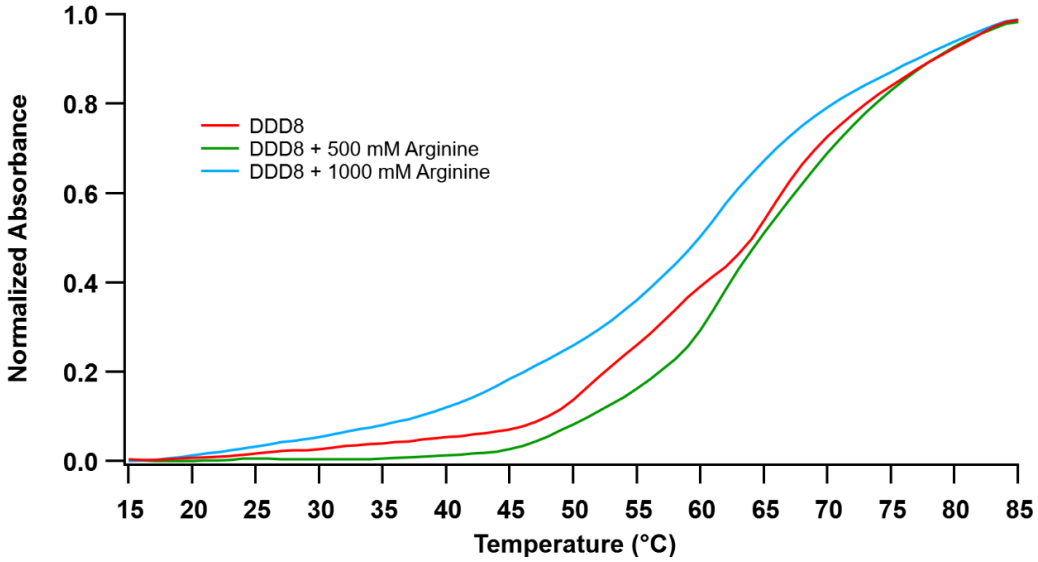

Figure 48. Thermal denaturation profiles of DDD8 in the absence and presence of Arg.

Figure 49 represents the changes in the melting temperature upon the addition of 500 mM and 1000 mM amino acid to DDD8. These results show that the DDD sequence is more easily destabilized than DDD8. The reason is probably that the methyl groups in the grooves reduce the effect of cations by shielding the charges. Hence, d5mC

substituted DDD becomes less flexible, resulting in an increase in the melting temperature and stability [162,163]. Moreover, it was observed that Arg affected the melting temperatures of DDD and DDD8 samples more than Lys. A similar case has been reported in the literature by Solovyev et al. [164]. In their study, thermal degredation of poly(dA)•poly(dT) was investigated in the presence of L-amino acids namely Lys, Arg, Pro, Glu and Asp. DNA melting temperature comparison in the presence of amino acids reveals a slight increase in T_m in the case of basic amino acids (Arg, Lys), whereas the acidic amino acids (Glu, Asp) decrease the T_m. Moreover, the change in the T_m with Arg was + 3.9°C and with Lys, it was + 0.6°C. The stability change was greater with Arg than with Lys, in a consistency with our results. Arg and Lys both are positively charged amino acids at pH 7.0. However, they interact with DNA molecule in different ways because the charge distribution is different [165]. Arg has a guanidinium moiety with three amine groups in its side chain whereas only one amine group is present in the Lys side chain. Even though electrostatic interactions occur in between the negatively charged phosphate group of DNA and both Lys and Arg, the interaction mode may differ. The guanidinium moiety with three amine group of Arg permits zwitterion H-bonding with the phosphate group of DNA. By doing so, it provides binding strength which is coming from its charge and structural organization. The interaction of Arg through additional H-bonding with the DNA backbone and the bases such as guanine is also possible [166]. Furthermore, the guanidinium group containing three amine group is bulkier than only one amine group, which might provide steric constrains that might alter the interactions [167]. Therefore, Arg can interact with DNA in several manners. On the other hand, less steric hindrance is expected in the Lys side chain with a single amine group. Previously, it was reported that the Lys peptides can interact with DNA cooperatively, with a higher chance of a second peptide associating with Lys homopeptide-bound DNA than with the free DNA molecule [168]. On the other hand, for homoarginine peptides, interactions occur in a noncooperative way. Partial cationic residues of polyarginine were found to be effective for occupying DNA

phosphate groups in DNA-homoarginine complexes, whereas all residues in polylysine were found to be capable of occupying phosphate groups [165,169,170].

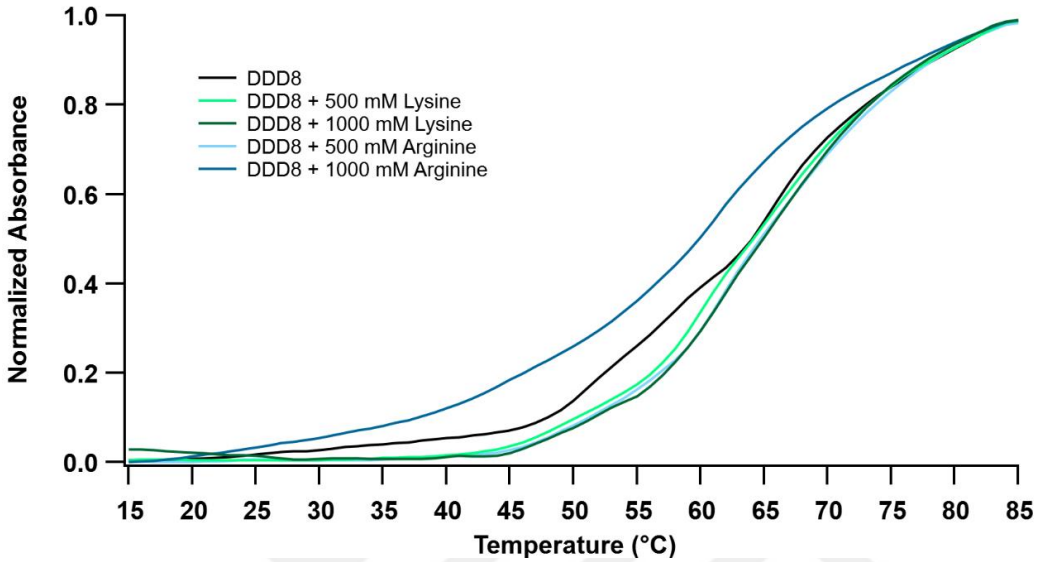

Figure 49. Thermal denaturation profiles of DDD8 upon addition of different concentrations of Lys or Arg.

Table 2. Melting temperatures of samples

Sample	**T_m (°C)**	**Sample**	**T_m (°C)**
DDD	61	DDD8	63.5
DDD + 50 mM Lys	61		
DDD + 250 mM Lys	62		
DDD + 500 mM Lys	63	DDD8 + 500 mM Lys	64
DDD + 1000 mM Lys	62.5	DDD8 + 1000 mM Lys	65
DDD + 250 mM Arg	60		
DDD + 500 mM Arg	58.5	DDD8 + 500 mM Arg	65
DDD + 1000 mM Arg	56	DDD8 + 1000 mM Arg	60

3.2.3 CD Spectroscopy Experiments

CD spectroscopy gives characteristic information about oligonucleotides and polynucleotides. Its working principle is based on the differential interactions of molecules with left and right polarized light. Information about secondary structures of nucleic acids and their conformational changes upon interactions and binding (with small molecules and amino acids) can be revealed by using CD spectroscopy. In this study, CD spectroscopy was used to determine the conformational changes observed in DDD and DDD8 in the presence of Lys or Arg.

In order to determine DNA-amino acid interactions by CD spectroscopy, samples were prepared by adding different concentrations of amino acids into a buffer solution containing 60.0 μM nucleic acid base. Only Lys and only Arg samples at 250 mM concentration were prepared as controls to show that they did not give rise to a CD peak in the absorbing region of DNA. DNA is a chiral molecule, and it gives to CD spectrum. The local maximum ellipticities of DDD and DDD8 (at wavelengths of approximately 245 nm and 275 nm) indicate that these sequences adopt the B-form of DNA [158]. Little to no effect was observed in the structure of DDD upon methylation since the main features in the spectrum were conserved.

In Figure 50, changes in the CD absorption spectra of DDD upon addition of increasing concentrations of Lys are displayed. Sample containing DDD only (represented with the red line in Figure 13) has a local maximum around 279 nm and a local minimum at 250 nm with ellipticities 6.80 mdeg and -9.46 mdeg, respectively. The addition of 250 mM Lys to DDD (the light blue line) significantly increased the minimum ellipticity without a shift in the wavelength to -20.3 mdeg. The addition of 500 mM Lys to DDD (the blue line) slightly raised the minimum ellipticity value to -10.22 mdeg, with a shift in the wavelength to 253 nm. Sample containing DDD and 1000 mM Lys (the yellow line) increased the minimum ellipticity value of DDD to -15.9 mdeg with a shift in the wavelength to 255 nm. The addition of increasing concentrations of Lys did not change the structural form of DDD.

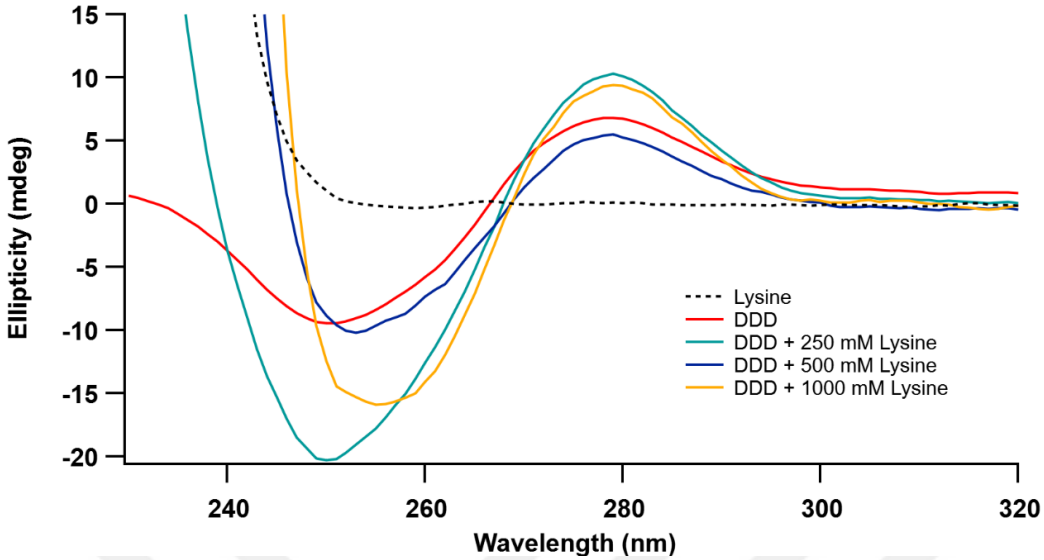

Figure 50. CD spectra of Lys, DDD and DDD + Lys at 5°C.

Figure 51 represents the addition of different concentrations of Arg to DDD. Slight changes in the ellipticities occurred with the addition of Arg. Upon addition of 250 mM Arg (denoted with the light blue line), the minimum ellipticity wavelength shifted to 253 nm and its intensity was raised to -10.6 mdeg from -9.46 mdeg. The maximum ellipticity did not change. The addition of 500 mM Arg (the yellow line) increased the minimum ellipticity to -10.9 mdeg at 254 nm and decreased the maximum ellipticity to 5.6 mdeg at 281 nm. Moreover, the addition of 1000 mM Arg to the DDD sample (the blue line) has a similar profile with the sample DDD + 500 mM Arg sample. As observed compared to the addition of Lys, the addition of Arg did not change the structure of DDD. Local maximum and minimum ellipticities kept their position (with slight shifts) in the spectra, and the CD absorption profile of DDD remained similar with increasing concentrations of Arg.

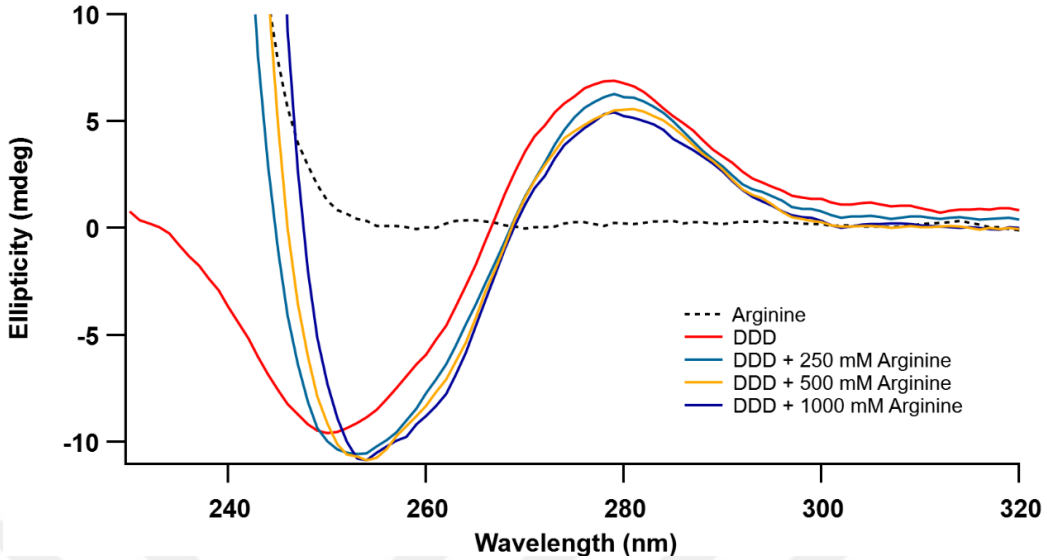

Figure 51. CD spectra of Arg, DDD and DDD + Arg at 5°C.

Figure 52 displays the CD spectra of DDD8 in the absence and presence of Lys. DDD8 was represented with the red line in the spectra. It has a local minimum at 252 nm with an ellipticity of -16.1 mdeg and a local maximum at 280 nm with an ellipticity of 8.42 mdeg. The blue and yellow lines represent the DDD8 samples with 500 mM and 1000 mM Lys, respectively. The profiles of the spectra are pretty similar to each other. The minimum ellipticity value was slightly decreased to ~ -16.5 with a shift to 254 nm. The addition of 500 mM and 1000 mM Lys to DDD8 also decreased the maximum ellipticity value. Overall, DDD8 kept its B-form structure as its profile did not change with the addition of Lys.

Figure 53 represents the changes in the CD spectra of DDD8 upon the addition of increasing concentrations of Arg. Again, DDD8 was represented with the red line. The addition of 500 mM (the blue line) and 1000 mM (the yellow line) Arg to DDD8 increased the local minimum ellipticity, with a 2 nm shift to 254 nm, to -16.5 mdeg and -16.9 mdeg, respectively. On the other hand, the local maximum ellipticity was decreased to 7.12 mdeg and 7.71 mdeg, respectively.

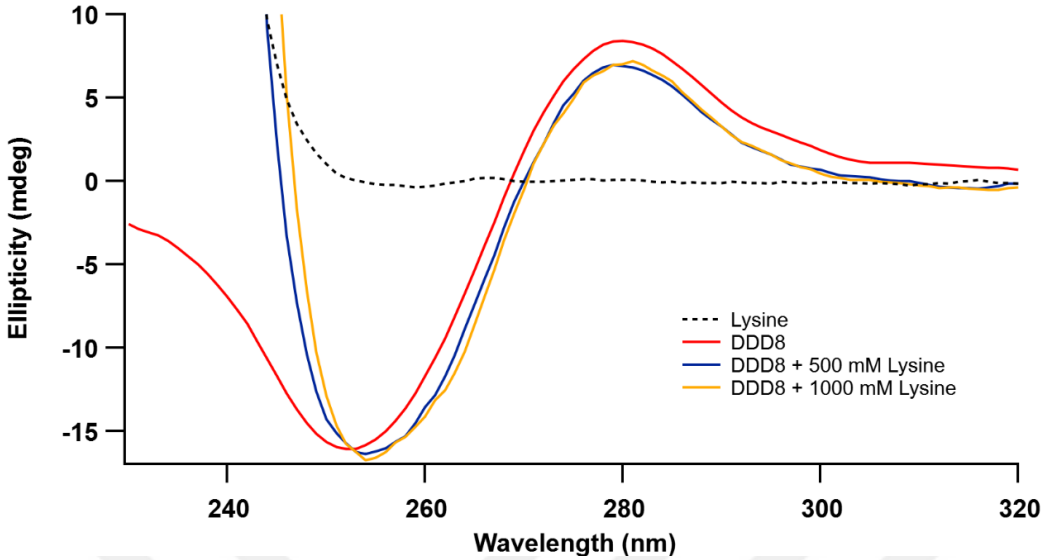

Figure 52. CD spectra of Lys, DDD8 and DDD8 + Lys at 5°C.

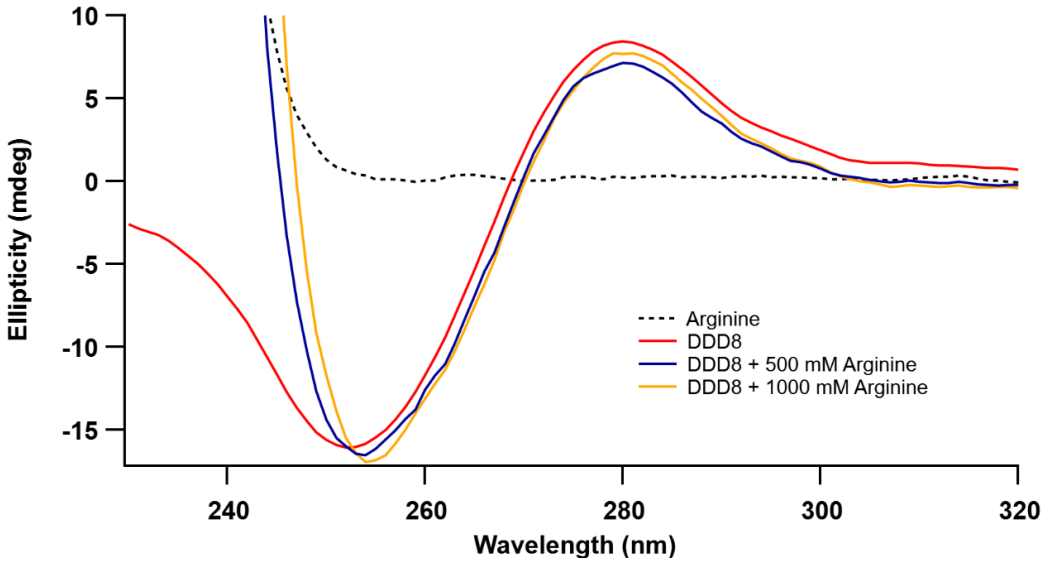

Figure 53. CD spectra of Arg, DDD8 and DDD8 + Arg at 5°C.

Figures 54 and 55 represent the change in the spectra of DDD and DDD8 upon the addition of Lys and Arg, respectively. Since Lys and Arg do not absorb at wavelengths where the absorption of DDD and DDD8 occurs, decreases in the spectra were associated with the interaction of Arg and Lys with DDD and DDD8. Although these interactions do not change the B form structure of DDD and DDD8, it shows that the DNA structure and base interactions are affected by Lys and Arg [63].

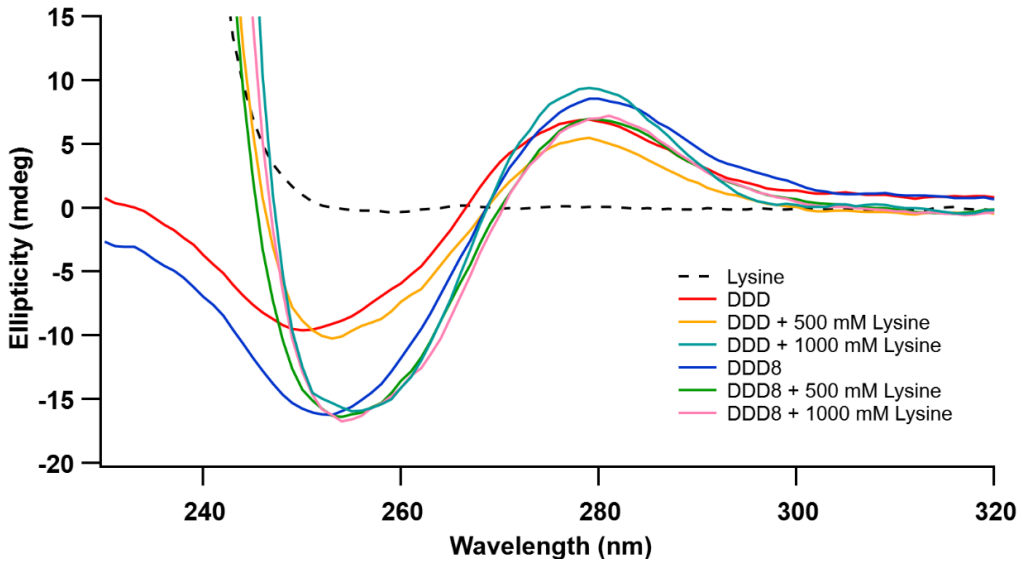

Figure 54. CD spectra of Lys, DDD, DDD8, DDD + Lys and DDD8 + Lys at 5°C.

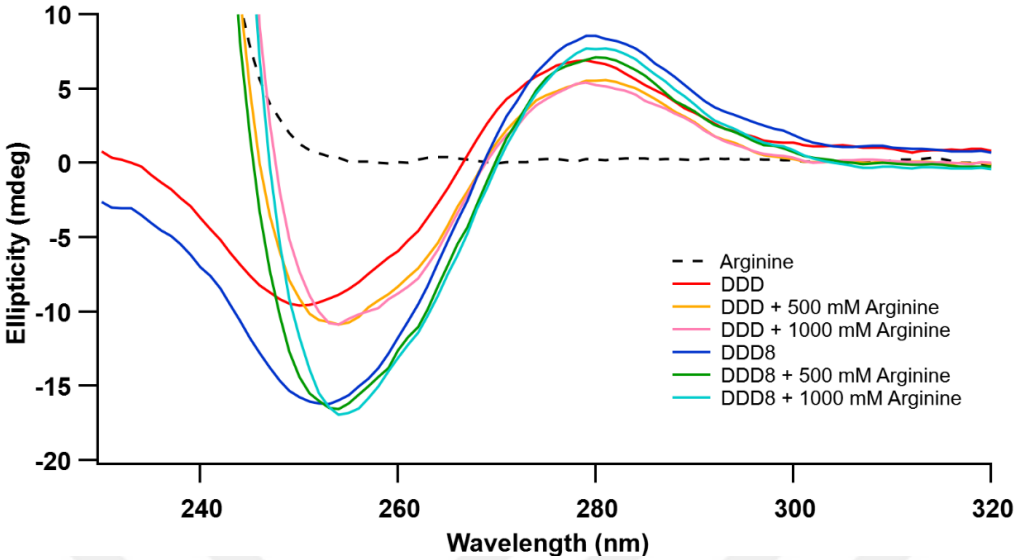

Figure 55. CD spectra of Arg, DDD, DDD8, DDD + Arg and DDD8 + Arg at 5°C.

CHAPTER 4

CONCLUSION

4.1 Investigating the Interactions of Poly(A)-COR in Crowded Environments

Within the scope of this thesis, interactions of poly(A) and COR in the presence of crowding agents were investigated. PEG200, sucrose and glycerol were used as cosolutes to mimic the cellular environment. UV-Vis absorption spectra results revealed that the absorption of poly(A) increased in crowded environments. Absorption maximum point increased with increasing concentrations of PEG and among crowding agents, the maximum increase in the absorption of poly(A) was observed in the sample which contains 20% sucrose. CD spectroscopy was used in order to determine the conformational changes upon the addition of crowding agents to poly(A) + COR. Induced self-structure of poly(A) (formed in the presence of COR) did not change with cosolutes. Yet, intensities of the CD peaks were altered upon changing the medium with crowding agents. Thermal denaturation experiments were employed in order to determine the melting temperatures, consequently, the stabilities of the samples. Melting temperatures of the samples were lowered upon addition of crowding agents. The greatest decrease in stability was observed in the sample containing 20% PEG. These results were reasonable since gradual increase of the cosolute concentration was reflected as a gradual decrease in the stability. Also, fluorescence spectroscopy experiments showed that the binding of COR to poly(A), in other words, the formation of self-structure of poly(A) was affected from the presence of PEG. In the light of these information, one can conclude that the mechanism of formation of self-structure of poly(A) and its interactions with COR in the cellular environment will probably differ from dilute and buffered conditions.

4.2 Investigating the Effect of DNA Methylation on DDD-Lysine and DDD-Arginine Interactions

In the second part of this thesis, we investigated the effects of DNA methylation, the most common epigenetic modification, on interactions of DDD with Lys and Arg amino acids. UV-Vis absorption measurements displayed that the absorption of DDD and DDD8 were increased upon increasing the amino acid concentration of the samples. We did not observe any significant changes in the CD spectra of the samples. It was determined that the B-form structure of DDD and DDD8 did not change noticeably upon interactions with Lys or Arg. Thermal denaturation experiment results revealed that positively charged amino acids stabilized the DNA structure. However, as we increase the concentration of amino acids, phosphate groups were pulled by amino acids and resulted in a decrease in the melting temperature and hence, the stability. DDD sequence is found to be more easily destabilized than DDD8 by the Lys or Arg. And the effect of Arg on the melting temperatures of DDD or DDD8 was greater than the effect of Lys on the melting temperatures of DDD or DDD8. However, further studies may be with longer DNA sequences and longer peptide sequences, or proteins are required to have a comprehensive understanding of the effect of DNA methylation on protein binding.

REFERENCES

[1] O. Avery, C. MacLeod, M. Mccarty, Studies on the Chemical Nature of the Substance Inducing Transformation of Pneumococcal Types, J. Exp. Med. 79 (1944) 137–158.

[2] J. Watson, F. Crick, Molecular Structure of Nucleic Acids, Nature. 171 (1953) 737–738. https://doi.org/10.1038/171737a0.

[3] F.H.C. Crick, On protein synthesis, in: Symp Soc Exp Biol, (1958) 8–9.

[4] F. Crick, Central Dogma of Molecular Biology, Nature. 228 (1970) 726–734.

[5] M. Meselson, F.W. Stahl, The replication of DNA in Escherichia coli, PNAS. 44 (1958) 671-682.

[6] R. Okazaki, T. Okazaki, K. Sakabe, K. Sugimoto, R. Kainuma, A. Sugino, N. Iwatsuki, In vivo mechanism of DNA chain growth, in: Cold Spring Harb. Symp. Quant. Biol., Cold Spring Harbor Laboratory Press, (1968)129–143.

[7] B.-K. Tye, P.-O. Nyman, I.R. Lehman, S. Hochhauser, B. Weiss, Transient accumulation of Okazaki fragments as a result of uracil incorporation into nascent DNA, Proc. Natl. Acad. Sci. 74 (1977) 154–157.

[8] D. Latchman, M. Sawadogo, Gene Regulation: A Eukaryotic Perspective (2nd edn), Trends Genet. 11 (1995) 332-336.

[9] W.C. Merrick, The pathway and mechanism of eukaryotic protein synthesis, Transl. Control. (1996) 31–69.

[10] V.M. Pain, Initiation of protein synthesis in eukaryotic cells, Eur. J. Biochem. 236 (1996) 747–771.

[11] I. Stansfield, K.M. Jones, M.F. Tuite, The end in sight: terminating translation in eukaryotes, Trends Biochem. Sci. 20 (1995) 489–491.

[12] Z. Chen, P. Zhao, F. Li, Y. Wang, A.I. Smith, G.I. Webb, T. Akutsu, A. Baggag, H. Bensmail, J. Song, Comprehensive review and assessment of computational methods for predicting RNA post-transcriptional modification sites from RNA sequences, Brief. Bioinform. 21 (2020) 1676–1696.

[13] T. Kiss, Small nucleolar RNA-guided post-transcriptional modification of cellular RNAs, EMBO J. 20 (2001) 3617–3622.

[14] W. Gilbert, Why Genes in Pieces, Nature. 271 (1978) 501. https://doi.org/10.1108/eb035499.

[15] F.S. Collins, E.S. Lander, J. Rogers, R.H. Waterson, Finishing the euchromatic sequence of the human genome, Nature. 431 (2004) 931–945.

[16] M. Irimia, D. Penny, S.W. Roy, Coevolution of genomic intron number and splice sites, 23 (2006) 321–325. https://doi.org/10.1016/j.tig.2007.03.015.

[17] G. Fu, K.C. Condon, M.J. Epton, P. Gong, L. Jin, G.C. Condon, N.I. Morrison, T.H. Dafa, L. Alphey, Female-specific insect lethality engineered using alternative splicing, 25 (2007) 353–357. https://doi.org/10.1038/nbt1283.

[18] B.J. Blencowe, Review Alternative Splicing : New Insights from Global Analyses, (2006) 37–47. https://doi.org/10.1016/j.cell.2006.06.023.

[19] F. Rottman, A.J. Shatkin, R.P. Perry, Sequences containing methylated nucleotides at the 5′ termini of messenger RNAs: Possible implications for processing, Cell. 3 (1974) 197–199. https://doi.org/10.1016/0092-8674(74)90131-7.

[20] K. Dower, N. Kuperwasser, H. Merrikh, M. Rosbash, A synthetic A tail rescues yeast nuclear accumulation of a ribozyme-terminated transcript, Rna. 10 (2004) 1888–1899. https://doi.org/10.1261/rna.7166704.

[21] M. Wickens, P. Anderson, R.J. Jackson, Life and death in the cytoplasm: Messages from the 3’ end, Curr. Opin. Genet. Dev. 7 (1997) 220–232. https://doi.org/10.1016/S0959-437X(97)80132-3.

[22] N. Sarkar, Polyadenylation of mRNA in prokaryotes, Annu. Rev. Biochem. 66 (1997) 173–197. https://doi.org/10.1146/annurev.biochem.66.1.173.

[23] S.L. Topalian, S. Kaneko, M.I. Gonzales, G.L. Bond, Y. Ward, J.L. Manley, Identification and Functional Characterization of Neo-Poly(A) Polymerase, an RNA Processing Enzyme Overexpressed in Human Tumors, Mol. Cell. Biol. 21 (2001) 5614–5623. https://doi.org/10.1128/mcb.21.16.5614-5623.2001.

[24] S.L. Topalian, M.I. Gonzales, Y. Ward, X. Wang, R.F. Wang, Revelation of a cryptic major histocompatibility complex class II-restricted tumor epitope in a novel RNA-processing enzyme, Cancer Res. 62 (2002) 5505–5509.

[25] F. Xing, G. Song, J. Ren, J.B. Chaires, X. Qu, Molecular recognition of nucleic acids: Coralyne binds strongly to poly(A), FEBS Lett. 579 (2005) 5035–5039. https://doi.org/10.1016/j.febslet.2005.07.091.

[26] P. Giri, M. Hossain, G.S. Kumar, Molecular aspects on the specific interaction of cytotoxic plant alkaloid palmatine to poly(A), Int. J. Biol. Macromol. 39 (2006) 210–221. https://doi.org/10.1016/j.ijbiomac.2006.03.026.

[27] P. Giri, G.S. Kumar, Specific binding and self-structure induction to poly(A) by the cytotoxic plant alkaloid sanguinarine, Biochim. Biophys. Acta - Gen. Subj. 1770 (2007) 1419–1426. https://doi.org/10.1016/j.bbagen.2007.05.005.

[28] R.C. Yadav, G.S. Kumar, K. Bhadra, P. Giri, R. Sinha, S. Pal, M. Maiti, Berberine, a strong polyriboadenylic acid binding plant alkaloid: Spectroscopic, viscometric, and thermodynamic study, Bioorganic Med. Chem. 13 (2005) 165–174. https://doi.org/10.1016/j.bmc.2004.09.045.

[29] Ö. Persil, C.T. Santai, S.S. Jain, N. V. Hud, Assembly of an antiparallel homo-adenine DNA duplex by small-molecule binding, J. Am. Chem. Soc. 126 (2004) 8644–8645. https://doi.org/10.1021/ja0492891.

[30] K.Y. Zee-Cheng, C.C. Cheng, Interaction between dna and coralyne

acetosulfate, an antileukemic compound, J. Pharm. Sci. 62 (1973) 1572–1573. https://doi.org/10.1002/jps.2600620949.

[31] J. Ren, J.B. Chaires, Sequence and structural selectivity of nucleic acid binding ligands, Biochemistry. 38 (1999) 16067–16075. https://doi.org/10.1021/bi992070s.

[32] S.S. Jain, M. Polak, N. V. Hud, Controlling nucleic acid secondary structure by intercalation: Effects of DNA strand length on coralyne-driven duplex disproportionation, Nucleic Acids Res. 31 (2003) 4608–4615. https://doi.org/10.1093/nar/gkg648.

[33] A.A. Moraru-Allen, S. Cassidy, J.L.A. Alvarez, K.R. Fox, T. Brown, A.N. Lane, Coralyne has a preference for intercalation between TA.T triples in intramolecular DNA triple helices, Nucleic Acids Res. 25 (1997) 1890–1896. https://doi.org/10.1093/nar/25.10.1890.

[34] H. Ihmels, K. Faulhaber, D. Vedaldi, F. Dall'Acqua, G. Viola, Intercalation of Organic Dye Molecules into Double-stranded DNA. Part 2: The Annelated Quinolizinium Ion as a Structural Motif in DNA Intercalators†, Photochem. Photobiol. 81 (2005) 1107-1115. https://doi.org/10.1562/2005-01-25-ir-427.

[35] J.S. Lee, L.J.P. Latimer, K.J. Hampel, Coralyne Binds Tightly to Both T·A·T- and C·G·C+-Containing DNA Triplexes, Biochemistry. 32 (1993) 5591–5597. https://doi.org/10.1021/bi00072a014.

[36] Ö.P. Çetinkol, N. V. Hud, Molecular recognition of poly(A) by small ligands: An alternative method of analysis reveals nanomolar, cooperative and shape-selective binding, Nucleic Acids Res. 37 (2009) 611–621. https://doi.org/10.1093/nar/gkn977.

[37] J.-H. Lin, W.-L. Tseng, Fluorescence Detection of Polyadenylation Reaction Through the Coordination of Adenosine 2–Coralyne–Adenosine 2, in: Polyadenylation, Springer, 2014: pp. 75–79.

[38] S.-Y. Hung, W.-L. Tseng, A polyadenosine–coralyne complex as a novel fluorescent probe for the sensitive and selective detection of heparin in plasma, Biosens. Bioelectron. 57 (2014) 186–191.

[39] M.S. Han, J.W. Hu, J. Luo, Unmodified Goldnanoparticles Used as Probes for Detection of Coralyne with poly (A40), in: Adv. Mater. Res., Trans Tech Publ, 2013: pp. 136–140.

[40] Y. Wang, X. Sun, J. Zeng, M. Deng, N. Li, Q. Chen, H. Zhu, F. Liu, X. Xing, Label-free and sensitive detection assay for terminal deoxynucleotidyl transferase via polyadenosine-coralyne fluorescence enhancement strategy, Anal. Biochem. 567 (2019) 85–89.

[41] E. Westhof, Water: an integral part of nucleic acid structure., Annu. Rev. Biophys. Biophys. Chem. 17 (1988) 125–144. https://doi.org/10.1146/annurev.bb.17.060188.001013.

[42] L.A. Marky, D.W. Kupke, potential for providing information about the linkage between sodium ion binding and the binding of other cationic ligands , including proteins , cationic peptides , or positively charged drugs . The method could also be of value in examining the role of, Methods Enzymol. 323 (2000) 419–441.

[43] S.I. Nakano, L. Wu, H. Oka, H.T. Karimata, T. Kirihata, Y. Sato, S. Fujii, H. Sakai, M. Kuwahara, H. Sawai, N. Sugimoto, Conformation and the sodium ion condensation on DNA and RNA structures in the presence of a neutral cosolute as a mimic of the intracellular media, Mol. Biosyst. 4 (2008) 579–588. https://doi.org/10.1039/b718806d.

[44] M.T. Record, W. Zhang, C.F. Anderson, Analysis of effects of salts and uncharged solutes on protein and nucleic acid equilibria and processes: A practical guide to recognizing and interpreting polyelectrolyte effects, hofmeister effects, and osmotic effects of salts, Elsevier Masson SAS, (1998) 281-353. https://doi.org/10.1016/s0065-3233(08)60655-5.

[45] D.H. Mathews, J. Sabina, M. Zuker, D.H. Turner, Expanded sequence dependence of thermodynamic parameters improves prediction of RNA secondary structure, J. Mol. Biol. 288 (1999) 911–940. https://doi.org/10.1006/jmbi.1999.2700.

[46] N. Sugimoto, S. ichi Nakano, M. Katoh, A. Matsumura, H. Nakamuta, T. Ohmichi, M. Yoneyama, M. Sasaki, Thermodynamic Parameters To Predict Stability of RNA/DNA Hybrid Duplexes, Biochemistry. 34 (1995) 11211–11216. https://doi.org/10.1021/bi00035a029.

[47] N. Sugimoto, S.I. Nakano, M. Yoneyama, K.I. Honda, Improved thermodynamic parameters and helix initiation factor to predict stability of DNA duplexes, Nucleic Acids Res. 24 (1996) 4501–4505. https://doi.org/10.1093/nar/24.22.4501.

[48] T. Xia, J. SantaLucia, M.E. Burkard, R. Kierzek, S.J. Schroeder, X. Jiao, C. Cox, D.H. Turner, Thermodynamic parameters for an expanded nearest-neighbor model for formation of RNA duplexes with Watson - Crick base pairs, Biochemistry. 37 (1998) 14719–14735. https://doi.org/10.1021/bi9809425.

[49] M. Zuker, Mfold web server for nucleic acid folding and hybridization prediction, Nucleic Acids Res. 31 (2003) 3406–3415. https://doi.org/10.1093/nar/gkg595.

[50] D.H. Mathews, Using an RNA secondary structure partition function to determine confidence in base pairs predicted by free energy minimization, Rna. 10 (2004) 1178–1190. https://doi.org/10.1261/rna.7650904.

[51] M.G. Seetin, D.H. Mathews, RNA structure prediction: An overview of methods, Methods Mol. Biol. 905 (2012) 99–122. https://doi.org/10.1007/978-1-61779-949-5_8.

[52] N. Sugimoto, M. Nakano, S.I. Nakano, Thermodynamics - Structure relationship of single mismatches in RNA/DNA duplexes, Biochemistry. 39

(2000) 11270–11281. https://doi.org/10.1021/bi000819p.

[53] N.E. Watkins, W.J. Kennelly, M.J. Tsay, A. Tuin, L. Swenson, H.R. Lee, S. Morosyuk, D.A. Hicks, J. Santalucia, Thermodynamic contributions of single internal rAdA, rCdC, rGdG and rUdT mismatches in RNA/DNA duplexes, Nucleic Acids Res. 39 (2011) 1894–1902. https://doi.org/10.1093/nar/gkq905.

[54] A.B. Fulton, How crowded is the prokaryotic cytoplasm?, Cell. 30 (1982) 345–347.

[55] S.B. Zimmerman, A.P. Minton, Macromolecular crowding, Annu. Rev. Biomoleular Struct. 22 (1993) 27–65. https://doi.org/10.1016/j.cub.2006.03.047.

[56] H.J. Guttman, C.F. Anderson, M.T. Record, Analyses of thermodynamic data for concentrated hemoglobin solutions using scaled particle theory: implications for a simple two-state model of water in thermodynamic analyses of crowding in vitro and in vivo, Biophys. J. 68 (1995) 835–846. https://doi.org/10.1016/S0006-3495(95)80260-2.

[57] J.R. Wenner, V.A. Bloomfield, Crowding effects on EcoRV kinetics and binding, Biophys. J. 77 (1999) 3234–3241. https://doi.org/10.1016/S0006-3495(99)77154-7.

[58] H.X. Zhou, G. Rivas, A.P. Minton, Macromolecular crowding and confinement: Biochemical, biophysical, and potential physiological consequences, Annu. Rev. Biophys. 37 (2008) 375–397. https://doi.org/10.1146/annurev.biophys.37.032807.125817.

[59] D. Miyoshi, N. Sugimoto, Molecular crowding effects on structure and stability of DNA, Biochimie. 90 (2008) 1040–1051. https://doi.org/10.1016/j.biochi.2008.02.009.

[60] J.R. Ellis, A.P. Minton, Join the Crowd, Nature. 425 (2003) 27–28.

https://doi.org/10.4103/2348-8832.201790.

[61] S. Pramanik, K. Nakamura, K. Usui, S.I. Nakano, S. Saxena, J. Matsui, D. Miyoshi, N. Sugimoto, Thermodynamic stability of Hoogsteen and Watson-Crick base pairs in the presence of histone H3-mimicking peptide, Chem. Commun. 47 (2011) 2790–2792. https://doi.org/10.1039/c0cc05776b.

[62] H. Karimata, S.I. Nakano, N. Sugimoto, Effects of polyethylene glycol on DNA duplex stability at different NaCl concentrations, Bull. Chem. Soc. Jpn. 80 (2007) 1987–1994. https://doi.org/10.1246/bcsj.80.1987.

[63] V.A. Bloomfield, D.M. Crothers, I. Tinoco, Nucleic Acids: Structures, Properties and Functions, in: Nucleic Acids Struct. Prop. Funct., University Science Books Press: Herndon VA, (2000) 443-444.

[64] M.H. Chow, K.T.H. Yan, M.J. Bennett, J.T.Y. Wong, Liquid crystalline chromosomes: Birefringence and DNA condensation, Eukaryot. Cell. (2010) 1577-1587.

[65] A.L. Olins, D.E. Olins, Spheroid chromatin units (v bodies), Science (80-.). 183 (1974) 330–332. https://doi.org/10.1126/science.183.4122.330.

[66] V.B. Teif, K. Bohinc, Condensed DNA: condensing the concepts, Prog. Biophys. Mol. Biol. 105 (2011) 208–222.

[67] M. Ptashne, On the use of the word “epigenetic,” Curr. Biol. 17 (2007) 233–236. https://doi.org/10.1016/j.cub.2007.02.030.

[68] A.P. Feinberg, B. Tycko, The history of cancer epigenetics, Nat. Rev. Cancer. 4 (2004) 143–153. https://doi.org/10.1038/nrc1279.

[69] A. Portela, M. Esteller, Epigenetic modifications and human disease, Nat. Biotechnol. 28 (2010) 1057–1068. https://doi.org/10.1038/nbt.1685.

[70] R.G. Urdinguio, J. V. Sanchez-Mut, M. Esteller, Epigenetic mechanisms in neurological diseases: genes, syndromes, and therapies, Lancet Neurol. 8

(2009) 1056–1072. https://doi.org/10.1016/S1474-4422(09)70262-5.

[71] E. Karouzakis, R.E. Gay, S. Gay, M. Neidhart, Epigenetic control in rheumatoid arthritis synovial fibroblasts, Nat. Rev. Rheumatol. 5 (2009) 266–272. https://doi.org/10.1038/nrrheum.2009.55.

[72] F. Miao, D.D. Smith, L. Zhang, A. Min, W. Feng, R. Natarajan, Lymphocytes from patients with type 1 diabetes display a distinct profile of chromatin histone H3 lysine 9 dimethylation an epigenetic study in diabetes, Diabetes. 57 (2008) 3189–3198. https://doi.org/10.2337/db08-0645.

[73] B.M. Javierre, A.F. Fernandez, J. Richter, F. Al-Shahrour, J. Ignacio Martin-Subero, J. Rodriguez-Ubreva, M. Berdasco, M.F. Fraga, T.P. O'Hanlon, L.G. Rider, F. V. Jacinto, F. Javier Lopez-Longo, J. Dopazo, M. Forn, M.A. Peinado, L. Carreño, A.H. Sawalha, J.B. Harley, R. Siebert, M. Esteller, F.W. Miller, E. Ballestar, Changes in the pattern of DNA methylation associate with twin discordance in systemic lupus erythematosus, Genome Res. 20 (2010) 170–179. https://doi.org/10.1101/gr.100289.109.

[74] L.D. Moore, T. Le, G. Fan, DNA methylation and its basic function, Neuropsychopharmacology. 38 (2013) 23–38. https://doi.org/10.1038/npp.2012.112.

[75] M. Ehrlich, M. Gama-Sosa, L.-H. Huang, Amount and distribution of 5-methylcytosine in human DNA from different types of tissues or cells, Nucleic Acids Res. 9 (1982) 2589–2598. https://linkinghub.elsevier.com/retrieve/pii/S1874391913002522.

[76] T.T.M. Ngo, J. Yoo, Q. Dai, Q. Zhang, C. He, A. Aksimentiev, T. Ha, Effects of cytosine modifications on DNA flexibility and nucleosome mechanical stability, Nat. Commun. 7 (2016) 1–9. https://doi.org/10.1038/ncomms10813.

[77] A.C.D. Machado, T. Zhou, S. Rao, P. Goel, C. Rastogi, A. Lazarovici, H.J. Bussemaker, R. Rohs, Evolving insights on how cytosine methylation affects protein-DNA binding, Brief. Funct. Genomics. 14 (2014) 61–73.

https://doi.org/10.1093/bfgp/elu040.

[78] M.M. Taqi, S.K.T.S. Wärmländer, O. Yamskova, F. Madani, I. Bazov, J. Luo, R. Zubarev, D. Verbeek, A. Gräslund, G. Bakalkin, Conformation effects of CpG methylation on single-stranded DNA oligonucleotides: Analysis of the opioid peptide dynorphin-coding sequences, PLoS One. 7 (2012) 1-11. https://doi.org/10.1371/journal.pone.0039605.

[79] A. Bird, M. Taggart, M. Frommer, O.J. Miller, D. Macleod, A fraction of the mouse genome that is derived from islands of nonmethylated, CpG-rich DNA, Cell. 40 (1985) 91–99. https://doi.org/10.1016/0092-8674(85)90312-5.

[80] S. Saxonov, P. Berg, D.L. Brutlag, A genome-wide analysis of CpG dinucleotides in the human genome distinguishes two distinct classes of promoters, Proc. Natl. Acad. Sci. U. S. A. 103 (2006) 1412–1417. https://doi.org/10.1073/pnas.0510310103.

[81] J. Tazi, A. Bird, Alternative chromatin structure at CpG islands, Cell. 60 (1990) 909–920. https://doi.org/10.1016/0092-8674(90)90339-G.

[82] V.R. Ramirez-Carrozzi, D. Braas, D.M. Bhatt, C.S. Cheng, C. Hong, K.R. Doty, J.C. Black, A. Hoffmann, M. Carey, S.T. Smale, A Unifying Model for the Selective Regulation of Inducible Transcription by CpG Islands and Nucleosome Remodeling, Cell. 138 (2009) 114–128. https://doi.org/10.1016/j.cell.2009.04.020.

[83] J.K. Choi, Contrasting chromatin organization of CpG islands and exons in the human genome, Genome Biol. 11 (2010) 1-8. https://doi.org/10.1186/gb-2010-11-7-r70.

[84] V.K. Rakyan, T. Hildmann, K.L. Novik, J. Lewin, J. Tost, A. V. Cox, T.D. Andrews, K.L. Howe, T. Otto, A. Olek, J. Fischer, I.G. Gut, K. Berlin, S. Beck, DNA methylation profiling of the human major histocompatibility complex: A pilot study for the Human Epigenome Project, PLoS Biol. 2 (2004) e405. https://doi.org/10.1371/journal.pbio.0020405.

[85] F. Eckhardt, J. Lewin, R. Cortese, V.K. Rakyan, J. Attwood, M. Burger, J. Burton, T. V. Cox, R. Davies, T.A. Down, C. Haefliger, R. Horton, K. Howe, D.K. Jackson, J. Kunde, C. Koenig, J. Liddle, D. Niblett, T. Otto, R. Pettett, S. Seemann, C. Thompson, T. West, J. Rogers, A. Olek, K. Berlin, S. Beck, DNA methylation profiling of human chromosomes 6, 20 and 22, Nat. Genet. 38 (2006) 1378–1385. https://doi.org/10.1038/ng1909.

[86] A. Meissner, T.S. Mikkelsen, H. Gu, M. Wernig, J. Hanna, A. Sivachenko, X. Zhang, B.E. Bernstein, C. Nusbaum, D.B. Jaffe, A. Gnirke, R. Jaenisch, E.S. Lander, Genome-scale DNA methylation maps of pluripotent and differentiated cells, Nature. 454 (2008) 766–770. https://doi.org/10.1038/nature07107.

[87] R.S. Illingworth, U. Gruenewald-Schneider, S. Webb, A.R.W. Kerr, K.D. James, D.J. Turner, C. Smith, D.J. Harrison, R. Andrews, A.P. Bird, Orphan CpG Islands Identify numerous conserved promoters in the mammalian genome, PLoS Genet. 6 (2010) e1001134. https://doi.org/10.1371/journal.pgen.1001134.

[88] A.K. Maunakea, R.P. Nagarajan, M. Bilenky, T.J. Ballinger, C. Dsouza, S.D. Fouse, B.E. Johnson, C. Hong, C. Nielsen, Y. Zhao, G. Turecki, A. Delaney, R. Varhol, N. Thiessen, K. Shchors, V.M. Heine, D.H. Rowitch, X. Xing, C. Fiore, M. Schillebeeckx, S.J.M. Jones, D. Haussler, M.A. Marra, M. Hirst, T. Wang, J.F. Costello, Conserved role of intragenic DNA methylation in regulating alternative promoters, Nature. 466 (2010) 253–257. https://doi.org/10.1038/nature09165.

[89] R.A. Irizarry, C. Ladd-Acosta, B. Wen, Z. Wu, C. Montano, P. Onyango, H. Cui, K. Gabo, M. Rongione, M. Webster, H. Ji, J.B. Potash, S. Sabunciyan, A.P. Feinberg, The human colon cancer methylome shows similar hypo- and hypermethylation at conserved tissue-specific CpG island shores, Nat. Genet. 41 (2009) 178–186. https://doi.org/10.1038/ng.298.

[90] F. Mohn, M. Weber, M. Rebhan, T.C. Roloff, J. Richter, M.B. Stadler, M. Bibel, D. Schübeler, Lineage-Specific Polycomb Targets and De Novo DNA Methylation Define Restriction and Potential of Neuronal Progenitors, Mol. Cell. 30 (2008) 755–766. https://doi.org/10.1016/j.molcel.2008.05.007.

[91] T. Caspary, M.A. Cleary, C.C. Baker, X.-J. Guan, S.M. Tilghman, Multiple Mechanisms Regulate Imprinting of the Mouse Distal Chromosome 7 Gene Cluster, Mol. Cell. Biol. 18 (1998) 3466–3474. https://doi.org/10.1128/mcb.18.6.3466.

[92] A. Wutz, D. P. Barlow, Imprinting of the mouse Igf2r gene depends on an intronic CpG island, Mol. Cell. Endocrinol. 140 (1998) 9–14. https://doi.org/10.1016/S0303-7207(98)00022-7.

[93] J.D. Choi, L.A. Underkoffler, A.J. Wood, J.N. Collins, P.T. Williams, J.A. Golden, E.F. Schuster, K.M. Loomes, R.J. Oakey, A Novel Variant of Inpp5f Is Imprinted in Brain, and Its Expression Is Correlated with Differential Methylation of an Internal CpG Island , Mol. Cell. Biol. 25 (2005) 5514–5522. https://doi.org/10.1128/mcb.25.13.5514-5522.2005.

[94] C.P. Ponting, P.L. Oliver, W. Reik, Evolution and Functions of Long Noncoding RNAs, Cell. 136 (2009) 629–641. https://doi.org/10.1016/j.cell.2009.02.006.

[95] T.R. Mercer, L. Rnas, M.E. Dinger, J.S. Mattick, Long non-coding RNAs: insights into functions, Nat. Rev. Genet. 10 (2009) 155–159.

[96] A. Mortazavi, B.A. Williams, K. McCue, L. Schaeffer, B. Wold, Mapping and quantifying mammalian transcriptomes by RNA-Seq, Nat. Methods. 5 (2008) 621–628. https://doi.org/10.1038/nmeth.1226.

[97] B.T. Wilhelm, S. Marguerat, S. Watt, F. Schubert, V. Wood, I. Goodhead, C.J. Penkett, J. Rogers, J. Bähler, Dynamic repertoire of a eukaryotic transcriptome surveyed at single-nucleotide resolution, Nature. 453 (2008) 1239–1243. https://doi.org/10.1038/nature07002.

[98] S. Djebali, P. Kapranov, S. Foissac, J. Lagarde, A. Reymond, C. Ucla, C. Wyss, J. Drenkow, E. Dumais, R.R. Murray, C. Lin, D. Szeto, F. Denoeud, M. Calvo, A. Frankish, J. Harrow, P. Makrythanasis, M. Vidal, K. Salehi-Ashtiani, S.E. Antonarakis, T.R. Gingeras, R. Guigó, Efficient targeted transcript discovery via array-based normalization of RACE libraries, Nat. Methods. 5 (2008) 629–635. https://doi.org/10.1038/nmeth.1216.

[99] Q. Pan, O. Shai, L.J. Lee, B.J. Frey, B.J. Blencowe, Deep surveying of alternative splicing complexity in the human transcriptome by high-throughput sequencing, Nat. Genet. 40 (2008) 1413–1415. https://doi.org/10.1038/ng.259.

[100] J.O. Korbel, A.E. Urban, J.P. Affourtit, B. Godwin, F. Grubert, J.F. Simons, P.M. Kim, D. Palejev, N.J. Carriero, L. Du, B.E. Taillon, Z. Chen, A. Tanzer, A.C.E. Saunders, J. Chi, F. Yang, N.P. Carter, M.E. Hurles, S.M. Weissman, T.T. Harkins, M.B. Gerstein, M. Egholm, M. Snyder, Paired-end mapping reveals extensive structural variation in the human genome, Science (80-.). 318 (2007) 420–426. https://doi.org/10.1126/science.1149504.

[101] M. Guttman, I. Amit, M. Garber, C. French, M.F. Lin, D. Feldser, M. Huarte, O. Zuk, B.W. Carey, J.P. Cassady, M.N. Cabili, R. Jaenisch, T.S. Mikkelsen, T. Jacks, N. Hacohen, B.E. Bernstein, M. Kellis, A. Regev, J.L. Rinn, E.S. Lander, Chromatin signature reveals over a thousand highly conserved large non-coding RNAs in mammals, Nature. 458 (2009) 223–227. https://doi.org/10.1038/nature07672.

[102] A.M. Khalil, M. Guttman, M. Huarte, M. Garber, A. Raj, D.R. Morales, K. Thomas, A. Presser, B.E. Bernstein, A. Van Oudenaarden, A. Regev, E.S. Lander, J.L. Rinn, Many human large intergenic noncoding RNAs associate with chromatin-modifying complexes and affect gene expression, Proc. Natl. Acad. Sci. U. S. A. 106 (2009) 11667–11672. https://doi.org/10.1073/pnas.0904715106.

[103] R.J. Taft, E.A. Glazov, N. Cloonan, C. Simons, S. Stephen, G.J. Faulkner, T. Lassmann, A.R.R. Forrest, S.M. Grimmond, K. Schroder, K. Irvine, T. Arakawa, M. Nakamura, A. Kubosaki, K. Hayashida, C. Kawazu, M. Murata, H. Nishiyori, S. Fukuda, J. Kawai, C.O. Daub, D.A. Hume, H. Suzuki, V. Orlando, P. Carninci, Y. Hayashizaki, J.S. Mattick, Tiny RNAs associated with transcription start sites in animals, Nat. Genet. 41 (2009) 572–578. https://doi.org/10.1038/ng.312.

[104] H. Neil, C. Malabat, Y. D'Aubenton-Carafa, Z. Xu, L.M. Steinmetz, A. Jacquier, Widespread bidirectional promoters are the major source of cryptic transcripts in yeast, Nature. 457 (2009) 1038–1042. https://doi.org/10.1038/nature07747.

[105] Z. Xu, W. Wei, J. Gagneur, F. Perocchi, S. Clauder-Münster, J. Camblong, E. Guffanti, F. Stutz, W. Huber, L.M. Steinmetz, Bidirectional promoters generate pervasive transcription in yeast, Nature. 457 (2009) 1033–1037. https://doi.org/10.1038/nature07728.

[106] G.J. Faulkner, Y. Kimura, C.O. Daub, S. Wani, C. Plessy, K.M. Irvine, K. Schroder, N. Cloonan, A.L. Steptoe, T. Lassmann, K. Waki, N. Hornig, T. Arakawa, H. Takahashi, J. Kawai, A.R.R. Forrest, H. Suzuki, Y. Hayashizaki, D.A. Hume, V. Orlando, S.M. Grimmond, P. Carninci, The regulated retrotransposon transcriptome of mammalian cells, Nat. Genet. 41 (2009) 563–571. https://doi.org/10.1038/ng.368.

[107] F. Ferri, H. Bouzinba-Segard, G. Velasco, F. Hubé, C. Francastel, Non-coding murine centromeric transcripts associate with and potentiate Aurora B kinase, Nucleic Acids Res. 37 (2009) 5071–5080. https://doi.org/10.1093/nar/gkp529.

[108] V.A. Burzio, C. Villota, J. Villegas, E. Landerer, E. Boccardo, L.L. Villa, R. Martínez, C. Lopez, F. Gaete, V. Toro, X. Rodriguez, L.O. Burzio, Expression of a family of noncoding mitochondrial RNAs distinguishes normal from

cancer cells, Proc. Natl. Acad. Sci. U. S. A. 106 (2009) 9430–9434. https://doi.org/10.1073/pnas.0903086106.

[109] F.F. Costa, Non-coding RNAs: Meet thy masters, BioEssays. 32 (2010) 599–608. https://doi.org/10.1002/bies.200900112.

[110] A. Wolffe, Chromatin: structure and function, Academic press, (1998) 26-30.

[111] K.E. van Holde, Chromatin structure and transcription, in: Chromatin, Springer, (1989) 355–408.

[112] R.D. Kornberg, Y. Lorch, Twenty-five years of the nucleosome, fundamental particle of the eukaryote chromosome, Cell. 98 (1999) 285–294. https://doi.org/10.1016/S0092-8674(00)81958-3.

[113] K. Luger, A.W. Mäder, R.K. Richmond, D.F. Sargent, T.J. Richmond, Crystal structure of the nucleosome core particle at 2.8 Å resolution, Nature. 389 (1997) 251–260.

[114] A.L. Lehninger, D.L. Nelson, M.M. Cox, M.M. Cox, Lehninger principles of biochemistry, Macmillan, (2005) 271-287.

[115] R.M. Youngson, Collins dictionary of human biology, Collins, (2006) 216-217.

[116] T. Jenuwein, C.D. Allis, Translating the Histone Code, 293 (2001) 1074–1080.

[117] T. Kouzarides, Chromatin Modifications and Their Function, Cell. 128 (2007) 693–705. https://doi.org/10.1016/j.cell.2007.02.005.

[118] A. Razin, A.D. Riggs, DNA Methylation and Gene Function, Cell. 210 (1980) 604–609. https://doi.org/10.1016/0092-8674(88)90479-5.

[119] C. Martin, Y. Zhang, The diverse functions of histone lysine methylation, Nat. Rev. Mol. Cell Biol. 6 (2005) 838–849. https://doi.org/10.1038/nrm1761.

[120] F. Miao, Z. Chen, S. Genuth, A. Paterson, L. Zhang, X. Wu, S.M. Li, P.

Cleary, A. Riggs, D.M. Harlan, G. Lorenzi, O. Kolterman, W. Sun, J.M. Lachin, R. Natarajan, Evaluating the role of epigenetic histone modifications in the metabolic memory of type 1 diabetes, Diabetes. 63 (2014) 1748–1762. https://doi.org/10.2337/db13-1251.

[121] D.A. Dougherty, Cation-π interactions in chemistry and biology: A new view of benzene, Phe, Tyr, and Trp, Science (80-.). 271 (1996) 163–168. https://doi.org/10.1126/science.271.5246.163.

[122] N. Zacharias, D.A. Dougherty, Cation-π interactions in ligand recognition and catalysis, Trends Pharmacol. Sci. 23 (2002) 281–287. https://doi.org/10.1016/S0165-6147(02)02027-8.

[123] L. Mao, Y. Wang, Y. Liu, X. Hu, Molecular Determinants for ATP-binding in Proteins: A Data Mining and Quantum Chemical Analysis, J. Mol. Biol. 336 (2004) 787–807. https://doi.org/10.1016/j.jmb.2003.12.056.

[124] L. McFail-Isom, X. Shui, L.D. Williams, Divalent cations stabilize unstacked conformations of DNA and RNA by interacting with base II systems, Biochemistry. 37 (1998) 17105–17111. https://doi.org/10.1021/bi982201+.

[125] R. Wintjens, J. Liévin, M. Rooman, E. Buisine, Contribution of cation-π interactions to the stability of protein-DNA complexes, J. Mol. Biol. 302 (2000) 393–408. https://doi.org/10.1006/jmbi.2000.4040.

[126] M. Rooman, E. Buisine, J. Lie, Cation – p / H-bond Stair Motifs at Protein – DNA Interfaces, 2836 (2002) 67–76. https://doi.org/10.1061/S0022-2836(02)00263-2.

[127] B. Basham, G.P. Schroth, P.S. Ho, An A-DNA triplet code: thermodynamic rules for predicting A-and B-DNA, Proc. Natl. Acad. Sci. 92 (1995) 6464–6468.

[128] A.H.-J. Wang, G.J. Quigley, F.J. Kolpak, J.L. Crawford, J.H. Van Boom, G. van der Marel, A. Rich, Molecular structure of a left-handed double helical

DNA fragment at atomic resolution, Nature. 282 (1979) 680–686.

[129] K. Rippe, V. Fritsch, E. Westhof, T.M. Jovin, Alternating d (G-A) sequences form a parallel-stranded DNA homoduplex., EMBO J. 11 (1992) 3777–3786.

[130] M.D. Frank-Kamenetskii, S.M. Mirkin, Triplex DNA structures, Annu. Rev. Biochem. 64 (1995) 65–95.

[131] K. Gehring, J.-L. Leroy, M. Gueron, A tetrameric DNA structure with protonated cytosine-cytosine base pairs, Nature. 363 (1993) 561–565.

[132] F.W. Smith, J. Feigon, Quadruplex structure of Oxytricha telomeric DNA oligonucleotides, Nature. 356 (1992) 164–168.

[133] A. Rich, D.R. Davies, F.H.C. Crick, J.D. Watson, The molecular structure of polyadenylic acid, J. Mol. Biol. 3 (1961) 71-IN19.

[134] E. Paleček, J. Doskočil, Pulse-polarographic analysis of double-stranded RNA, Anal. Biochem. 60 (1974) 518–530.

[135] W.M. Scovell, Structural and conformational studies of polyriboadenylic acid in neutral and acid solution, Biopolym. Orig. Res. Biomol. 17 (1978) 969–984.

[136] A.G. Petrovic, P.L. Polavarapu, Structural transitions in polyriboadenylic acid induced by the changes in pH and temperature: vibrational circular dichroism study in solution and film states, J. Phys. Chem. B. 109 (2005) 23698–23705.

[137] M.I. Zarudnaya, D.M. Hovorun, Hypothetical double-helical poly (A) formation in a cell and its possible biological significance, IUBMB Life. 48 (1999) 581–584.

[138] P. Giri, G.S. Kumar, Binding of protoberberine alkaloid coralyne with double stranded poly (A): a biophysical study, Mol. Biosyst. 4 (2008) 341–348.

[139] F. Xing, G. Song, J. Ren, J.B. Chaires, X. Qu, Molecular recognition of nucleic acids: Coralyne binds strongly to poly(A), FEBS Lett. 579 (2005)

5035–5039. https://doi.org/10.1016/j.febslet.2005.07.091.

[140] M. Polak, N. V. Hud, Complete disproportionation of duplex poly(dT).poly(dA) into triplex poly(dT).poly(dA).poly(dT) and poly(dA) by coralyne, Nucleic Acids Res. 30 (2002) 983–992.

[141] W.D. Wilson, S. Mizan, F.A. Taniuos, S. Yao, G. Zon, The interaction of intercalators and groove-binding agents with DNA triple-helical structures: the influence of ligand structure, DNA backbone modifications and sequence, J. Mol. Recognit. 7 (1994) 89–98.

[142] K. Sandström, S. Wärmländer, J. Bergman, R. Engqvist, M. Leijon, A. Gräslund, The influence of intercalator binding on DNA triplex stability: correlation with effects on A-tract duplex structure, J. Mol. Recognit. 17 (2004) 277–285.

[143] V. Římal, O. Socha, J. Štěpánek, H. Štěpánková, Spectroscopic study of cytosine methylation effect on thermodynamics of DNA duplex containing CpG motif, J. Spectrosc. 2015 (2015) 1-8.

[144] L. Nardo, M. Lamperti, D. Salerno, V. Cassina, N. Missana, M. Bondani, A. Tempestini, F. Mantegazza, Effects of non-CpG site methylation on DNA thermal stability: a fluorescence study, Nucleic Acids Res. 43 (2015) 10722–10733.

[145] P. Giri, G. Suresh Kumar, Isoquinoline Alkaloids and their Binding with Polyadenylic Acid: Potential Basis of Therapeutic Action, Mini-Reviews Med. Chem. 10 (2010) 568–577. https://doi.org/10.2174/138955710791384009.

[146] P. Giri, G. Suresh Kumar, Molecular recognition of poly(A) targeting by protoberberine alkaloids: In vitro biophysical studies and biological perspectives, Mol. Biosyst. 6 (2009) 81–88. https://doi.org/10.1039/b910706a.

[147] P. Giri, G. Kumar, Molecular Aspects of Small Molecules-Poly(A) Interaction: An Approach to RNA Based Drug Design, Curr. Med. Chem. 16 (2009) 965–987. https://doi.org/10.2174/092986709787581932.

[148] T. Biver, Use of UV-vis spectrometry to gain information on the mode of binding of small molecules to DNAs and RNAs, Appl. Spectrosc. Rev. 47 (2012) 272–325. https://doi.org/10.1080/05704928.2011.641044.

[149] Y.M. Chang, C.K.M. Chen, M.H. Hou, Conformational changes in DNA upon ligand binding monitored by circular dichroism, Int. J. Mol. Sci. 13 (2012) 3394–3413. https://doi.org/10.3390/ijms13033394.

[150] J. Jaumot, R. Gargallo, Experimental Methods for Studying the Interactions between G-Quadruplex Structures and Ligands, Curr. Pharm. Des. 18 (2012) 1900–1916. https://doi.org/10.2174/138161212799958486.

[151] Z. He, J. Liu, J. Zhang, N. Zhang, Spectroscopic study on the intermolecular interaction of SO2 absorption in poly-ethylene glycol+H2O systems, Korean J. Chem. Eng. 31 (2014) 514–521. https://doi.org/10.1007/s11814-013-0249-7.

[152] C.H. Spink, J.B. Chaires, Effects of hydration, ion release, and excluded volume on the melting of triplex and duplex DNA, Biochemistry. 38 (1999) 496–508. https://doi.org/10.1021/bi9820154.

[153] C.H. Spink, J.B. Chaires, Selective Stabilization of Triplex DNA by Poly(ethylene glycols), J. Am. Chem. Soc. 117 (1995) 12887–12888. https://doi.org/10.1021/ja00156a038.

[154] P. Woolley, P.R. Wills, Excluded-volume effect of inert macromolecules on the melting of nucleic acids, Biophys. Chem. 22 (1985) 89–94. https://doi.org/10.1016/0301-4622(85)80029-6.

[155] J.Q. Wu, R.B. Macgregor, Pressure Dependence of the Melting Temperature of Solids, Biochemistry. 32 (1993) 12531–12537.

https://doi.org/10.1002/pssb.2221780234.

[156] P. Del Vecchio, D. Esposito, L. Ricchi, G. Barone, The effects of polyols on the thermal stability of calf thymus DNA, Int. J. Biol. Macromol. 24 (1999) 361–369. https://doi.org/10.1016/S0141-8130(99)00058-6.

[157] L. Homchaudhuri, R. Swaminathan, Novel absorption and fluorescence characteristics of L-lysine, Chem. Lett. (2001) 844–845. https://doi.org/10.1246/cl.2001.844.

[158] V.A. Bloomfield, D.M. Crothers, I. Tinoco, Nucleic Acids: Structures, Properties and Functions, in: Nucleic Acids Struct. Prop. Funct., University Science Books Press: Herndon VA, (2000) 598-601.

[159] Z.-J. Tan, S.-J. Chen, Nucleic acid helix stability: effects of salt concentration, cation valence and size, and chain length, Biophys. J. 90 (2006) 1175–1190.

[160] D.W. Gruenwedel, C. -H Hsu, Salt effects on the denaturation of DNA, Biopolymers. 7 (1969) 557–570. https://doi.org/10.1002/bip.1969.360070412.

[161] R. Owczarzy, B.G. Moreira, Y. You, M.A. Behlke, J.A. Wälder, Predicting stability of DNA duplexes in solutions containing magnesium and monovalent cations, Biochemistry. 47 (2008) 5336–5353. https://doi.org/10.1021/bi702363u.

[162] D. Renciuk, O. Blacque, M. Vorlickova, B. Spingler, Crystal structures of B-DNA dodecamer containing the epigenetic modifications 5-hydroxymethylcytosine or 5-methylcytosine, Nucleic Acids Res. 41 (2013) 9891–9900. https://doi.org/10.1093/nar/gkt738.

[163] A. Thalhammer, A.S. Hansen, A.H. El-Sagheer, T. Brown, C.J. Schofield, Hydroxylation of methylated CpG dinucleotides reverses stabilisation of DNA duplexes by cytosine 5-methylation, Chem. Commun. 47 (2011) 5325–5327.

[164] A.Y. Solovyev, S.I. Tarnovskaya, I.A. Chernova, L.K. Shataeva, Y.A. Skorik, The interaction of amino acids, peptides, and proteins with DNA, Int. J. Biol. Macromol. 78 (2015) 39–45. https://doi.org/10.1016/j.ijbiomac.2015.03.054.

[165] S. Ichimura, M. Zama, Quantitative study of dye binding to DNA-polylysine and DNA-polyarginine complexes, Biochem. Biophys. Res. Commun. 49 (1972) 840–847.

[166] J.-P. Vigneron, N. Oudrhiri, M. Fauquet, L. Vergely, J.-C. Bradley, M. Basseville, P. Lehn, J.-M. Lehn, Guanidinium-cholesterol cationic lipids: efficient vectors for the transfection of eukaryotic cells, Proc. Natl. Acad. Sci. 93 (1996) 9682–9686.

[167] J. Tao, A.D. Frankel, Specific binding of arginine to TAR RNA, Proc. Natl. Acad. Sci. 89 (1992) 2723–2726.

[168] G. Liu, M. Molas, G.A. Grossmann, M. Pasumarthy, J.C. Perales, M.J. Cooper, R.W. Hanson, Biological properties of poly-l-lysine-DNA complexes generated by cooperative binding of the polycation* 210, J. Biol. Chem. 276 (2001) 34379–34387.

[169] M. Piscopo, L. De Petrocellis, M. Conte, G. Pulcrano, G. Geraci, On the possibility that H1 histone interaction with DNA occurs through phosphates connecting lysine and arginine side chain groups, Acta Biochim. Pol. 53 (2006) 507–513. https://doi.org/10.18388/abp.2006_3321.

[170] A. Mann, G. Thakur, V. Shukla, A.K. Singh, R. Khanduri, R. Naik, Y. Jiang, N. Kalra, B.S. Dwarakanath, U. Langel, M. Ganguli, Differences in DNA condensation and release by lysine and arginine homopeptides govern their DNA delivery efficiencies, Mol. Pharm. 8 (2011) 1729–1741. https://doi.org/10.1021/mp2000814.

APPENDICES

A. Preparation of 10X BPE Buffer and Stock Solutions

10X BPE Buffer (100.0 mL, pH = 7.0) contains

- 60.0 mM Na_2HPO_4 (from 300.0 mM stock)
- 20.0 mM NaH_2PO_4 (from 300.0 mM stock)
- 10.0 mM Na_2EDTA (pH = 8.0) (from 100.0 mM stock)

Preparation of 300.0 mM 50.0 mL Na_2HPO_4 (stock)

$M = \frac{n}{V}$, $M = 0.300\ M$, $V = 50.0\ mL$ therefore, $n = 0.015\ mol$

$n = \frac{m}{M_W}$, $M_W = 141.96\ g/mol$, $m = 2.13\ g$

2.13 g Na_2HPO_4 is dissolved in 50.0 mL Millipore water.

Preparation of 300.0 mM 50.0 mL NaH_2PO_4 (stock)

$M = \frac{n}{V}$, $M = 0.300\ M$, $V = 50.0\ mL$ therefore, $n = 0.015\ mol$

$n = \frac{m}{M_W}$, $M_W = 119.98\ g/mol$, $m = 1.80\ g$

1.80 g NaH_2PO_4 is dissolved in 50.0 mL Millipore water.

Preparation of 100.0 mM 100.0 mL Na_2EDTA (stock)

$M = \frac{n}{V}$, $M = 0.100\ M$, $V = 100.0\ mL$ therefore, $n = 0.010\ mol$

$n = \frac{m}{M_W}$, $M_W = 372.24\ g/mol$, $m = 3.72\ g$

3.72 g Na_2EDTA is dissolved in 100.0 mL Millipore water.

Preparation of 250.0 mM 250.0 mL NaOH (stock)

$M = \frac{n}{V}$, $M = 0.25\ M$, $V = 250.0\ mL$ therefore, $n = 0.063\ mol$

$n = \frac{m}{M_W}$, $M_W = 39.997\ g/mol$, $m = 2.50\ g$

2.50 g NaOH is dissolved in 250.0 mL Millipore water.

Dilution from stock HCl

Stock HCl concentration: 11.457 M, desired dilution: 10% (1.1457 M)

$M_1V_1 = M_2V_2$, $11.457\ M * V = 1.1457\ M * 100.0\ mL$, therefore V = 10.0 mL

10.0 mL HCl from stock is diluted to 100 mL with Millipore water.

Using the formula $M_1V_1 = M_2V_2$,

60.0 mM 100.0 mL Na_2HPO_4: $300.0\ mM * V = 60.0\ mM * 100.0\ mL$,

$V = 20.0\ mL$, 20.0 mL from stock Na_2HPO_4

20.0 mM 100.0 mL NaH_2PO_4: $300.0\ mM * V = 20.0\ mM * 100.0\ mL$,

$V = 6.67\ mL$, 6.67 mL from stock NaH_2PO_4

10.0 mM 100.0 mL Na_2EDTA: $100.0\ mM * V = 10.0\ mM * 100.0\ mL$,

$V = 10.0\ mL$, 10.0 mL from stock Na_2EDTA

20.0 + 6.67 + 10.0 = 36.7 mL

50.00 mL – 36.67 mL = 13.33 mL dH_2O is added.

pH is adjusted to 7.0 with prepared HCl solution. Added HCl volume is recorded as V_{HCl}. Desired buffer volume is 100.0 mL.

$100.0\ mL - 50.00\ mL - V_{HCl} = V_{dH_2O}$, V_{dH_2O} is added accordingly.

Preparation of 200 mM 100 mL NaCl (stock)

$M = \frac{n}{V}$, $M = 0.200\ M$, $V = 100\ mL$ therefore, $n = 0.020\ mol$

$n = \frac{m}{M_W}$, $M_W = 58.44 g/mol$, $m = 1.17\ g$

1.17 g NaCl is dissolved in 100.0 mL Millipore water.

Preparation of Amino Acid Stock Solutions

- **Preparation of 2.0 M Arginine Stock Solution**

$M = \frac{n}{V}$, $M = 2.00\ M$, $V = 10.0\ mL$ therefore, $n = 0.020\ mol$

$n = \frac{m}{M_W}$, $M_W = 210.67\ g/mol$, $m = 4.21\ g$

4.21 g Arginine is dissolved in 10.0 mL Millipore water.

- **Preparation of 2.0 M Lysine Stock Solution**

$\mathrm{M} = \frac{\mathrm{n}}{\mathrm{V}}$, $M = 2.00\ M$, $V = 10.0\ mL$ therefore, $n = 0.020\ mol$

$n = \frac{m}{M_W}$, $M_W = 182.65\ g/mol$, $m = 3.65\ g$

3.65 g Lysine is dissolved in 10.0 mL Millipore water.

B. Thermal Denaturation Experiments

Investigating the Interactions of Poly(A)-COR in Crowded Environments

UV-Vis Spectra of Samples

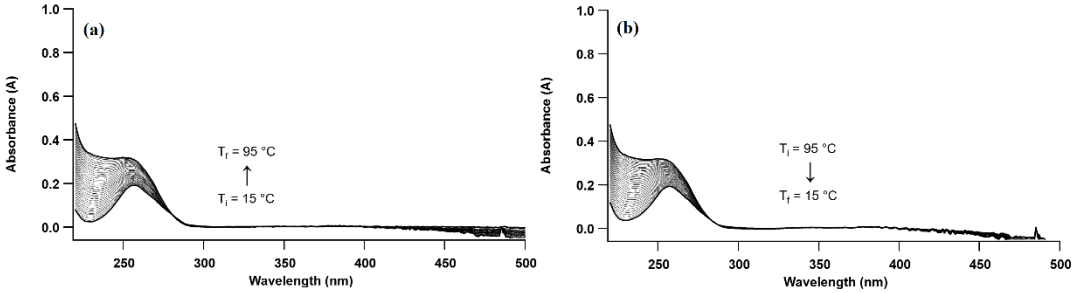

Figure 56. UV-Vis absorption spectra of 30.0 μM poly(A) sample obtained during thermal denaturation experiment (a) heating and (b) cooling.

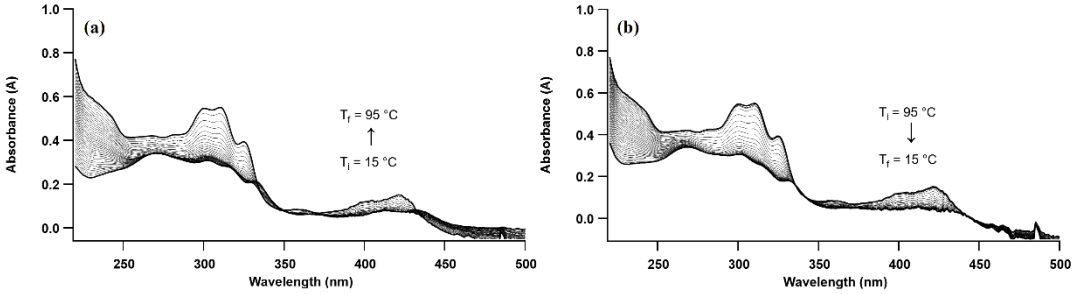

Figure 57. UV-Vis absorption spectra of 30.0 μM poly(A) + 7.5 μM COR sample obtained during thermal denaturation experiment (a) heating and (b) cooling.

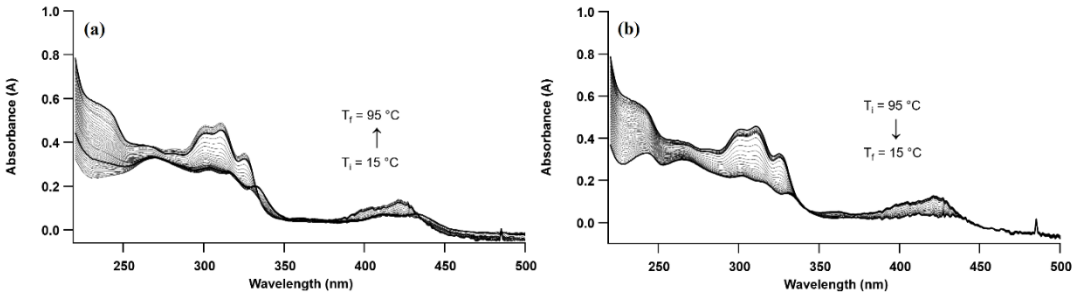

Figure 58. UV-Vis absorption spectra of 30.0 μM poly(A) + 7.5 μM COR + 5% PEG sample obtained during thermal denaturation experiment (a) heating and (b) cooling.

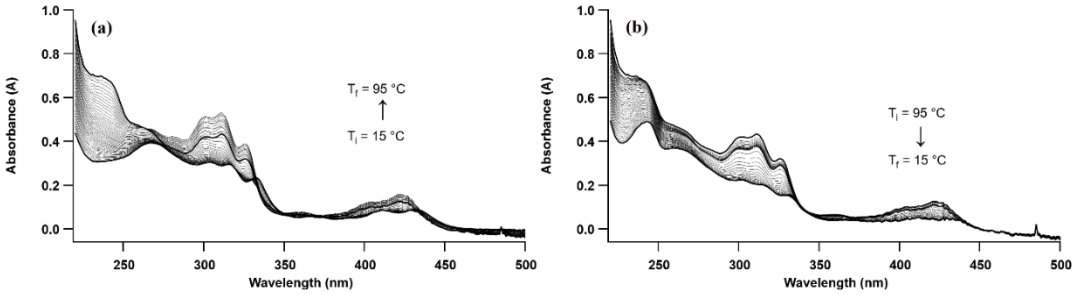

Figure 59. UV-Vis absorption spectra of 30.0 μM poly(A) + 7.5 μM COR + 10% PEG sample obtained during thermal denaturation experiment (a) heating and (b) cooling.

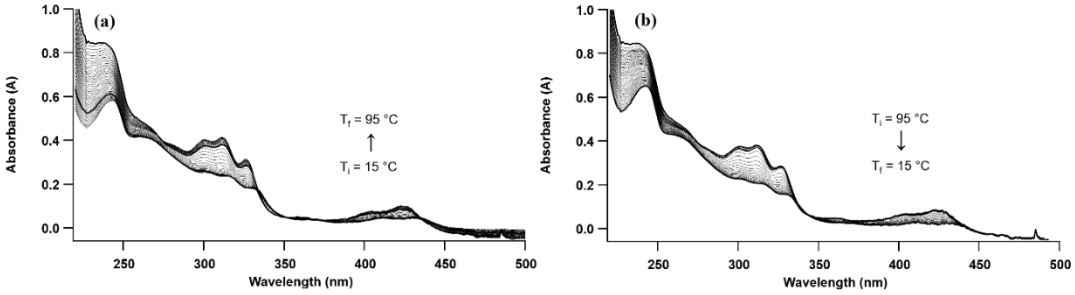

Figure 60. UV-Vis absorption spectra of 30.0 μM poly(A) + 7.5 μM COR + 20% PEG sample obtained during thermal denaturation experiment (a) heating and (b) cooling.

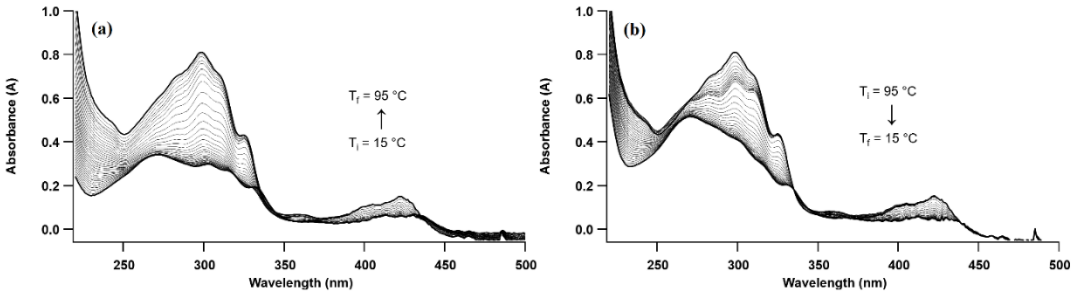

Figure 61. UV-Vis absorption spectra of 30.0 μM poly(A) + 7.5 μM COR + 20% glycerol sample obtained during thermal denaturation experiment (a) heating and (b) cooling.

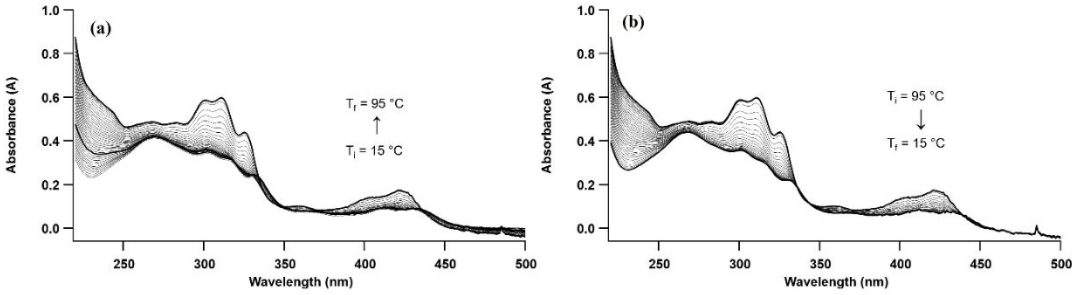

Figure 62. UV-Vis absorption spectra of 30.0 μM poly(A) + 7.5 μM COR + 20% sucrose sample obtained during thermal denaturation experiment (a) heating and (b) cooling.

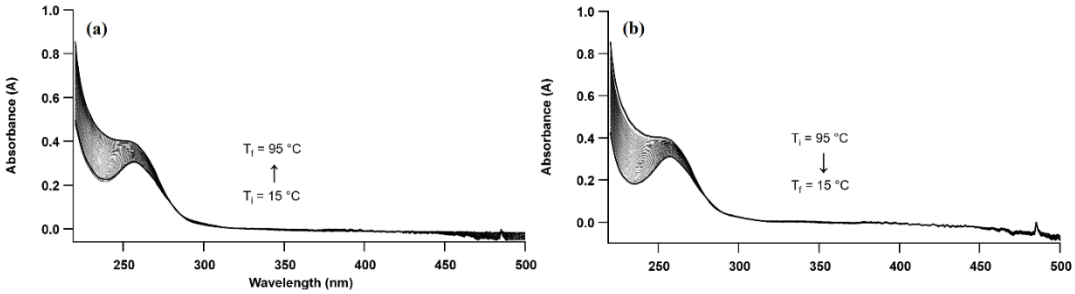

Figure 63. UV-Vis absorption spectra of 30.0 μM poly(A) + 20% PEG sample obtained during thermal denaturation experiment (a) heating and (b) cooling.

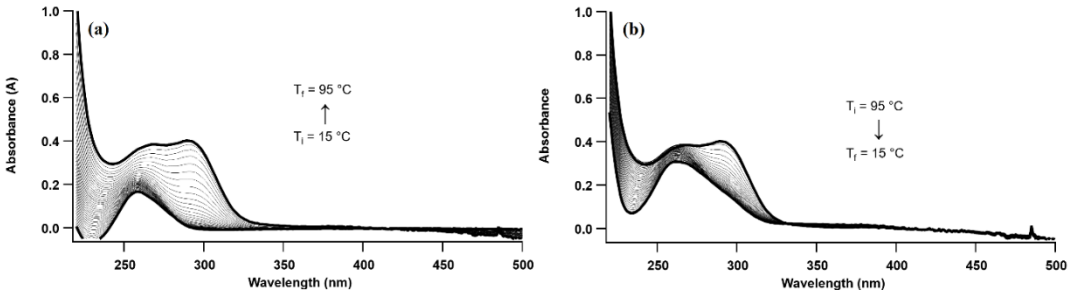

Figure 64. UV-Vis absorption spectra of 30.0 μM poly(A) + 20% glycerol sample obtained during thermal denaturation experiment (a) heating and (b) cooling.

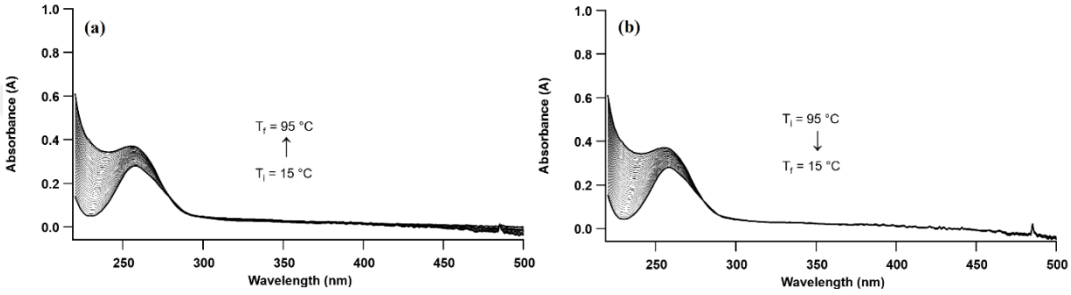

Figure 65. UV-Vis absorption spectra of 30.0 μM poly(A) + 20% sucrose sample obtained during thermal denaturation experiment (a) heating and (b) cooling.

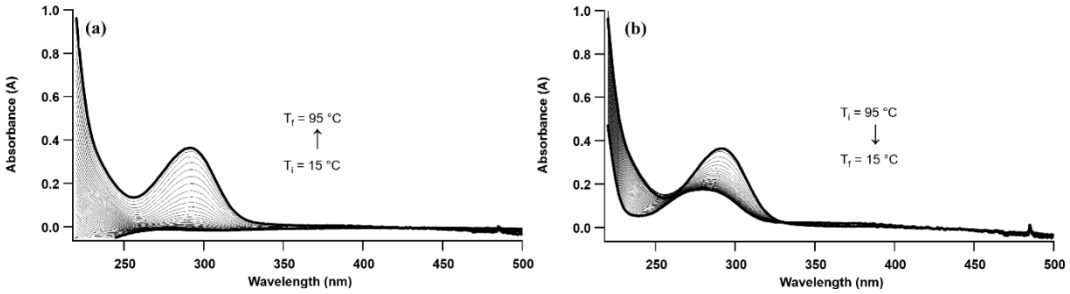

Figure 66. UV-Vis absorption spectra of 20% glycerol obtained during thermal denaturation experiment (a) heating and (b) cooling.

Investigating the Effect of DNA Methylation on DDD-Lysine and DDD-Arginine Interactions

Comparison of Thermal Denaturation Profiles

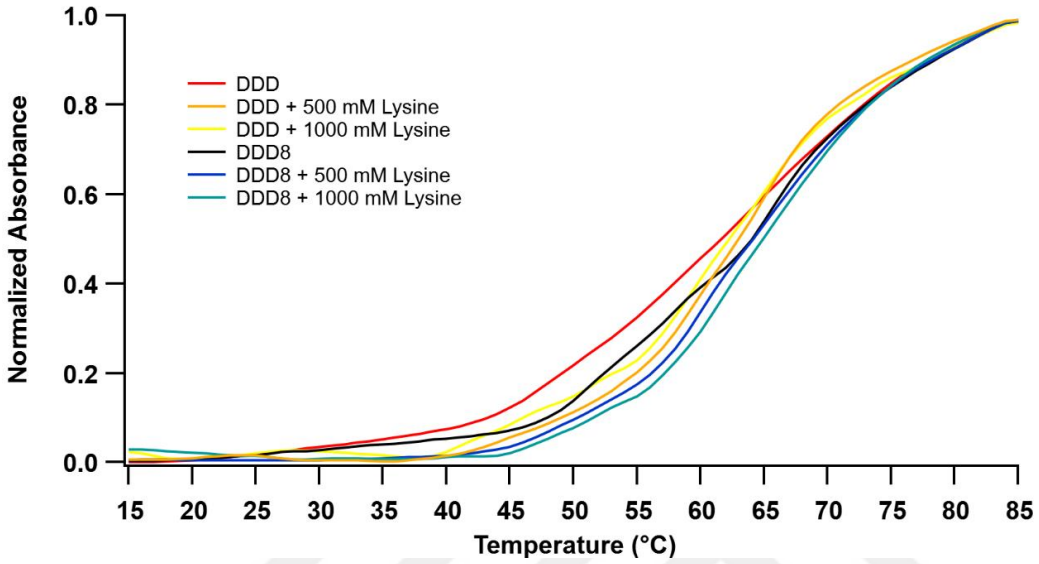

Figure 67. Thermal denaturation profiles of DDD and DDD8 in the presence and absence of Lys obtained by monitoring the change in absorbance at 260 nm with varying temperature.

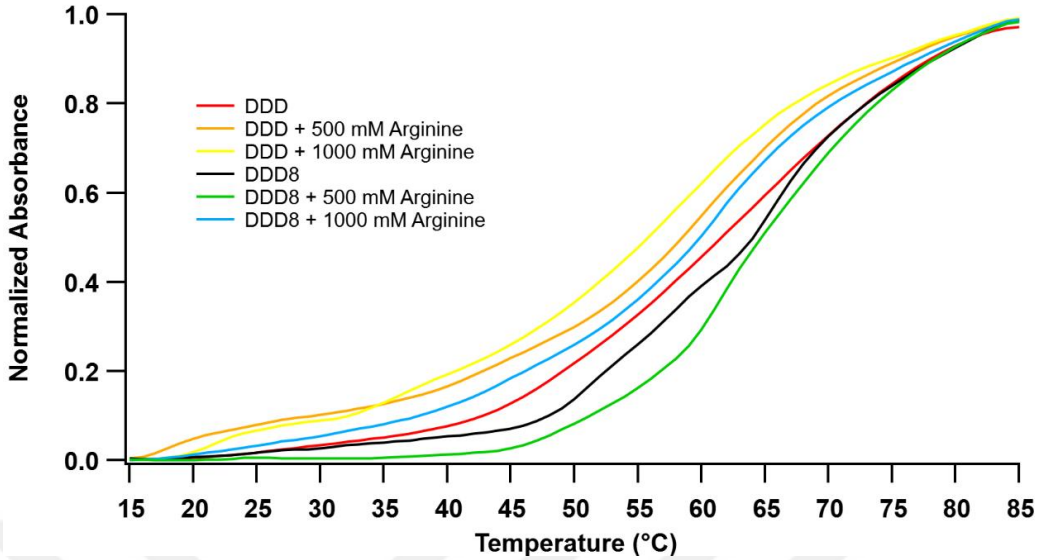

Figure 68. Thermal denaturation profiles of DDD and DDD8 in the presence and absence of Arg obtained by monitoring the change in absorbance at 260 nm with varying temperature.

C. DDD and DDD8 Sequences Used in DNA-Amino Acid Interactions

Table 3. DDD and DDD8 sequences used in DNA-amino acid interactions

Sequence Name	DNA Sequence	Double Helical Structure
DDD (Dickerson dodecamer)	5’-CGCGAATTCGCG-3’	5’-CGCGAATTCGCG-3’ 3’-GCGCTTAAGCGC-5’
DDD8 (Methylated Dickerson dodecamer)	5’-^{me}CG^{me}CGAATT^{me}CG^{me}CG-3’	5’-^{me}CG^{me}CGAATT^{me}CG^{me}CG-3’ 3’-G^{me}CG^{me}CTTAAG^{me}CG^{me}C-5’